Nonlinear Modeling on Viscoelastic Contact Interface: Theoretical Study and Experimental Validation

A Dissertation Presented

by

Chia-Hung Dylan Tsai

to

The Graduate School

in Partial Fulfillment of the

Requirements

for the Degree of

Doctor of Philosophy

in

Mechanical Engineering

Stony Brook University

December 2010

Stony Brook University

The Graduate School

Chia-Hung Dylan Tsai

We, the dissertation committee for the above candidate for the
Doctor of Philosophy degree,
hereby recommend acceptance of this dissertation.

Dr. Imin Kao, Dissertation Advisor
Mechanical Engineering, Stony Brook University

Dr. Robert Kukta, Chairperson of Defense
Mechanical Engineering, Stony Brook University

Dr. Chad S Korach
Mechanical Engineering, Stony Brook University

Dr. Yu Zhou
Mechanical Engineering, Stony Brook University

Dr. Makoto Kaneko
Mechanical Engineering, Osaka University

This dissertation is accepted by the Graduate School

Lawrence Martin
Dean of the Graduate School

Abstract of the Dissertation

Nonlinear Modeling on Viscoelastic Contact Interface: Theoretical Study and Experimental Validation

by

Chia-Hung Dylan Tsai

Doctor of Philosophy

in

Mechanical Engineering

Stony Brook University

2010

Viscoelasticity is a phenomenon of time-dependent strain and/or stress in elastic solids. Various contact interfaces with anthropomorphic end-effectors and polymeric solids found in robots and manipulators are intrinsically viscoelastic. It is therefore important to model such behavior and to study the effects of such time-dependent strain and stress on the stability and sustainability of grasping and manipulation. Both theoretical modeling and experimental study are presented in this dissertation. In theoretical modeling, a new nonlinear latency model is proposed for the application of contact interface involving viscoelasticity in robotics. Latency model can describe well various features of viscoelastic materials, such as stress relaxation, creep, and strain stiffening. The theoretical modeling was supported by experiments and computational simulation. Experiments were conducted by applying displacement-based control to study the stress relaxation and force-based control to explore the creep phenomenon, respectively, in order to validate the proposed theory. The experimental results of viscoelastic responses were observed, and found to match well with the proposed model as well as simulation results.

Table of Contents

Appendix

List of Figures

List of Tables

Acknowledgements

First and foremost, I would like to express my appreciation to my advisor, Professor Imin Kao, for his guidance and encouragement throughout this research. Professor Kao's expert insights into the subjects of robotics and contact modeling provided the inspiration for my research. I would also like to thank him for providing me with a comfortable and supportive research environment.

It is my pleasure to acknowledge Professor Robert Kukta, Professor Chad Korach, Professor Yu Zhou and Professor Makoto Kaneko for taking on the responsibilities of being on my dissertation reading committee. I heartily appreciate their efforts in reading through my dissertation and providing comments and criticisms despite their busy schedules. I am especially grateful to Professor Kaneko and Professor Korach for their support and providing me with their laboratories for conducting experimental studies. Many thanks are also due to Professor Mitsuru Higashimori for fruitful discussions.

I have particularly enjoyed the friendship and many thought-provoking discussions with my colleagues, Craig Capria, Chunhui Chung, Kunbo Zhang, Roosevelt Moreno, and others in the lab. A special thanks to Craig and Mrs. Cara Capria for their help in reading and giving comments about this dissertation.

The road in pursuing the Ph.D. program would not be as smooth without the support from all the friends I have met at Stony Brook, and especially my girlfriend HuiJu Yang. I am grateful for meeting HuiJu here, and appreciate her support and understanding throughout my Ph.D. study.

Last but not least, I would like to express my love and gratitude to my family, especially my parents. Their continuous encouragement has helped push me through these learning and trying years. Without their spiritual and financial support, this dissertation would not have been possible.

Chapter 1

INTRODUCTION

1.1 Contact Interface and Viscoelasticity

Viscoelasticity is a physical, and sometimes chemical phenomenon of time dependent strain [6] and stress. Robotic contacts typically involve end-effectors and grasped objects that are anthropomorphic or polymeric solids [7]. It is therefore important to model such behavior. Viscoelastic contact interface results in time-dependent displacement or force during grasping and manipulation.

In the context of robotics research, we will discuss viscoelasticity as a property of solids. The majority of viscoelastic solids display nonlinear elastic behavior, as opposed to the linear elastic behavior. The response of viscoelastic materials in contact exhibits both time-dependent and displacement-dependent nature that causes changes in force or displacement when contact is being made. Such time-dependent responses always approach equilibrium asymptotically. Thus, theoretical modeling and experiments need to be conducted to capture the physical response of transient when load or displacement is applied while the viscoelastic material tries to achieve equilibrium from a transient state. In the process of achieving the equilibrium from a transient state, the latency caused by the redistribution within the solid constitutes the time-dependent nature of the response.

1.2 Outline of Viscoelastic Properties

Viscoelastic materials, specifically in the context of robotic grasping and manipulation, exhibit the properties of: (1) *Relaxation*: the evolution of force in grasping while the displacement is held constant; (2) *Creep*: the evolution of displacement in contact and grasping while the external force is held constant; (3) *Strain History Dependence*: The response of the material depends on prior strain history; (4) *Energy Dissipation*: a net energy dissipation associated with a complete cycle of loading and unloading.

1.3 Overview of Chapters in the Proposal

The introduction to the viscoelasticity and literature survey are presented in Chapters 1 and 2, respectively. In Chapter 3, the consistency of the parameters of Fung's model is shown by using the experimental results. These results demonstrate a main difference from the spring-damper model (e.g. Maxwell model, Kelvin model, ..., etc). The Maxwell model suffers from the lack of consistency in their parameters (quantitative values of springs and dampers) which varies with the change of experimental setup and boundary conditions, in addition to the material properties.

In Chapter 4, a novel "latency model" is proposed. The latency model is a strain-based model. The main concept of this model is that viscoelastic materials always try to achieve a new equilibrium state under different boundary conditions. When the external force is first applied to the material, the strain distribution inside the material is uneven and under a transient state. With time elapsing, a new equilibrium state is reached based on the latency model. This causes the stress relaxation and creep, as the temporal responses of viscoelastic contact interface. Both simulation and experimental results are presented in this chapter. Moreover, different types of relaxation are discovered and discussed in this chapter.

Based on the latency model presented in Chapter 4, more experimental studies are presented and discussed in Chapter 5. The strain stiffening effect has been brought into the viscoelasticity study and modeling in this chapter.

The strain creep phenomenon is studied in Chapter 6 with modeling and experiments with force control. The model has also been applied to the analysis of grasp stability in this chapter as a practical application.

In the experimental results from different experiments with viscoelastic contact interface, we observed that the relation between the strain and strain rate is nonlinear. Based on this observation, we extend the latency model to a more realistic model, which models the relation between the strain and strain rate by a power law function in Chapter 7.

Finally, the investigations of nonlinear viscoelastic contact interface are summarized in Chapter 8. In addition, two potential biomedical applications are proposed with a brief literature survey and preliminary. The topics of the proposed future work are : (1) Bio-inspired Tactile Sensor, and (2) Modeling of Viscoelastic Contact for Calibrating Cochlear Models.

Chapter 2

LITERATURE REVIEW

2.1 Fung's Model of Viscoelasticity

A popular viscoelastic model in the biomedical field is the Fung's model [8], proposed by Y. C. Fung in 1993. The main idea of the model is to represent the reacting force as the multiplication of two independent responses: the temporal response and the elastic response while incorporating the history of the stress response. The model may be written as

$$T(t) = \int_{-\infty}^{t} G(t-\tau) \frac{\partial T^{(e)}[\lambda(t)]}{\partial \lambda} \frac{\partial \lambda(\tau)}{\partial \tau} \, d\tau \tag{2.1}$$

where $T(t)$ is the tensile stress at time, t, with a step increase of size λ in elongation on the specimen. $T^{(e)}(\lambda)$ is the so-called the elastic response and $G(t)$, a normalized function of time, is the reduced relaxation function.

Tiezzi and Kao [9, 10, 11] simplified this model to study the soft contact interface assuming no past stress history, as shown in (2.2). It was shown that the viscoelastic model has an important implication on the stability of grasp which cannot be captured by rigid or linear elastic modeling.

$$\mathscr{G}(\delta,t) = N^{(e)}(\delta) \cdot g(t) \tag{2.2}$$

where $\mathscr{G}(\delta,t)$ represents the grasping force as a function of the displacement δ and time t. the $N^{(e)}(\delta)$ represents the elastic response of normal force as a function of the displacement (or depression unto the object). $g(t)$, represents the temporal response of relaxation

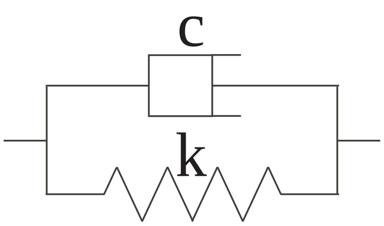

Figure 2.1: Schematic representation of Kelvin-Voigt model.

or creep. The important property of this model is the separation of spatial response and temporal response as two independent functions.

Tsai *et al.* [12] showed the consistency of parameters of the same viscoelastic material under different experimental setup.

2.2 Spring-Damper Models of Viscoelasticity

Linear model of spring and damper has been widely used in the modeling of viscoelasticity [1]. In 1966, Yang proposed a viscoelastic model for the contact problem by assuming the elastic modulus is a function of time [13]. Kelvin-Voigt's solid model was constructed by a spring and a damper connected in parallel [14] as shown in Fig. 2.1, and the relation of stress, σ, and strain, ε, can be formulated as:

$$\sigma = k\varepsilon + c\frac{d\varepsilon}{dt} \tag{2.3}$$

Maxwell proposed in 1867 the Maxwell fluid model [15] as a single set of spring and damper in series as shown in Fig. 2.2. The relation of stress, σ, and strain, ε, can be formulated as.

$$\frac{1}{k}\frac{d\sigma}{dt} + \frac{\sigma}{c} = \frac{d\varepsilon}{dt} \tag{2.4}$$

The "generalized Maxwell model" utilizes multiple serial spring-damper sets and a spring connected in parallel. However, the problem of this model is the inconsistency of the parameters (stiffness constants and damping factors) obtained from the model. Such pa-

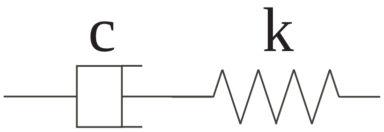

Figure 2.2: Schematic representation of Maxwell model.

rameters can have discrepancies of numerical values, often in two orders of magnitude or higher, while representing the same material with sets of supposedly similar springs and dampers. These parameters sometimes can also present unrealistic difference in scales under different experimental setup (*e.g.* in [1, 16]).

2.3 Rheology Model of Viscoelasticity

Research of viscoelasticity also has been done from the rheology viewpoint [17, 18, 19]. Golik proposed a model based on the diffusion of holes inside rubber under an external force [20]. In 1974, a new concept of viscoelasticity was proposed by Golik [20]. It was concluded that creep and stress relaxation in folded polymers are resulted from hole diffusion, in which the boundaries of the crystallites act as sources and sinks with respect to holes. Based on these studies, we construed that one cause of viscoelastic behavior should be the internal re-arrangement and alignment of materials.

2.4 Models from Molecular Perspective

B. H. Zimm [21] in 1956 proposed a model which represented a viscoelastic solid by a chain of beads connected with ideal springs immersed in viscous fluid. Zimm treated the problem as a three-dimensional chain problem with Brownian motion and a special type of interaction. By employing Kirkwood's general formalism, he obtained the exact solution of the eigenvalue problem. Before this, Alfrey [22] presented a study of the viscoelastic behavior of an amorphous linear polymer from molecular point of view. Rouse, Jr. [23] studied three factors of linear polymeric molecules; namely, the length of polymer molecules, the flexibility of the molecular chains, and the interaction of the segments of polymer molecules. In addition, Bueche [24] derived the equations of a viscoelastic polymer to predict the viscoelastic behavior of plastics from molecular viewpoint.

In [6], Meyers and Chawla suggested that a continuous displacement of atoms or molecules takes place with time at a constant load. This flow mechanism of non-crystalline materials is associated with the diffusion of atoms or molecules within the material. This model provides another supporting argument for stress relaxation and creep phenomena as being due to a certain kind of continuous internal movement while the configuration of the material under grasping is held constant.

In [25], the author applied statistical solution to the rubber elasticity problem. Although viscoelasticity was not discussed much in this book, the molecular structure of rubber showed similar construction as the studies mentioned above [20, 6]. Recently, Goktekin [26] modified the Navier-Stokes equation with an additional elastic term in it, which results in a very vivid simulation of viscoelastic material.

2.5 Model from Energy Perspective

In 2007, Adolf proposed the idea of “material clock” in modeling of viscoelasticity [19]. The “material clock” is the model which depends on the potential energy of the system, also known as “potential energy clock model.” The model is derived from the Williams-Landel-Ferry model (WLF), a temperature dependent viscosity model. As shown in many other studies, the same experimental setup may produce different results due to this “clock” effect (*e.g.* the periodic loading-unloading experiment performed by Viidik in 1973).

2.6 Models from the Perspective of Stress Wave Propagation

Research studies have been conducted on the dynamic behavior of viscoelastic materials, especially the stress wave propagation. Theocaris and Papadopoulou studied the propagation of stress waves in viscoelastic media based on the Kelvin-Voigt model [27]. Turhan and Mengi proposed three types of inhomogeneities of the stress wave within the viscoelastic media [28]. Stucky and Lord utilized the finite element modeling method (FEM) to analyze the properties of ultrasonic waves in linear viscoelastic media [29]. Pereira, Mansour and Davis employed a wave propagation technique to measure the dynamic viscoelastic properties of excised skin when subjected to a low incremental strain [30]. Fowles and Williams derived two different phase velocities from conservation relations, mass and energy [31].

Chapter 3

AN EXPERIMENTAL STUDY OF GRASPING SUSHI WITH VISCOELASTIC MODELING

In this chapter, we employ Fung's viscoelastic model discussed by Tiezzi and Kao to study the experimental data presented by Sakamoto *et al.* [1] for grasping viscoelastic objects using a parallel-jaw gripper. The viscoelastic contact modeling presented in this chapter is characterized by two separate responses: elastic response and temporal response. Two main and intriguing results were found in the modeling and analysis of experimental data. The first is the consistency on the normalized coefficients for the curve fitting of the temporal response during the relaxation period of the grasping. Such consistency suggests that the proposed model is applicable to the grasping task at hand. The other result is the generic pattern of the elastic response deduced from the experimental data. The pattern of elastic response represents different physical significance of grasping which involves viscoelastic contact interface [12].

3.1 Introduction

Viscoelastic contacts can be found in many applications in daily life and robotic tasks. One study of viscoelastic grasping was presented in [1] in which the authors performed a grasping experiments with sushi using a parallel-jaw gripper. The grasping task as illustrated in Figure 3.1: loading, holding, and unloading. In the loading and unloading phases, the elastic response of sushi as the grasped object is dominant. During the holding phase in which the gripper was held stationary, the viscoelastic response of "*relaxation*" is dominant. Figure 3.2 and Figure 3.3 show the experimental setup and snapshots of the grasping task. Three groups of experiments were performed with displacement of the parallel-jaw gripper at 4*mm*, 8*mm*, and 12*mm*, respectively. Figure 3.4 shows a typical response of forces measured by the gripper as a function of time for the three displacements.

The first and last phases of the grasping displayed in Figure 3.1 can be controlled arbitrarily with appropriate control algorithm, and are independent of the material's viscoelastic behavior[1] . The middle segment, in which the viscoelasticity dominates, can be modeled according to the models described in the Chapter 2

In this chapter, we will describe Tiezzi and Kao's [10] model along with the study of the experimental data presented in [1]. The study will focus on both the temporal and the elastic responses.

3.2 Viscoelastic Modeling in Tiezzi and Kao

The viscoelastic model proposed by Tiezzi and Kao [10] calls for the representation of the contact and grasping by the following general equation

$$\mathscr{G}(\delta,t) = N^{(e)}(\delta)\cdot g(t) \tag{3.1}$$

The term to the left of the equal sign in equation (3.1), $\mathscr{G}(\delta,t)$, represents the grasping force as a function of the displacement δ, and time t. The important property of this model is the separation of spatial response and temporal response as two independent functions. On the right-hand side, the $N^{(e)}(\delta)$ represents the elastic response of normal force as a function of the displacement (or depression unto the object). This elastic function can em-

---

[1] Unless the application of the normal force is so slow as to be comparable to the shortest time constant of the exponentially decaying characteristics such as that in equation (3.3) or equation (3.6). See the following equations and modeling.

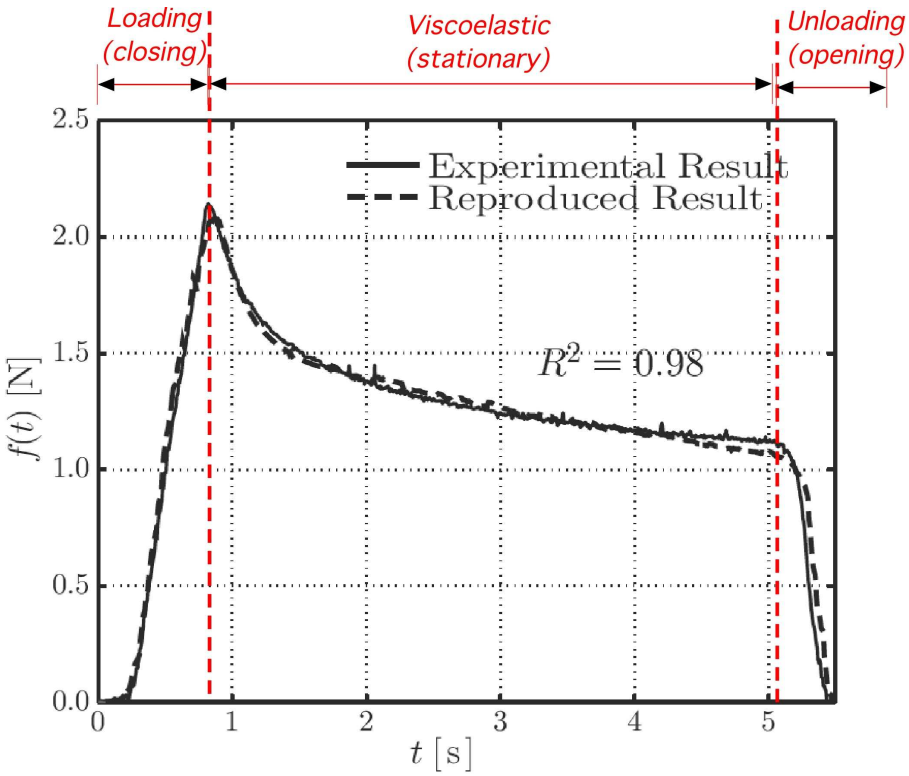

Figure 3.1: The three phases of a grasping task performed on sushi using parallel-jaw gripper [1]. The grasping task can be broken into 3 phases: loading holding, and unloading

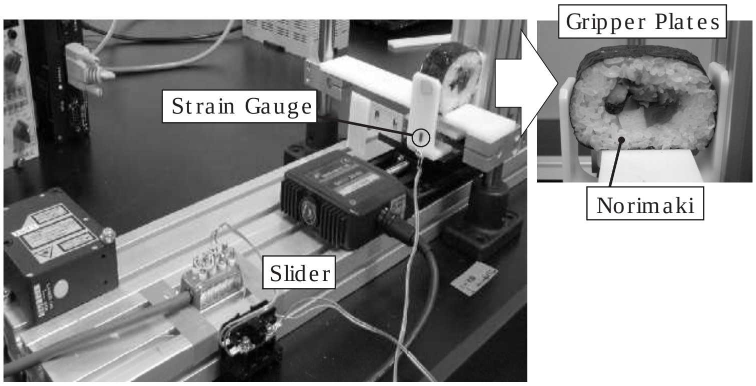

Figure 3.2: The experimental setup and a typical grasp of sushi by a parallel-jaw gripper [1].

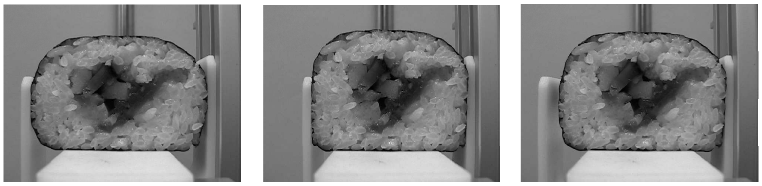

(a) t = 0[s] (b) t = 3[s] (c) t = 6[s]

Figure 3.3: Photos showing three instances of grasps [1]. The grasping configuration and elapsed time can be compared with Figure 3.4.

ploy various models, with typically nonlinear elastic contact behavior, proposed by many researchers [32, 33, 34, 35, 36, 37, 38]. The second term in equation (3.1), $g(t)$, represents the temporal response of relaxation or creep. In the grasp task discussed here, both temporal response of relaxation and creep are considered. It is noted that one function may be constant while the other is varying in equation (3.1), for example, in the relaxation phase during which the parameters of temporal function can be singled out for curve fitting.

3.2.1 Elastic Response, $N^{(e)}(\delta)$

The elastic response function, $N^{(e)}(\delta)$, is the amplitude of the force generated instantaneously by a displacement δ from the undeformed configuration. In equation (3.2), the parameters p and q are dependent upon the materials and geometry [39], and was derived from the power-law equation proposed by Xydas and Kao [34].

$$N^{(e)}(\delta) = \frac{p}{(q+1)}\delta^{q+1} \tag{3.2}$$

It is noted that other models of non-linear elastic behavior can be used in place of equation (3.2) [36, 32, 40, 37, 38].

3.2.2 Temporal Response, $g(t)$

The relaxation function [10] is in the form of equation (3.3), as part of equation (3.1)

$$g(t) = \sum_{i=0}^{n} c_i e^{-v_i t} \quad \text{with} \quad v_0 = 0 \quad \text{and} \quad \sum_{i=0}^{n} c_i = 1 \tag{3.3}$$

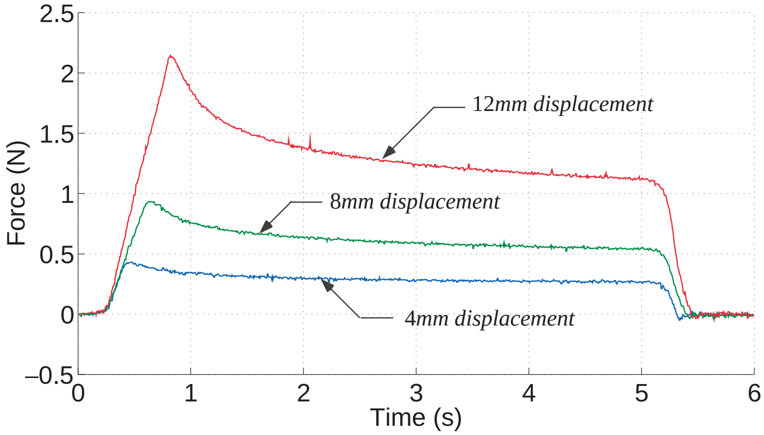

Figure 3.4: The measurements of forces by strain-gauge sensor mounted on the gripper are plotted as a function of time for total displacement of 4*mm*, 8*mm*, and 12*m*, respectively [1].

The temporal response in equation (3.3) is normalized such that $\sum_{i=0}^{n} c_i = 1$. In the following analysis, two exponentially decaying terms are used. See Appendix A for the justification of choosing two exponential terms. Therefore, equation (3.3) used in curve fitting of experimental data is

$$g(t) = c_0 + c_1 e^{-\nu_1 t} + c_2 e^{-\nu_2 t} \tag{3.4}$$

where $c_0 + c_1 + c_2 = 1$.

3.3 Experimental Results and Analysis

3.3.1 Experimental Setup

We use in this chapter the experimental results in [1]. The experiments were conducted by a pair of parallel-jaw gripper grasping sushi on a table as shown in Figure 3.2. The mass of the moving part of gripper is around $14g$ (including plate and wires) Strain gauges attached on the grippers measure the forces applied on sushi at a sampling rate of $200Hz$. "Normaki-sushi" was used in the experiments with a new sushi for each experiment. Experiments were conducted in three grasping displacements of $4mm$, $8mm$, and $12mm$, with the same maximum speed of movement and ramp-up and ramp-down profiles, as shown in phase one of the three curves in Figure 3.4. Figure 3.4 shows a typical sequence of the grasping task. For each displacement, several experiments were performed with data recorded for analysis.

3.3.2 The Procedure of Grasping Task

As shown in Figure 3.3, the gripper was first brought to contact with sushi. After $0.2\,sec$, the gripper starts to grasp the sushi with a speed of movement equal to $20\,mm/s$ until the prescribed displacement is achieved at $4mm$, $8mm$, or $12mm$. After that, the gripper holds steadily until the time is at $5.1\,s$. Finally, the gripper releases the sushi with the same speed of movement at $20\,mm/s$, during which the contact is broken and the gripper moves back to the starting position.

3.3.3 Elastic Response Based on Experimental Results

The force-displacement diagram in Figure 3.5 shows the elastic response for the entire grasping from loading to release. In the loading stage, the curve is approximately linear. On the other hand, the unloading curve appears to be nonlinear and similar to a typical response of unloading in a nano-indentation process. Further discussions will be presented in the next section. In Figure 3.5, we use three different legends in each diagram to mark different sets of data. The circle on the loading curve indicates the instant when the grasping force reaches the maximum value; the circle on the unloading curve indicates the breaking of contact when the contact force sensed by the strain gauge becomes zero; the triangle in the plot shows the instant when the maximum grasping displacement is reached.

A few observations are in order:

(1) loading to the largest displacement: This is marked by the first circle (red circle). We noted that the maximum normal force is achieve before the displacement reaches maximum, due to viscoelastic effect.

(2) holding with relaxation: The relaxation curve is characterized by the exponential decay of normal force, under the condition of constant displacement. The elastic response (force-displacement) shows a vertical straight line.

(3) unloading to dis-engagement: The unloading segment is a nonlinear curve in the elastic response plot.

(4) the creep effect after the gripper was no longer in contact: The creep takes place after the contact between the gripper and sushi is broken, in a gradual expansion of sushi after the external force is removed.

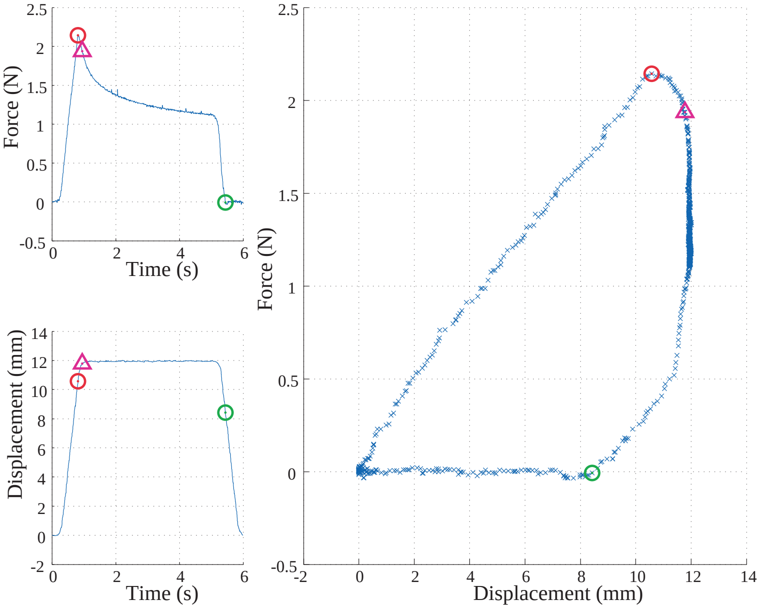

Figure 3.5: Experimental data of sushi grasping with 12*mm* displacement. The forces and displacement are plotted as a function of time. The elastic response of force-displacement is plotted with legends of circle(s) and triangle corresponding to labeled instants in each plot.

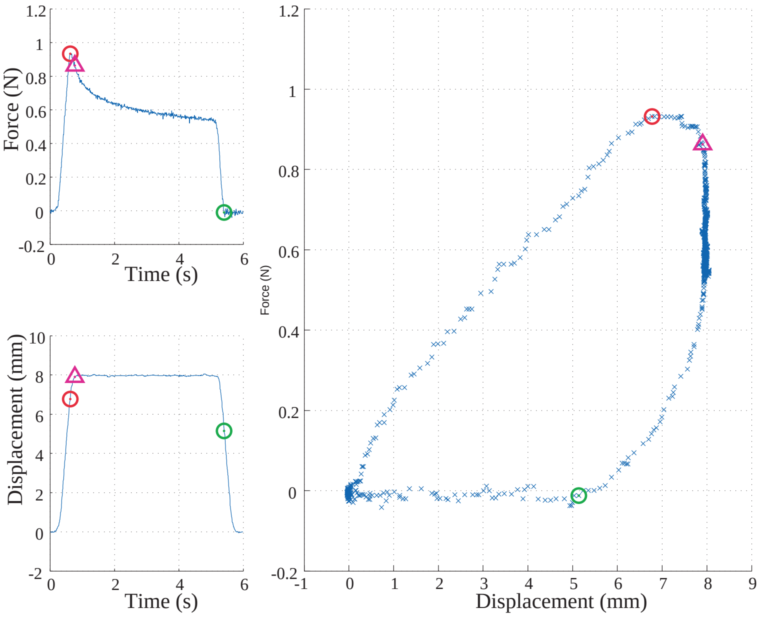

Figure 3.6: Experimental data of sushi grasping with 8*mm* displacement.

The elastic responses corresponding to the $8\,mm$ (plotted in Figures 3.6) and $4\,mm$ displacements are similar.

3.3.4 Inertia Effect of Gripper During Sushi Grasping

The force measured by the strain gauge contains not only the contact normal force of grasping but also the inertial force due to the acceleration and deceleration of the gripper. The mass of the gripper is $14\,g$, with accelerations corresponding to 12mm, 8mm and 4mm displacement being $0.6990\,m/s^2$, $0.7263\,m/s^2$ and $0.7110\,m/s^2$. The inertial forces are estimated at: $F_{12mm} = 9.786 \times 10^{-3}\,N$, $F_{8mm} = 1.017 \times 10^{-2}\,N$, and $F_{4mm} = 9.954 \times 10^{-3}\,N$, respectively. Comparing with the normal force from sushi, the inertial effect for 12*mm* experiments is less than 1%, for 8*mm* experiments is about 1%, and for 4*mm* experiments is about 2.5%. It is concluded that the inertial effect does not affect the outcomes of the experiments.

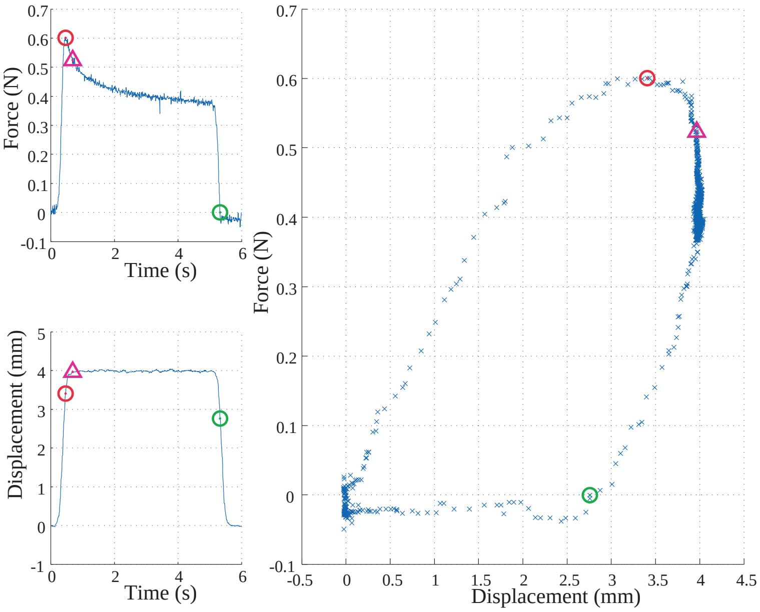

Figure 3.7: Experimental data of sushi grasping with 4*mm* displacement.

3.3.5 Data Analysis of the Viscoelastic Relaxation Phase

As presented in Tiezzi and Kao [10], when $g(t)$ is normalized to 1 at $t = 0$ at the onset of the viscoelastic response, the exponentially decaying "*relaxation*" behavior can be represented by the general function of linear combination of exponential terms [10]. Since equation (3.3) is normalized with time starting at $t = 0$, we have shifted the time reference of the viscoelastic phase in Figure 3.1 to start at $t = 0$ for the relaxation segment.

Employing the 'nonlinear least squares' curve-fitting technique with 'trust-region reflective newton' algorithm by using equation (3.4) and the data from the curve of the "*viscoelastic*" phase in the experimental result with displacement equal to 12*mm* renders the following best-fit equation with correlation of $R^2 = 0.9986$

$$N^{(e)}(\delta) = 2.187 \tag{3.5}$$

$$g(t) = 0.4852 + 0.2472.e^{-3.9810t} + 0.2676e^{-0.5325t} \tag{3.6}$$

Using the parameters in equation (3.6), we can plot the viscoelastic response of relaxation phase in Figure 3.4. The experimental data and best-fit function are plotted in Figure 3.8 for comparison.

In addition, the asymptotic response of the viscoelastic contact, when the time is elapsed for longer period, is plotted in Figure 3.9, using the same parameters in equation (3.6) with the best-fit curve. This provides us with a sense of the asymptotic behavior of grasping for the soft contact in grasping as time goes on.

Following the same procedure, the normalized temporal response for the 8*mm* grasping displacement is found with $R^2 = 0.9941$, and

$$N^{(e)}(\delta) = 0.957 \tag{3.7}$$

$$g(t) = 0.5275 + 0.2313.e^{-3.4930t} + 0.2411e^{-0.4247t} \tag{3.8}$$

The curve-fitting result for the 4*mm* grasping displacement is obtained with $R^2 = 0.965$, and

$$N^{(e)}(\delta) = 0.4254 \tag{3.9}$$

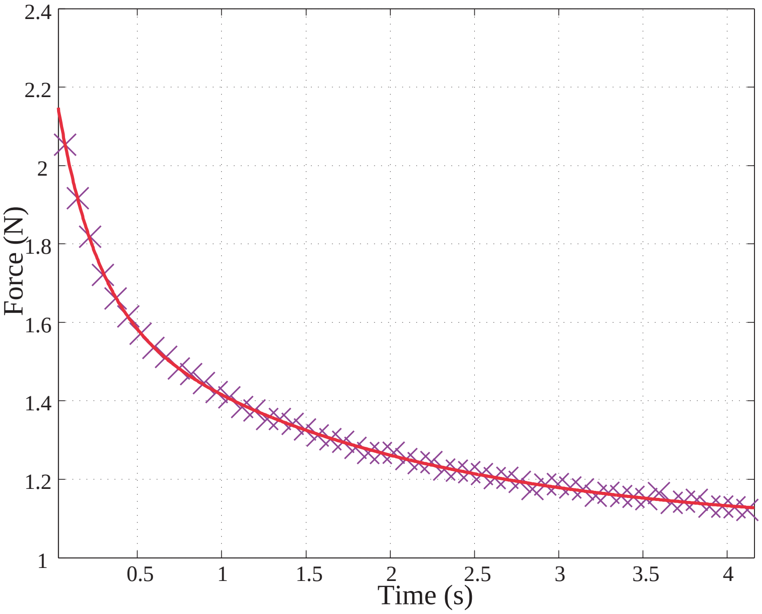

Figure 3.8: Comparison of the experimental data and best-fit function (12*mm*). The experimental data are shown with ‘x’; the best-fit curve is shown in solid line. The result shows good curve fitting.

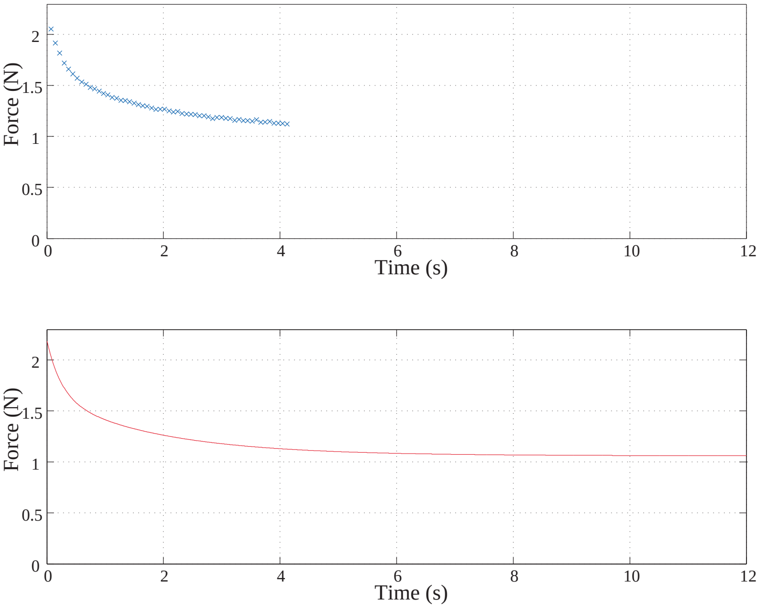

Figure 3.9: Comparison of best-fit curve with asymptotic value at the lower plot for the viscoelastic soft contact and grasping. The experimental data in the upper half plot are from [1]. The lower half plot illustrates the relaxation behavior with longer elapsed time to show the asymptotic behavior.

Table 3.1: The coefficients of the relaxation function in Eq (3.4) with 12*mm* Displacement. The results show 10 different sets of experimental data.

No.	c_0	c_1	v_1	c_2	v_2	$N^{(e)}$	R^2
01	0.5007	0.2390	3.666	0.2604	0.4860	2.285	0.9987
02	0.4872	0.2506	3.659	0.2622	0.4710	1.963	0.9983
03	0.4817	0.2552	3.525	0.2631	0.4838	1.434	0.9977
04	0.5127	0.2391	3.646	0.2482	0.4928	1.901	0.9985
05	0.5016	0.2401	3.672	0.2583	0.5145	1.991	0.9988
06	0.4852	0.2472	3.981	0.2676	0.5325	2.187	0.9986
07	0.4674	0.2740	3.743	0.2586	0.4704	1.530	0.9973
08	0.4345	0.2786	3.856	0.2869	0.5329	1.418	0.9980
09	0.4849	0.2605	3.699	0.2546	0.5016	1.944	0.9987
10	0.4894	0.2427	3.737	0.2679	0.5194	2.922	0.9995

$$g(t) = 0.6186 + 0.1651.e^{-3.7860t} + 0.2161e^{-0.6427t} \tag{3.10}$$

3.4 Discussions

3.4.1 Different Regions of the Elastic Response

In Figures 3.5 and 3.6, several common regions with different physical significance can be categorized. To summarize the experimental results, Figure 3.10 is plotted to illustrate different regions of grasping using viscoelastic contact model on sushi. The entire grasping process can be broken into six different regions as shown in Figure 3.10.

The six regions in Figure 3.10 are labeled as “Preloading region,” “Loading region,” “Transition region,” “Relaxation region,” “Unloading region” and “Creep region.” The details of each region will be explained in the following.

3.4.1.1 Preloading Phase

This segment happens at the beginning of the grasp to transition to point A at which the loading region starts. This region is normally nonlinear with response depending on the nature of grasp and materials.

Table 3.2: The coefficients of the relaxation function in Eq (3.4) with 8*mm* displacement

No.	c_0	c_1	v_1	c_2	v_2	$N^{(e)}$	R^2
01	0.5143	0.2371	3.758	0.2485	0.4561	1.166	0.9961
02	0.5188	0.2313	3.725	0.2499	0.4779	0.985	0.9957
03	0.5101	0.2701	3.180	0.2196	0.4300	1.089	0.9953
04	0.4738	0.2732	3.705	0.2529	0.4956	1.117	0.9960
05	0.4649	0.2506	3.948	0.2844	0.4546	0.956	0.9955
06	0.5275	0.2313	3.493	0.2411	0.4247	0.957	0.9941
07	0.5395	0.2242	3.935	0.2362	0.4769	1.336	0.9974
08	0.5572	0.2250	3.410	0.2178	0.4885	0.987	0.9923
09	0.5244	0.2415	3.351	0.2340	0.4523	1.427	0.9965
10	0.5296	0.2324	3.725	0.2379	0.4829	1.154	0.9956

Table 3.3: The coefficients of the relaxation function in Eq (3.4) with 4*mm* displacement

No.	c_0	c_1	v_1	c_2	v_2	$N^{(e)}$	R^2
01	0.5281	0.2517	2.711	0.2201	0.2828	0.4715	0.9724
02	0.5692	0.2133	3.584	0.2173	0.3972	0.4331	0.9770
03	0.6030	0.1918	3.731	0.2051	0.4896	0.6053	0.9824
04	0.6006	0.1833	3.960	0.2160	0.5163	0.6828	0.9849
05	0.5721	0.2120	4.160	0.2158	0.6349	0.3661	0.9542
06	0.6186	0.1651	3.786	0.2161	0.6427	0.4254	0.9650
07	0.5743	0.1885	5.111	0.2371	0.6607	0.3781	0.9455
08	0.5617	0.2342	3.124	0.2040	0.3497	0.4862	0.9495
09	0.5353	0.2439	3.497	0.2207	0.4513	0.4081	0.9630
10	0.5139	0.2355	2.958	0.2505	0.2553	0.5588	0.9842

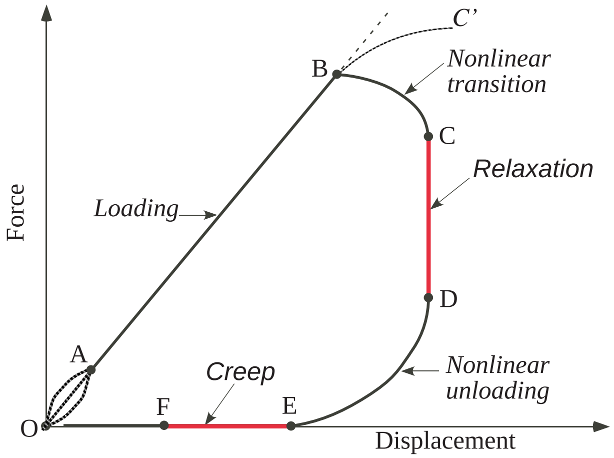

Figure 3.10: Model of elastic and temporal responses of grasping sushi with viscoelastic contact interface. The schematic model illustrated typical response with 6 regions: OA, AB, BC, CD, DE, EF.

Table 3.4: Statistic result: mean value and standard deviation of normalized coefficients

Displacement	Coefficient	Average	Standard Deviation
12mm	c_0	0.4845	0.0215
	c_1	0.2527	0.0144
	c_2	0.2628	0.0103
	v_1	3.7184	0.1249
	v_2	0.5005	0.0234
8mm	c_0	0.5161	0.0280
	c_1	0.2417	0.0176
	c_2	0.2422	0.0189
	v_1	3.6230	0.2541
	v_2	0.4639	0.0243
4mm	c_0	0.5677	0.0342
	c_1	0.2120	0.0291
	c_2	0.2203	0.0140
	v_1	3.6622	0.6814
	v_2	0.4681	0.1480

3.4.1.2 Loading Phase

The region from point A to B is the loading phase of grasping in which the normal force is gradually increased until a prescribed value is reached. The normal force is applied through the controller of the parallel-jaw gripper. It is also called the “closing phase” in the paper [1]. This segment looks fairly linear until it reaches point B when the maximum force is reached in Figure 3.10.

3.4.1.3 Transition Phase

The region BC represents the transition from the elastic loading to viscoelastic relaxation. Starting at point B, the force starts to decrease while displacement is increased to maximum at C. At point C, the gripper was held stationary with no change in displacement. Depending on the characteristics of the material being grasped, the point C can be higher than point B (as is in the case of biomedical tissues [41]) or lower than point B (as is in this case of grasping sushi). The transition region is nonlinear.

3.4.1.4 Relaxation Phase

The region CD is characterized by the gradual decrease of the normal force while the grasping configuration and displacement remains unchanged—demonstrating the *relaxation* behavior, as shown in Figure 3.10. Due to the viscoelastic characteristics of the object (in this case, the sushi being grasped), the normal force exhibits the typical behavior of an exponentially decaying curve—corresponding to the decrease in the normal force in the vertical line segment CD, as shown in Figure 3.10. This region is also called the “stationary phase” in the paper [1]. From equation (3.1), we can tell that the elastic response will keep as a constant if the δ keeps the same. In this segment, the equipment maintains the same displacement, δ, which results in the relaxation response. The reduction in force is a way of minimizing the energy through re-orienting the individual particles of the grasped object (rice and other garnish in sushi).

3.4.1.5 Unloading Phase

The region *DE* is the unloading stage in which the gripper retreats from grasp and finally breaks the contact at point E. After the contact is broken at point E when the normal force is reduced to zero, the gripper will continue to retreat until the original position at *O*. The region *DE* appears to be nonlinear, and resembles that of typical unloading in indentation or nano-indentation. This phase corresponds to the reverse of the "loading" phase. It is also called the "opening phase" in [1].

3.4.1.6 Recovery Phase

As soon as the contact is broken, the sushi continues to restore to its initial configuration, as shown in the region *EF* in Figure 3.10, through the creep phenomenon [10]. At the *EF* region, the sushi has no external force applied but continues to expand while the normal force applied is zero. Creep compliance is another side of the coin to the relaxation in *CD*.

3.4.2 Discussions and Statistical Analysis of Temporal Response

The temporal function $g(t)$ is the reduced relaxation function which describes the relaxation behavior of viscoelastic material. The coefficients of curve fitting using equation (3.4) for 12mm-displacement is listed in Tables 3.1.

The statistical analysis of the normalized coefficients (c_0 c_1 c_2 and ν_1 ν_2) in equation (3.4) from the 10 different data sets was conducted, with results of mean value and standard deviation listed in Table 3.4. It is clear from Table 3.4 that the standard deviation of the coefficients and exponents are very small compared to the mean value. Thus, the statistical analysis of the temporary response of relaxation yields results that are quite consistent. This suggests that the curve fitting employed to perform the analysis of grasping is consistent and yield repeatable results, and seems to capture the physics of relaxation in exponential decay.

The temporal response of relaxation represented by segment *CD* in Figure 3.10 presents another intriguing insight. It is observed in experiments that the particles (rice grains and garnish) rearrange themselves with a reduction in grasping force, while holding displacement at constant, during the relaxation stage *CD*. However, this *CD* segment of relaxation does not present any changes in energy due to the external force on the force-displacement diagram, because the integration of area is zero! Nevertheless, it is obvious that energy changes are taking place during the relaxation process. So what is the seeming paradox? The problem cannot be answered by the elastic energy alone, but should be tackled in a broader context using equations of thermodynamics and energy. The entropy is increased during the grasping stage from *O* to *C*, and is decreased during relaxation in *CD* while the internal particles are re-arranging themselves in an attempt to minimize the disorder. It is conjectured, however, that the sum of entropy of such increase (from *O* to *C*) and decrease (from *C* to *D*) is still positive, because this is not a reversible process.

3.5 Summary

In this chapter, we employ viscoelastic contact model to analyze the experimental data of grasping viscoelastic objects using a parallel-jaw gripper. Two main conclusions are presented. The first is the modeling of elastic and temporal responses which can be broken into six distinct regions, each with its physical meaning. The pattern is also consistent with the experimental data. The second result is regarding the consistency of the normalized coefficients of exponentially decaying equation of the relaxation response. The small standard deviation suggests that the modeling is statistically significant within the data group of the same displacement. The results suggest that the dual response model [41, 34] can capture the behavior of viscoelastic grasping task quite well.

Chapter 4

THEORY AND EXPERIMENTAL STUDY USING THE LATENCY MODEL

In this chapter, we propose the *latency model* to describe the viscoelastic contact behavior. This new model is built upon research from various fields of science and engineering. Experiments were conducted to validate the characteristics of the latency model. The work contained in this chapter has been published in [2].

4.1 Introduction

Viscoelasticity is the phenomenon of time-dependent strain and/or stress in elastic solids. Various contact interfaces with anthropomorphic end-effectors and polymeric solids found in robots and manipulators are intrinsically viscoelastic. It is therefore important to model such behavior and to study the effects of such time-dependent strain and stress on the stability and sustainability of grasping and manipulation. Various models have been proposed over the years to describe such behavior of time-dependent strain and stress. Furthermore, viscoelastic solids also display typically nonlinear elastic response. Built upon a variety of literature, a new and practical *latency model* is proposed in this chapter for the application of contact interface involving viscoelasticity in robotics. Latency model can describe various features of viscoelastic materials, such as stress relaxation, creep, and material clock. The theoretical modeling was supported by experiments in which we found two types of relaxation, depending on the loading and unloading of grasping or contact. One type is well documented in existing literature; but the other type has not been, to our best knowledge, presented before. The proposed theory can unify both types of time-dependent relaxation responses.

4.2 The Latency Model

The latency model we proposed here is a analytical model based on the movement of internal structure of material, as discussed in Section 4.1. It describes a latency of time and evolution of a transient response to sudden changes of external force or displacement in grasping. The external force, which can be measured in experiments, is the result of the normal stress on the contact surfaces. The internal strain and stress, however, will change as the density distribution inside the material changes in response to achieve an equilibrium state. The latency model tries to capture such temporal responses of relaxation or creep.

4.2.1 The Concept of Latency Model

The fundamental concept of latency model postulates that the density distribution is a function of time for viscoelastic material, and it is always moving toward the equilibrium state. The stress distribution will also vary with the density distribution, and macroscopically, results in the phenomenon of stress relaxation as the response of stress change on the contact surface.

This model is illustrated in Figure 4.1, which we assume the entire block as a uniform viscoelastic material starting at an equilibrium state. When an external force is applied, the latency model displays varied gaps of density distribution in the second plot in Figure 4.1 at the end of loading phase. The uneven distribution is a direct result of the *latency* with which the effect of external load has not been evenly propagated and developed to the central part of the material, and it results in the uneven stress distribution inside the material. At this moment, the maximum stress happens on the contact surface. There is a lag in

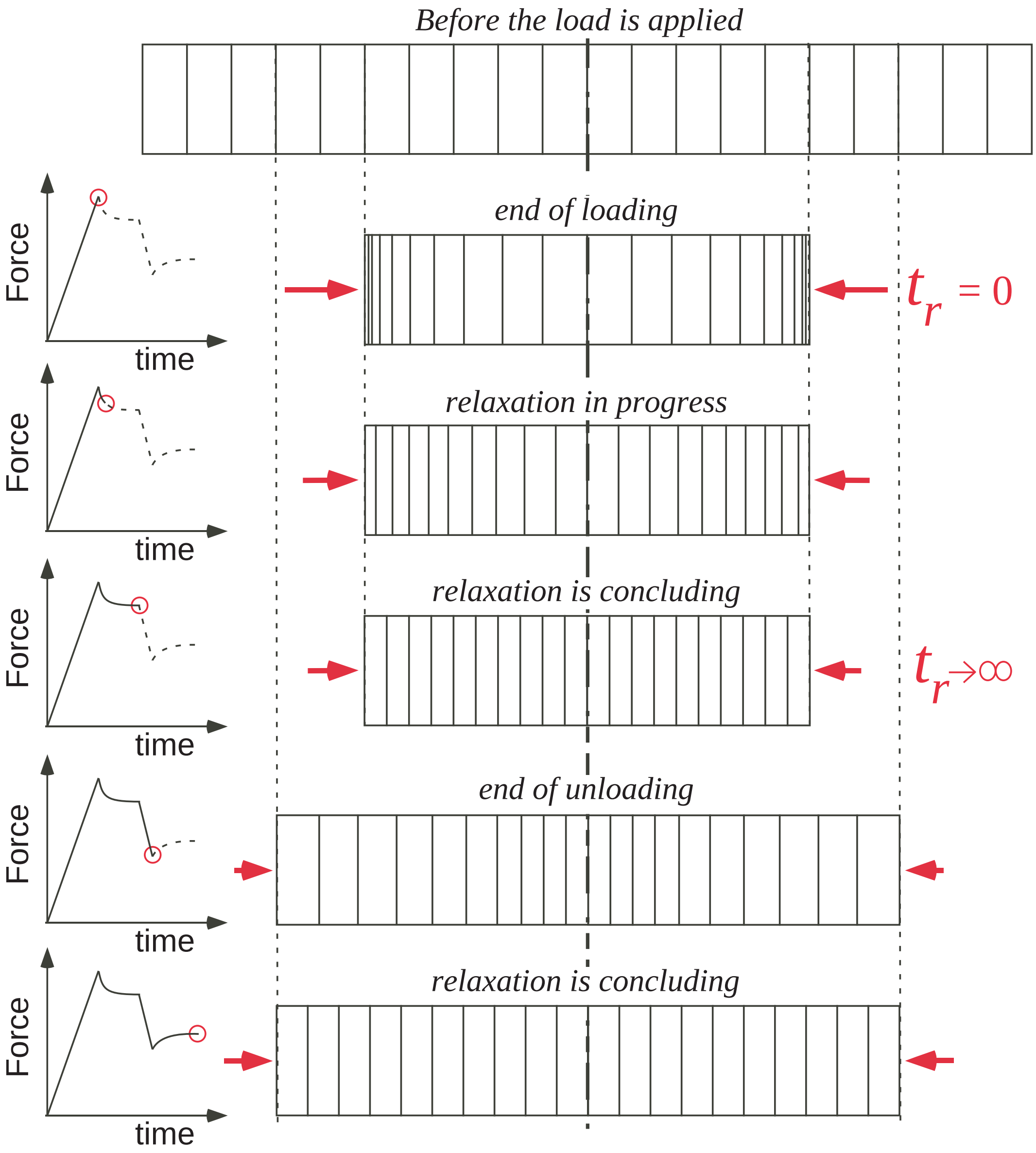

Figure 4.1: The latency model: **Loading:** The first subplot represents the density distribution before the external load is applied. The second subplot is the transient state when the external force is applied, with displacement held constant ($t_r = 0$). The relaxation phase after that is shown in subplots 3 and 4 when equilibrium is established ($t_r \to \infty$). **Unloading:** The displacement of the grasp is *partially* increased which causes another type of relaxation shown in subplots 5 and 6. *All:* The forces and their magnitudes are indicated with arrows of different lengths corresponding to their magnitudes. The force-time plots to the left of the figure indicate the state of the latency model with small circle.

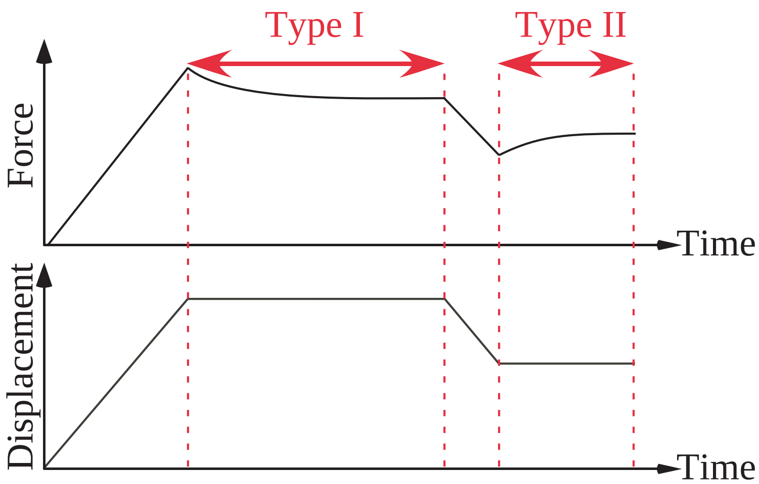

Figure 4.2: Type I and Type II relaxation curves in response to loading-holding and unloading-holding conditions, respectively.

the time-dependent response that causes subsequent redistribution via mechanisms of hole diffusion and/or chain of beads as discussed in Chapter 2. The external force is plotted with arrows acting at the contact interface with different magnitudes, based on the latency model. The corresponding force-time plot to the left of each state indicates the progression of force variation with a circle in the plot. When the relaxation is in progress from the third subplot to the fourth, the force decreases as the position is held constant in grasping. The relaxation phase will finally approach equilibrium when the density distribution asymptotically approaches uniform. At the fifth subplot, the displacement is increased with contact expanded. This *partial* unloading again causes transient response with uneven density distribution. As time progresses, the relaxation nature causes redistribution, which in turn causes the external force to increase.

It is important to notice these two types of relaxation based on whether it is loading-holding or unloading-holding. This is best illustrated in Figure 4.2, in which the displacement is controlled by the application of external force, as shown in the second half of the plot in Figure 4.2. First, the displacement is increased toward the grasped object, followed by holding the displacement at the maximum value until the “Type I” relaxation is asymptotically finished. The Type I relaxation is well-known and has been widely reported in the literature. This relaxation is characterized by an exponentially decaying time-dependent response, accompanied by a decrease in force while the displacement is held constant.

Next, the displacement is decreased partially and held. This unloading-holding phase causes the “Type II” relaxation. Instead of a decaying response in force, this relaxation is characterized by the increasing force while the displacement is held constant. This, to our best knowledge, has not been reported with a model.

The two types of relaxation represent the same physics, only with different initial condition and configuration of grasping. Conceptually, the latency model can explain the two different types of relaxation with an unified model. As a result, the latency model can capture both Type I and Type II relaxation satisfactorily.

4.2.2 The Analytical Latency Model

The latency model assumes that the stress is proportional to the strain; that is, $\sigma_c = \alpha \varepsilon_c$. The compressive normal force on the contact surfaces is $F_c = \sigma_c A$, which has the same magnitude as the grasp force, denoted as F. Because σ_c is a compressive stress, we can write the magnitude of the force

$$F = |F_c| = -\sigma_c A = -\alpha_c \varepsilon_c \tag{4.1}$$

where σ_c and ε_c are the compressive stress and strain at contact surface, respectively, A is the area of contact surface and $\alpha_c = \alpha A$ is the proportional constant for strain and applied force. Furthermore, the force function of viscoelastic materials is a combination of the elastic response, $N^{(e)}(\delta)$, and the temporal response, $g(t)$ [10]. The temporal function, $g(t)$, is an exponentially decaying function (the direction of decay depends on the type of relaxation). Thus, we have

$$F(\delta, t) = N^{(e)}(\delta) \cdot g(t) \tag{4.2}$$

with the temporal response being

$$g(t) = \sum_{i=0}^{n} c_i e^{-v_i t} \quad \text{with} \quad v_0 = 0 \quad \text{and} \quad \sum_{i=0}^{n} c_i = 1 \tag{4.3}$$

where c_i are the coefficients and ν_i are the exponents. It is noted that the elastic response, $N^{(e)}$, is a function of the displacement applied before the relaxation starts, and should remain constant thereafter. Thus, we can set $N^{(e)} = N_0$, the normal force at $t_r = 0$ before the relaxation starts, and simplify equation (4.2) as

$$F = N_0(c_0 + c_1 e^{-\nu_1 t}) \tag{4.4}$$

In equation (4.4), the exponential function is employed for $g(t)$ from equation (4.3) by taking $n = 1$ [10]. Substituting equation (4.1) into equation (4.4), we can derive

$$\varepsilon_c = -\frac{N_0}{\alpha_c}(c_0 + c_1 e^{-\nu_1 t}) \tag{4.5}$$

The strain rate of ε_c becomes

$$\dot{\varepsilon}_c = \frac{d}{dt}\varepsilon_c = \frac{\nu_1 N_0}{\alpha_c} c_1 e^{-\nu_1 t} \tag{4.6}$$

Finally, we substitute equation (4.6) into equation (4.5) to obtain

$$\dot{\varepsilon}_c = m\varepsilon_c + l \tag{4.7}$$

where $m = -\nu_1$ and $l = -(N_0 c_0 \nu_1)/(\alpha_c)$.

Figure 4.3 shows the result of equation (4.7). The trend of relaxation is always approaching the equilibrium state at the equilibrium strain, ε_e, with zero strain rate ($\dot{\varepsilon}_c = 0$) regardless of the type of relaxation. Moreover, we notice that Type I relaxation happens when the absolute value of the strain, ε_i, is greater than that of the equilibrium strain, ε_e. As a result, Type I relaxation stays above the equilibrium point on the horizontal axis and Type II stays below the horizontal axis.

Equation (4.7) can also be written as

$$\dot{\varepsilon}_c = -\nu_1(\varepsilon_c + \frac{N_0 c_0}{\alpha_c}) \tag{4.8}$$

When the strain rate $\dot{\varepsilon}_c$ in equation (4.8) becomes zero, the equilibrium is reached and the

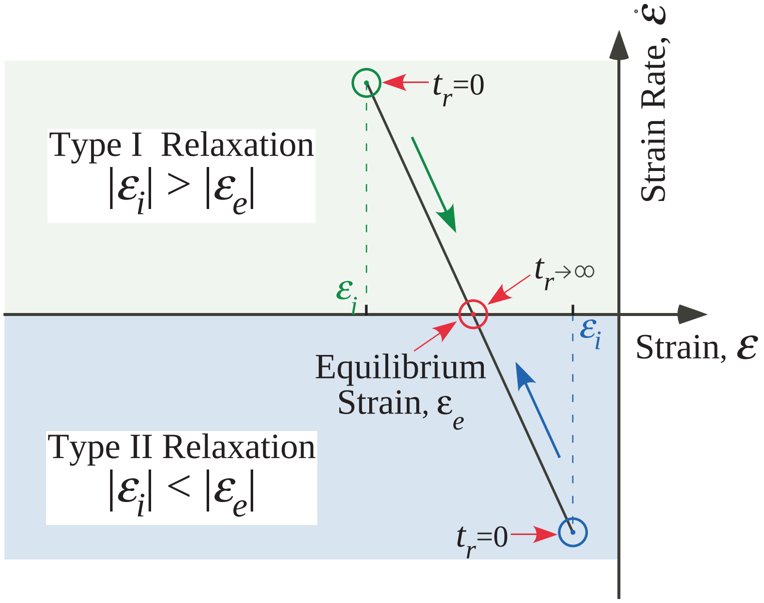

Figure 4.3: The relationship between the strain rate, $\dot{\varepsilon}$, and the strain, ε, during the relaxation phase. In this figure, ε_i is the strain on contact surface when $t_r = 0$, ε_e is the strain on contact surface in equilibrium state when $t_r \longrightarrow \infty$, and t_r is the relaxation time.

strain is equal to the equilibrium strain[1] . Therefore, we obtain

$$\dot{\varepsilon}_c = -\nu_1(\varepsilon_c - \varepsilon_e) \quad \& \quad \varepsilon_e = -\frac{N_0 c_0}{\alpha_c} \tag{4.9}$$

Equation (4.6) can be employed to obtain the time as a function of strain rate or strain on contact surface, as follows

$$t = \frac{1}{\nu_1} \ln \frac{N_0 c_1 \nu_1}{\alpha_c \dot{\varepsilon}_c} = \frac{1}{\nu_1} \ln \frac{N_0 c_1}{-\varepsilon_c \alpha_c - N_0 c_0} \tag{4.10}$$

4.2.3 Computational Simulation of the Latency Model by Finite Element Method (FEM)

The analytical latency model described in Sections 4.2.1 and 4.2.2 is a continuous model with varying density/strain distribution. The continuous latency model can be implemented in numerical simulations using discrete elements. For the purpose of discretization for simulation, we divide the material into n nodes with equal spaces between each other, similar to the first subplot in Figure 4.1 ($2n$ nodes).

The parameters ν_1 in equation (4.9) is constant for homogeneous material. The ε_e is determined by N_0. Thus, we can write for each node represented in the latency model

$$\dot{\varepsilon}_i = -\nu_1(\varepsilon_i - \varepsilon_e) \quad i = 2, \cdots, n \tag{4.11}$$

Equations (4.9) and (4.11) constitute the evolution of the distance between the nodes based on the latency model.

The simulation was implemented using the displacement control in Figure 4.4(b), similar to that in experiments. The nodes inside the material will react to the change of displacement based on equation (4.11). The *step-by-step algorithm* is: (*i*) Calculate the equilibrium strain, ε_e, base on the contact displacement; (*ii*) Substitute ε_e and ε_i into equation (4.11) to obtain the strain rate, $\dot{\varepsilon}_i$, of ith node; (*iii*) Displace the ith node based on the

---

[1] The equilibrium strain can also be obtained from equation (4.4) and (4.1) by assuming $t \to 0$. The same result for the equilibrium strain, $\varepsilon_e = -N_0 c_0/\alpha_c$, can be obtained.

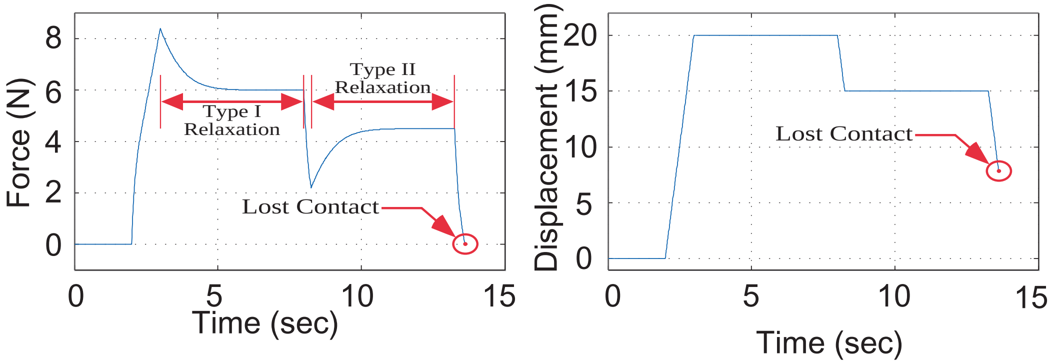

Figure 4.4: The results of simulation using the latency model by implementing the formulation in Section 4.2.2.

obtained strain rate, $\dot{\varepsilon}_i$; (*iv*) Go back to step (*i*) and perform the calculation on the $(i+1)$th node recursively until the last node, $i = n-1$ is reached.

Figure 4.4 shows the results of a simulation. The prescribed displacement sequence is in the right half of Figure 4.4(b). The left half of Figure 4.4(a) shows the contact force. Both Type I and Type II relaxations are seen in Figure 4.4(a).

4.3 Experimental Validation

Experiments were conducted to validate the proposed latency model. The experiments are designed to resemble the loading-holding-unloading presented in Section 4.2. In the following sections, the experimental setup will be discussed, followed by the presentation of experimental results.

4.3.1 Experimental Setup

The experiments were conducted using a tensile testing machine with a pair of parallel flat fixtures pressing upon the object, as shown in Figure 4.5. Since the system is identical to a parallel-jaw gripper, it will be referred to as such in this chapter. The load cell has a range of $2\,kN$ force with an accuracy of $0.2\,N$ and high repeatability. The displacement measurements have an accuracy of $10^{-3}\,mm$. Multiple experiments with varying loading rates, stationary and relaxation phase, and unloading phase were conducted. The parameters of the experiments are tabulated in Figure 4.5.

The inertia of the fixture is compensated by the design of the equipment in order to minimize the effect of force measurement due to acceleration or deceleration. Calibration experiments were conducted to measure the inertia force without contact to identify the amount of inertia force due to the fixture alone. The results indicate a maximum of $0.35N$ of inertia force (within the range of acceleration and deceleration used in the experiments) measured by the load cell, which is only slightly larger than the accuracy of the load cell. Based on the parameters used in the experiments, we conclude that the inertia effect is less than 1% of the typical range of forces; therefore, it is negligible.

The material of the grasped object is a soft silicone solid. The silicone solid is made of silicon powder by mixing the composition of 50% silicone powder with 50% thinner. The silicone is then cured for 48 hours after mixing.

4.3.2 Experimental Validation of the Latency Model

Experiments were conducted using the equipment shown in Figure 4.5 to compress a parallelepiped silicone material with a size of $61 \times 43 \times 22\,mm$. The video clip of the compress-and-hold experiments is submitted with this chapter. Six still photo frames of this video are extracted and illustrated in Figure 4.6 to show the correlation to the proposed latency model in Figure 4.1. The first part of the video clip shows the setup. The second part shows the relaxation with accelerated frame speed to see the movement of the line due to relaxation.

Figure 4.7 shows the profile of force measured by the load cell when the distance between the contact surfaces is held at constant. It is clear that the recorded force, when the relaxation starts, decreases and the gap widens (*cf.* Figure 4.6) as predicted by the latency model. This is an effective validation of the proposed latency model for viscoelastic materials.

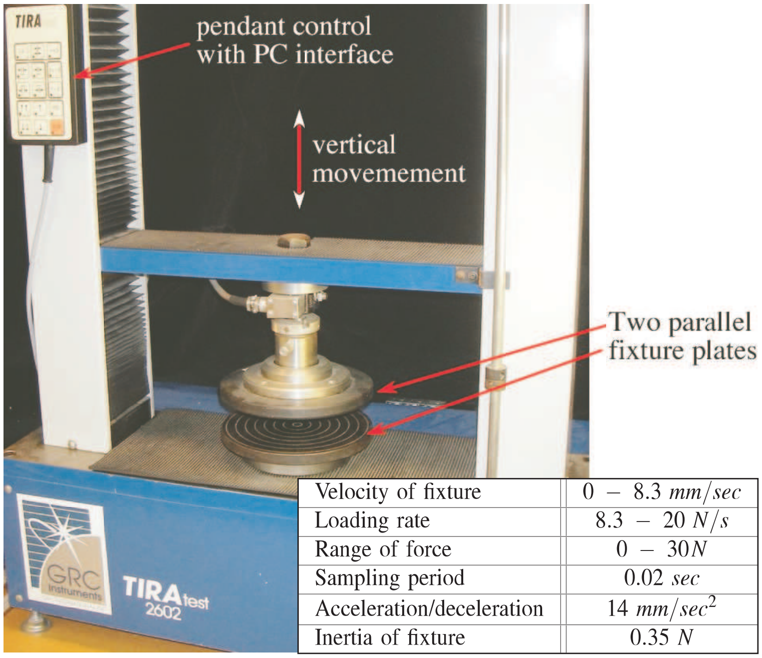

Velocity of fixture	$0 - 8.3\ mm/sec$
Loading rate	$8.3 - 20\ N/s$
Range of force	$0 - 30N$
Sampling period	$0.02\ sec$
Acceleration/deceleration	$14\ mm/sec^2$
Inertia of fixture	$0.35\ N$

Figure 4.5: The experimental setup on a tensile testing machine with a pair of parallel flat fixture plates.

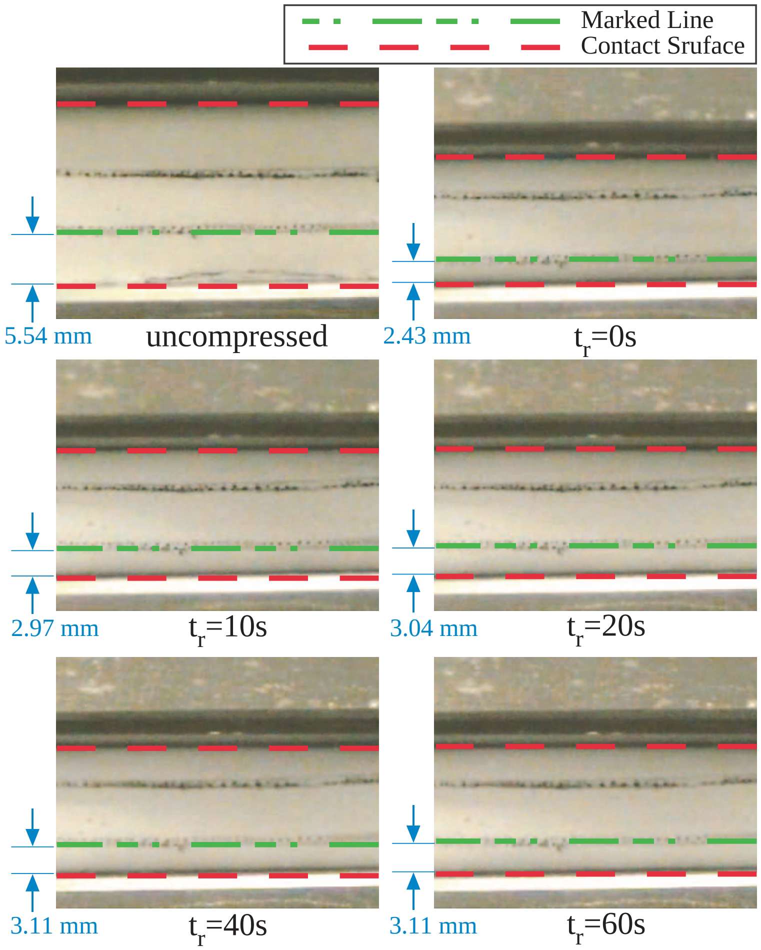

Figure 4.6: Still photos from the video of experiments conducted by compressing the silicone block and hold. The first still photo is when the material was not compressed at the beginning of the experiment. The two contact surfaces were shown in the photos. Marker lines were labeled on the block to show the movement of lines. The block was compressed to maximum displacement in the next still photo at $t_r = 0s$ with a distance between the two bottom lines being $2.43\,mm$. At this point, the fixtures maintain their positions, holding the total distance between the contact surfaces the same. The next four still photos show the widening of the distance between the two marker lines from $2.43\,mm$ at $t_r = 0s$ to $2.97\,mm$ at $t_r = 10s$ to $3.04\,mm$ at $t_r = 20s$ to $3.11\,mm$ at $t_r = 40s$, and asymptotically approaches $3.11\,mm$ at $t_r = 60s$. The video clip accompanying this chapter shows this relaxation and evolution clearly.

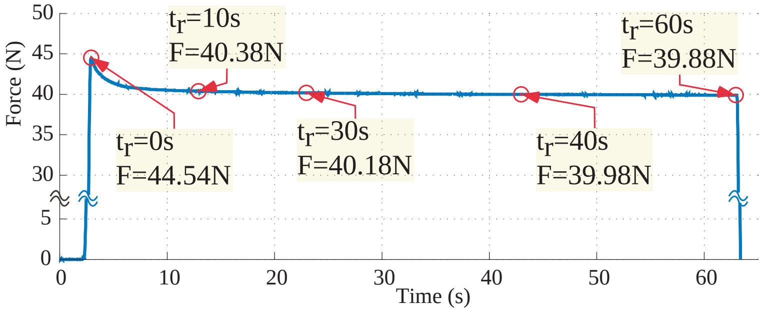

Figure 4.7: The experimental data corresponding to Figure 4.6. The evolution of force as the relaxation was taking place even though the total distance between fixtures is held the same, the silicone undergoes the changes described in the latency model presented in Figure 4.1.

4.3.3 Experimental Results about Type I and II Relaxation

To observe Type I and Type II relaxations, repeated loading and partial unloading were applied. In the experiments, a rubber ball was used as the test specimen. The results of force due to the prescribed displacements are shown in Figures 4.8, depending on loading or unloading.

It is noted that Type I relaxation occurs when the object is held at constant displacement after a loading stage with increasing force and displacement. This is illustrated by the exponentially decaying force in the upper-left plot of Figure 4.8. In addition, this is represented in the right plot of Figure 4.8 as corresponding to the vertical lines moving downward with the same displacement but decreasing forces at constant displacement of $20\,mm$.

On the other hand, Type II relaxation occurs when the displacement is held constant after an unloading phase. This is shown by the increasing force in the upper-left plot of Figure 4.8, and also represented in the right plot of Figure 4.8 as corresponding to the vertical lines moving upward with the same displacement but increasing forces at constant displacement of $15\,mm$.

Figure 4.9 shows the progression of the sequence of the experiment from 1 to 14, corresponding to each change of force/displacement in Figure 4.8.

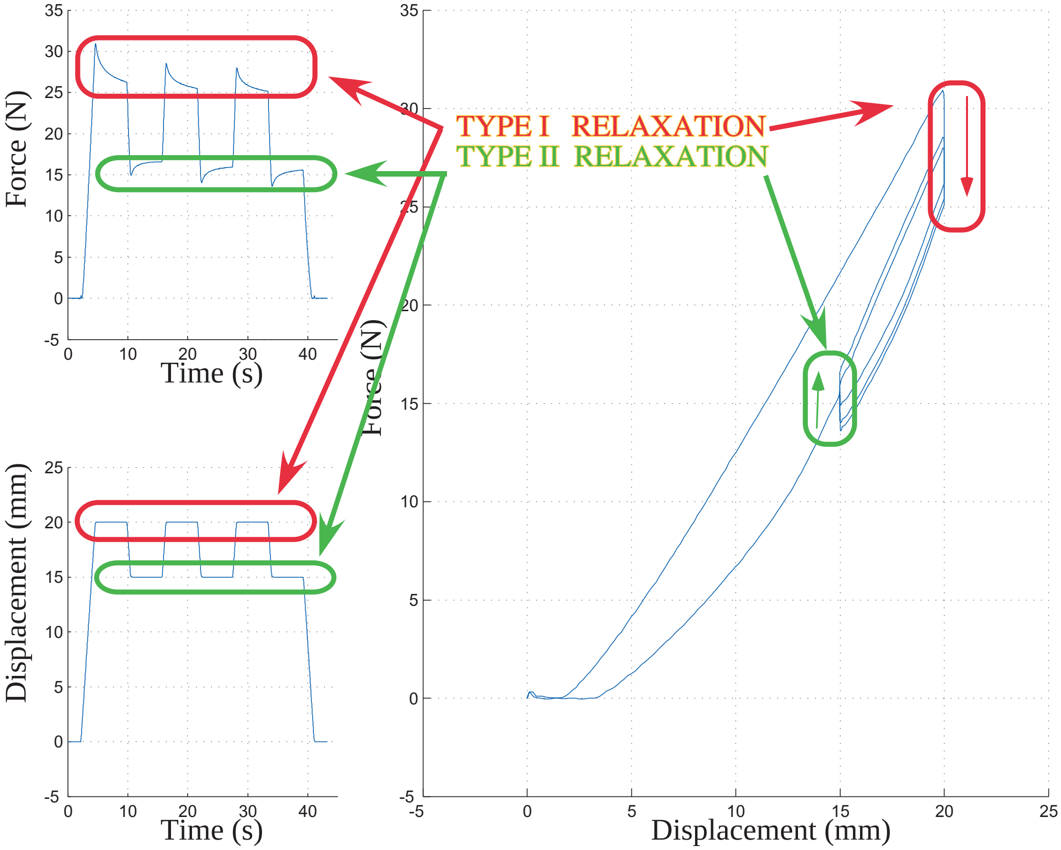

Figure 4.8: Experimental results illustrating Type I and Type II relaxation under repeated loading and unloading.

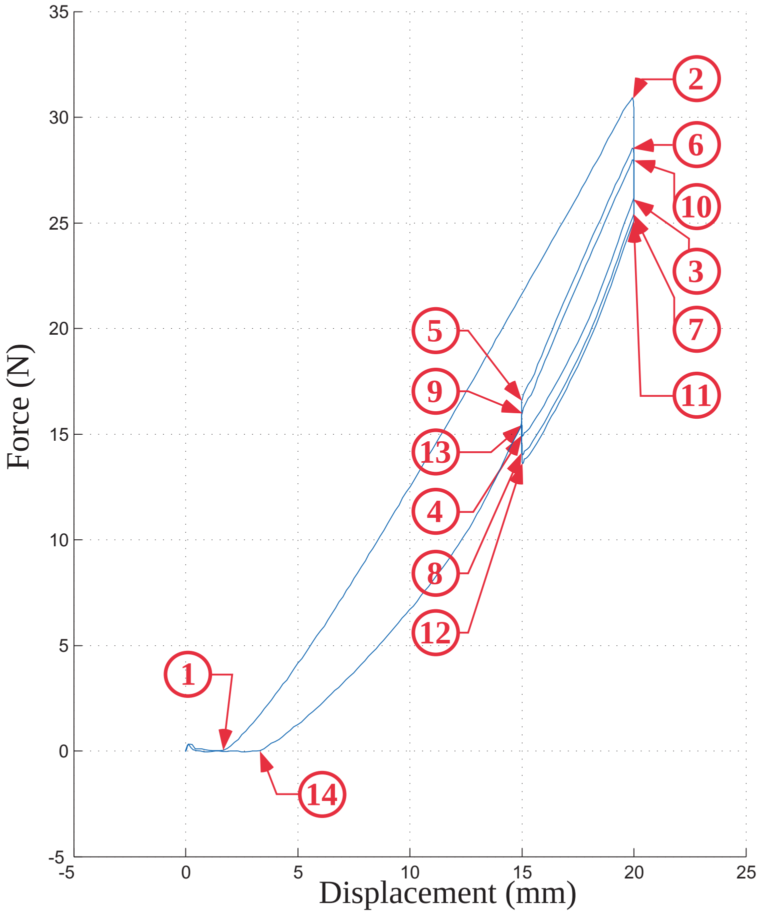

Figure 4.9: The time sequence of force-displacement relation shown in Figure 4.8.

4.4 Discussions

4.4.1 Computational Simulation

The simulation which implements the latency model in Figure 4.4 assumes that the strain rate is a function of the strain , as in equation (4.7). In other words, the strain rate will be higher when the current state is far from the equilibrium state than the state which is almost in equilibrium. We also assume that the stress is proportional to strain.

4.4.2 Solid Model

The stresses from the contact surface to the center of material decrease due to the inertial force of each mass as well as latency in hole diffusion [20]. When relaxation progresses, these different stresses start to become equal to each other via redistribution of strain between masses, accompanied by energy dissipation. These effects were captured by the modified Fung's model with formulation presented in Section 4.2.2.

4.4.3 Potential Energy

Type II relaxation is not commonly seen in the literature. However, it is reasonable when we consider potential energy of Type II relaxation process. When Type II relaxation is accompanied by an increase in force, as shown by the smaller counterclockwise loop in the left plot of Figure 4.10, the net energy dissipation is positive—which is consistent with physical systems. If Type II relaxation were to cause the force to decrease like Type I relaxation, then it will result in a clockwise loop of negative energy dissipation—which violates the physics.

4.5 Summary

In this chapter, we presented a latency model to describe the time-dependent behavior of viscoelastic materials commonly found in robotic contact interface or grasped objects.

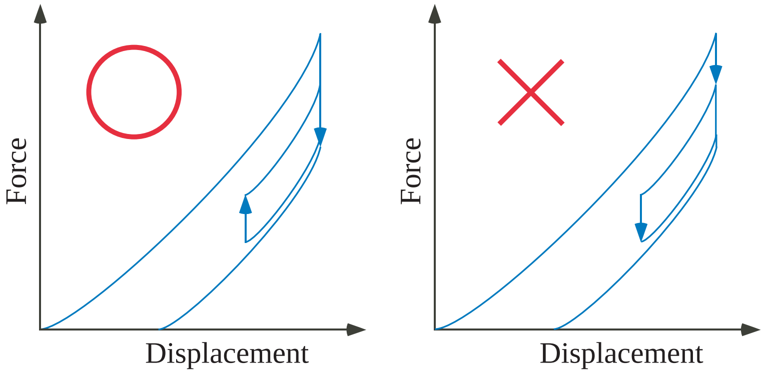

Figure 4.10: The direction of Type II relaxation in the force-displacement plot, showing the loop tracing the relaxation.

Implementation of the latency model with computer simulation as well as experimental results were presented. They are found to match with each other well. Video clip from experiments clearly depicts the relaxation response as an exponential function of time. The Type I and Type II relaxation behaviors are represented by the exponentially changing force when the displacement is held constant in grasping. Type I is well documented in literature; whereas, Type II relaxation has not been discussed previously. The physical significance of Type II relaxation (with increased force during relaxation) was discussed in relation to Type I. The latency model unifies both types of relaxation in a model with analytical formulation which can be utilized for modeling and simulation.

Chapter 5

EXPERIMENTAL STUDY AND MODELING OF LOADING AND UNLOADING OF NONLINEAR VISCOELASTIC CONTACTS

The latency model is an analytical model for describing the behavior of nonlinear viscoelastic contact interface in robotic grasping and manipulation. The latency model is based on experimental observation of viscoelastic materials which exhibit the behavior of both elastic and temporal responses when subject to external force or displacement. It is postulated that such materials display latency in response of external influence by the rearrangement of molecules, holes, and structures in order to achieve an equilibrium state corresponding to the instantaneous loading. As a result, we propose that there are temporal *latent activities* in progress before the material reaches the equilibrium state. In the previous study [2], the latent activity of strain re-distribution with a prescribed constant displacement was presented using both theoretical modeling and experimental results. In this chapter, we build upon this latency model to study the behavior of viscoelastic materials under different loading rates with experimental results. The latency model is employed to explain the behavior of responses of hard and soft viscoelastic materials typically found in robotic contact and grasping.

5.1 Introduction

This chapter builds upon the study of the latency model proposed in [2] to investigate the behaviors of grasping response observed in viscoelastic materials. The concept of “latency” refers to the latent activities in progress, while the state of viscoelastic material remains the same macroscopically (*e.g.* displacement or force remains the same after loading or unloading). In [2], the latent activity of strain re-distribution was studied based on experimental results when the displacement is held constant in a grasping task.

In this chapter, the strain hardening effect (or *stiffening effect*) is correlated with the latent activity postulated in the latency model, as observed from the experimental results. Furthermore, Gardel concluded that the stiffening effect is directly related to the concentration of cross-link structure [42], which can also correlate with the idea of uneven strain distribution in the latency model. The strain hardening effect in contact interface can complement the previously proposed latency model to explain the observed behavior under different loading/unloading rates presented with the experimental studies in this chapter.

5.2 The Latency Model for Viscoelastic Contact Interface

The latency model is an analytical model for describing the nonlinear contact behavior of viscoelastic materials based on experimental observation. In the latency model, we postulate that the strain distribution within the viscoelastic material is a function of time. When a viscoelastic material is subject to external displacement, the unevenly distributed strain, from the immediate contact interface inward to core of the material, will result in an uneven stress distribution; consequently, a change of contact force on the contact surface will happen [2]. Re-arrangement and re-distribution of the transient state will ensue until an equilibrium state is achieved. When the displacement of the deformed object is held constant, the force will decrease exponentially as a result of the re-arrangement. This is commonly known as the *relaxation* response. Likewise, when the external force deforming the subject is held constant, the rearrangement will occur with a tendency to reach towards the equilibrium, resulting in the exponential change of displacement. This is known as the *creep* response. In [2], the latent activity of strain distribution when subject to a constant displacement was investigated.

Tsai and Kao applied the modified Fung's model to formulate the latency model to study the strain rate when a viscoelastic contact is subject to a constant displacement after the loading is completed, as follows [2]

$$\dot{\varepsilon}_c = m\varepsilon_c + l = -v_1(\varepsilon_c + \varepsilon_0) = -v_1(\varepsilon_c + \frac{N_0 c_0}{\alpha_c}) \tag{5.1}$$

or

$$\dot{\varepsilon}_c = -v_1(\varepsilon_c + \frac{N_0(1-c_1)}{\alpha_c}) \tag{5.2}$$

where $m = -v_1$, $l = -(N_0 c_0 v_1)/\alpha_c$, $\dot{\varepsilon}_c$ and ε_c are the strain rate and strain of material on the contact interface, ε_o is the equilibrium strain for a given displacement, N_0 is the initial elastic response (force) due to the constant displacement after loading, and c_0, v_1, α_c are constant coefficients pertaining to the materials and their properties. The coefficients are defined in the following equation [2, 9, 10, 11]

$$F(t) = N_0(c_0 + c_1 e^{-v_1 t}) \quad \text{with} \quad c_0 + c_1 = 1 \tag{5.3}$$

In this chapter, we study the force response based on different loading/unloading rates. The specific stiffness, k_s, in the chapter is defined as

$$k_s = \frac{\partial\sigma}{\partial\varepsilon} \tag{5.4}$$

where σ and ε are the stress and strain, respectively.

5.3 Experiment and Analysis

In this section, we present the experimental setup first, followed by the experimental results and analysis.

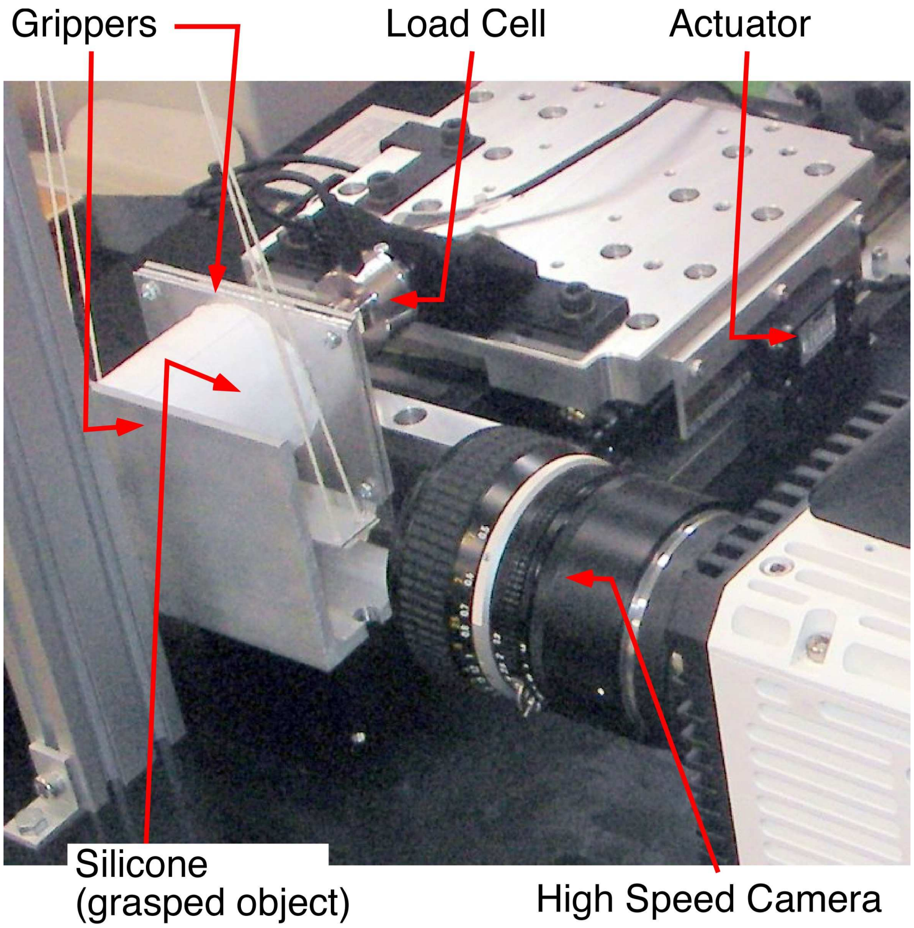

Figure 5.1: Experimental setup for the compressive loading and unloading tests, showing the parallel-jaw gripper, camera, and ancillary devices

Table 5.1: composition of the silicone used in the experiments

	silicone powder	thinner
hard silicone	90%	10%
soft silicone	50%	50%

5.3.1 Experimental setup

Figure 5.1 illustrates the experimental setup of a robotic parallel-jaw gripper and high-speed video camera. A grasped object is shown between the two gripper surfaces. The force of grasping is measured by the load cell mounted on the gripper that has an accuracy of $0.25N$. The accuracy of displacement of the system is $1\mu m$.

The mass of the gripper mounted on the load cell is $14g$, which moves with an acceleration up to $5000\,mm/s^2$ in all the experiments performed in this chapter. The grasped object has much smaller movement and thus its inertial effect is neglected. As a result, we can estimate the maximum amount of inertial force to be about $0.07\,N$ (during the ramp-up and ramp-down periods). This is much smaller than the accuracy level of the force sensor. The actual profile of motion, measured inertial force, and the estimated inertial force are shown in Figure 5.2. By comparing the data of force with the gripper moving at the highest loading rate versus that of stationary gripper, the same conclusion is also reached. That is, the inertial effect due to the acceleration at the loading or unloading in this experimental setup can indeed be neglected.

Two different silicone solids with “hard” and “soft” texture are fabricated for the experimental study, as shown in Figure 5.3. Both cylindrical silicones are 25mm in radius and 30mm in height with the compositions listed in Table 5.1.

Figure 5.4 shows a schematic of the experimental setup in Figure 5.1 with the grasped silicone solid and the fiducial marks, parallel-jaw gripper, and the camera.

The procedures of the various experiments conducted under different loading rates are enumerated in the following.

(1) The gripper is moved to barely touch the surface of the silicone solid.

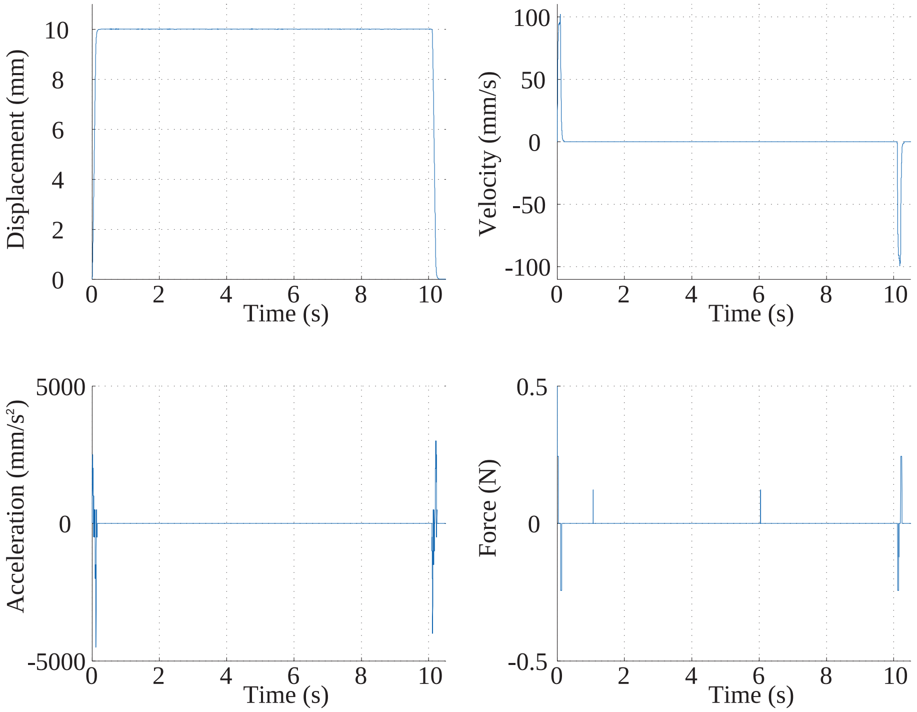

Figure 5.2: The profiles of motion of the gripper from which the acceleration is determined to judge the inertial effect of gripper in experiments. The bottom right plot shows the measured inertial force from the load cell.

Figure 5.3: The left and right cylindrical specimens are "hard" and "soft" silicone, respectively. The dimensions of both specimens are 25 *mm* in radius and 30 *mm* in height.

The silicone solid is supported freely by strings so that it will not fall due to gravity, but with least amount of interference to grasping.

(2) The loading process will begin based on a loading rate determined *a priori* by the amount of prescribed displacement and the duration of holding (for relaxation). Several loading rates are employed as follows: 20, 40, 60, 80, and $100\,mm/sec$.

(3) After the loading-and-hold procedure, the gripper unloads to break contacts, as shown in Figures 5.6 and 5.7.

The measurements of force and displacement, as well as the video camera capture are stored for further analysis.

5.3.2 Experimental results and analysis

5.3.2.1 Evidence of latency in relaxation

Figure 5.4 shows two still photo frames captured during holding after the loading phase is completed, to demonstrate the effect of relaxation. The first frame was captured when the loading process ended, followed by the beginning of the holding process at $t_r = 0\,sec$. The second fame was captured $5\,sec$ after holding at $t_r = 5\,sec$. We can clearly observe in Figure 5.4 the change of positions of the fiducial marks during the elapsed time. Hence, we use this as evidence of ongoing rearranging activities, so called "latent activities", during holding (constant displacement of compression). The position change follows an exponential function of time [2].

5.3.2.2 Elastic and temporal responses

Corresponding to the captured video, we can plot the results of force versus time, as well as the displacement versus time. These plots are shown in the two left plots in

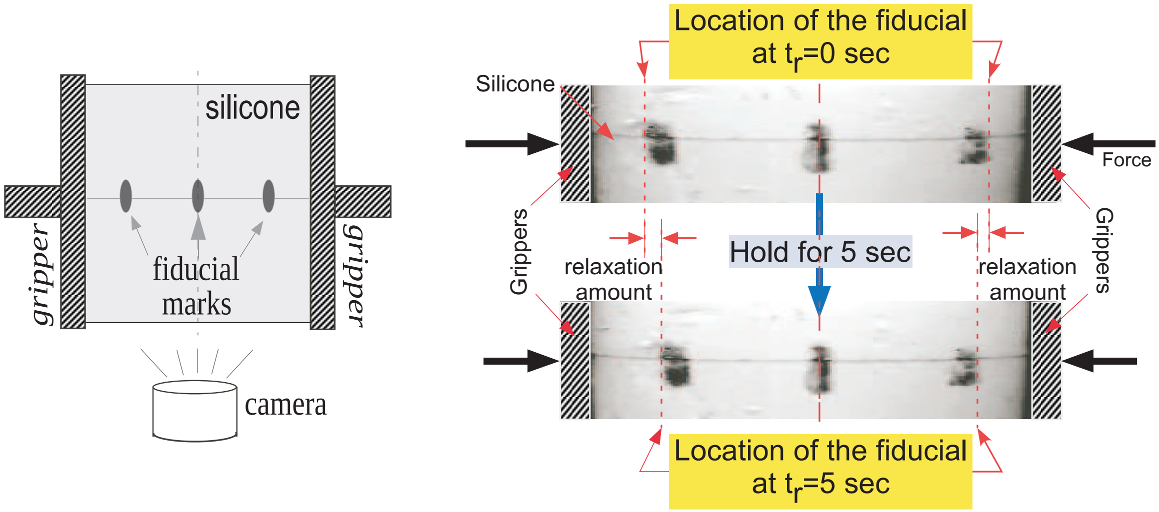

Figure 5.4: *Left*: The schematic of the grippers, camera and silicone object. *Right*: Still photos in grasping from the experiment showing the relation and movement of the fiducial marks on the surface of the silicone solid, with the displacement being held at constant for 5 seconds.

Figure 5.5. The response of force versus displacement is plotted in the right of Figure 5.5, showing the history of force as a result of prescribed displacement profile.

5.3.2.3 Loading phase under different loading rates

Figures 5.6 and 5.7 show, for soft and hard silicone solids, respectively, the force measured under different loading rates, subject to a prescribed displacement controlled sequence.

The viscoelastic materials share similar properties with elastic materials. First of all, the specific stiffness (defined by $\partial\sigma/\partial\varepsilon$ in equation 5.4) is different between soft and hard silicone solids in Figures 5.6 and 5.7. With the same amount of compression, the hard silicone shows higher specific stiffness and results in higher compression force.

Different properties are observed in Figures 5.8 and 5.9 which show the zoom-in views of forces, focusing on the end of loading phase in Figures 5.6 and 5.7, respectively. We found that the maximum compressive forces of soft silicone due to different loading rates are different, with higher loading rate producing higher maximum compressive force, as shown in Figure 5.8. On the other hand, the maximum compressive forces of the hard silicone due to different loading rates are nearly the same, as shown in Figure 5.9.

5.3.2.4 Holding phase under different loading rates

Next, let us focus on the end of holding phase shown in Figures 5.10 and 5.11. It appears that the asymptotic values of relaxation curves under different loading rates are the same for both hard and soft silicone, although the responses start with different initial values as shown in Figures 5.8 and 5.9. This suggests that the equilibrium state (i.e., the asymptotic value of relaxation) is related to the held displacement, but not dependent upon the loading rates. In other words, the asymptotic value is a path-independent property for viscoelastic material with a constant displacement.

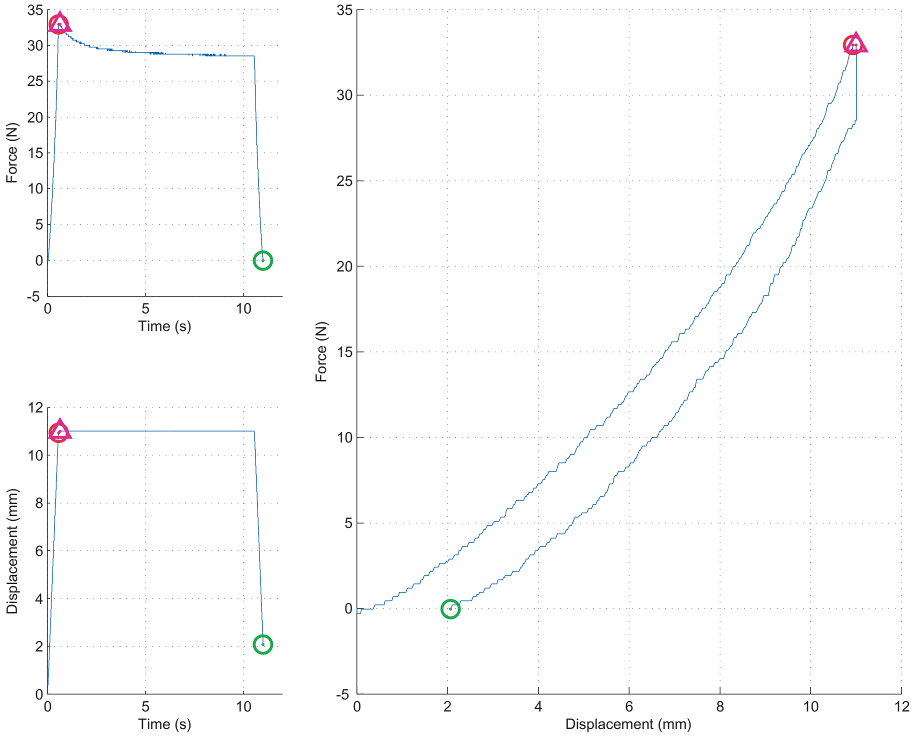

Figure 5.5: The experimental result: (top-left) the force as a function of time, (bottom-left) the prescribed displacement curve, and (right) the force vs. displacement. Data are plotted corresponding to the experimental results obtained from Figure 5.4.

Table 5.2: The material property of the specimen

	v_1 Equation (5.1)	$k_s(N/m^2)$ Specific Stiffness	ν Poisson Ratio
hard silicone	0.695	1.221×10^5	0.48
soft silicone	0.493	3.497×10^4	0.48

5.4 Discussions

5.4.1 Loading rates and the latency model

From the perspective of the latency model, the reaction force on a gripper is proportional to the stress on the contact surface. When the loading rate is high, the magnitude of strain on the contact surface will be high. The result of different maximum force in Figure 5.8 is due to the different loading process. When the loading rate is high, it does not allow the material enough time to re-distribute, and thus the build-up of force away from the equilibrium state is larger. The equilibrium state corresponds to the asymptotic state of the relaxation process. However, in the case of the hard silicone the maximum force of the higher loading rate is only slightly larger than that of the lower loading rate.

To apply the latency model to the experimental results, we first convert the measured force into stress on the contact surface, $\sigma = F/A_n$. Next, the strain is obtained using equation (5.4) at the steady-state (asymptotic) values with $\varepsilon = k_s \sigma$. The following derivation renders the nominal contact area with different loading displacements. The variables are corresponding to Figure 5.12 where A is the original contact area, ΔA is the change of contact area due to the Poisson effect, ν is the Poisson ratio which is 0.48 from the specification of the silicone, and d, Δd, l, and Δl are geometric parameters. We have

$$A + \Delta A = \frac{\pi}{4}(d + \Delta d)^2 = \frac{\pi d^2}{4}\left(1 - \frac{\nu \Delta l}{l}\right)^2 \tag{5.5}$$

The specific stiffness obtained from the asymptotic values at the end of loading is

$$k_s = \frac{\sigma_{asym}}{\varepsilon_{asym}} = \frac{F_{asym}/A_n}{\varepsilon_{asym}} \tag{5.6}$$

where σ_{asym} and ε_{asym} are the asymptotic values of stress and strain on the contact surface, F_{asym} and A_n are the corresponding force measured by load cell and nominal contact area. The specific stiffness is a constant where the steady-state temporal response is established asymptotically. The properties of the silicone specimen are listed in Table 5.2

Following the steps above, we can obtain the strain at every moment during grasping by the following equation:

$$\varepsilon = \frac{\sigma}{k_s} = \frac{F/A_n}{k_s} \tag{5.7}$$

where σ is the stress on the contact surface, k_s is the specific stiffness of the material, F is the force measured by the load cell on the gripper, and A_n is the nominal contact area. Based on the conclusion of [12], the exponent of force relaxation curve will be consistent for the same material. Thus, we can obtain v_1 by applying curve fitting to the relaxation curves in the form of equation (5.3). Consequently, we found $v_{1(soft)} = 0.493$ for the soft silicone and $v_{1(hard)} = 0.695$ for the hard silicone, listed in Table 5.2.

The latency model shown in equation (5.1) still requires the equilibrium strain, ε_o. We note that the material will be uniformly distributed at the final equilibrium state. Therefore, the equilibrium strain is

$$\varepsilon_o = \frac{\Delta l}{l} \tag{5.8}$$

where ε_o is the strain at equilibrium state, Δl is the compression displacement, and l is the initial length of the material.

Now we can substitute the values from the experimental results into equation (5.1) and obtain the strain rate, $\dot{\varepsilon}_c$, during the operation. Figures 5.13 and 5.14 show the results of the analysis at the end of loading phase and during the relaxation, respectively. (For the convenience of reading, we plot the compression strain as positive in the figures which originally is negative.) Since the loading rate of the grippers is much faster than the strain rate inside the material, it results in larger strain on the contact surface than the equilibrium strain at the loading phase (the first plots in Figure 5.13). The second plot is the internal strain rate of material obtained from the latency model in equation (5.1).

This phenomenon is consistent with the latency model that utilizes the re-arrangement and re-distribution of structures and molecules in order to achieve a new equilibrium based on the external force or displacement.

5.4.2 Asymptotic value of relaxation and the latency model

The asymptotic value of relaxation curves is found to be the same, and depends on the material and the total external force. If the same external force is applied to a viscoelastic object, the equilibrium state will be the same when the time approaches infinity, regardless of the loading rate. This also suggests that the strain/stress distribution will be uniform for any isotropic material.

In Figure 5.14, the analysis of relaxation phase is shown. The first plot shows that the actual strain (blue curve) on the contact surface initially is greater than the equilibrium strain (red curve). However, the strain on the contact surface will eventually reach the equilibrium value. Thus, the results match with the prediction of the latency model very well.

The existence of the asymptotic value is predicted by the latency model in that the localized strained states will return to its equilibrium state when the disturbance is removed with the change of strain given in equation (5.1).

5.4.3 Strain stiffening/hardening and the latency model

Strain stiffening, a well-known phenomenon, delineates the increase of stiffness at the contact interface when an external force is applied. Instead of considering the stiffening effect being due to the change of the material property called *stiffness*, the latency model provides an alternative explanation of the effect in the sense of uneven strain distribution inside the viscoelastic material. Because the strain propagation inside viscoelastic material is slower than the loading rate applied by the external force, as presented in the preceding experimental results, an uneven strain distribution will be created. To this end, a higher loading rate will result in a more uneven strain distribution. A comparison of material movement between a high and a low loading rate is illustrated in Figure 5.15. We notice that at the end of loading, the strain on the contact surface (yellow shade area) will be higher at the high loading rate than low loading rate, resulting in the difference of reaction forces for the same amount of displacement compression. This is known as the strain stiffening effect. When time is allowed for the uneven strains to propagate and reach a new equilibrium state, the asymptotic reaction force will then become the same again. This has been presented experimentally in this chapter, as illustrated in (III) in Figure 5.15.

5.5 Summary

In this chapter, we present the results of experimental studies and modeling of the latency model as applied to the loading and unloading of viscoelastic materials in contact. We found that the latency model is consistent with the well-known strain stiffening/hardening effect. From the perspective of the latency model, this effect can be explained by the uneven strain distribution inside the material. We also deduce from the experimental results that there is an asymptotic equilibrium state of the viscoelastic material when subject to external force or displacement. It depends on the property of the material and the external force or displacement applied, but not on the loading rate. The latency model can be applied to explain the experimental results of relaxation observed in a displacement-controlled grasping task.

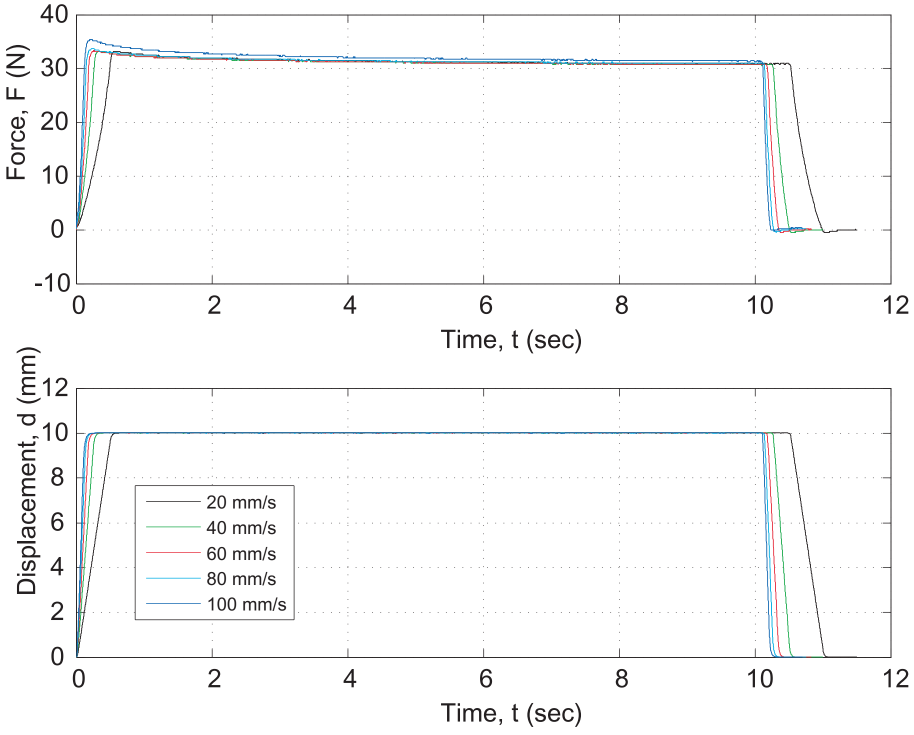

Figure 5.6: The loading-holding-unloading process on soft silicone.

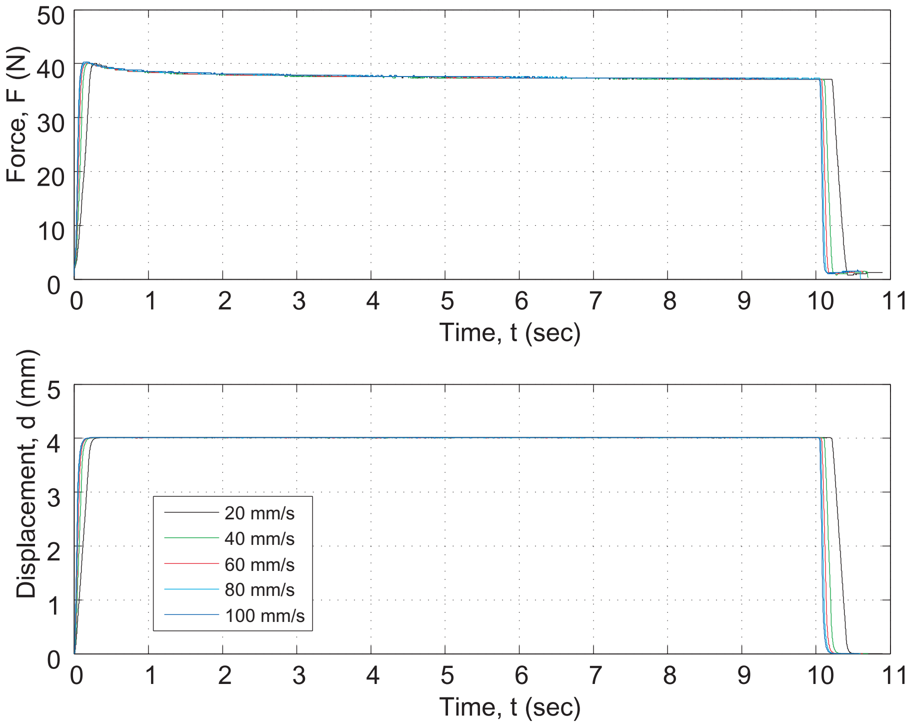

Figure 5.7: The loading-holding-unloading process on hard silicone.

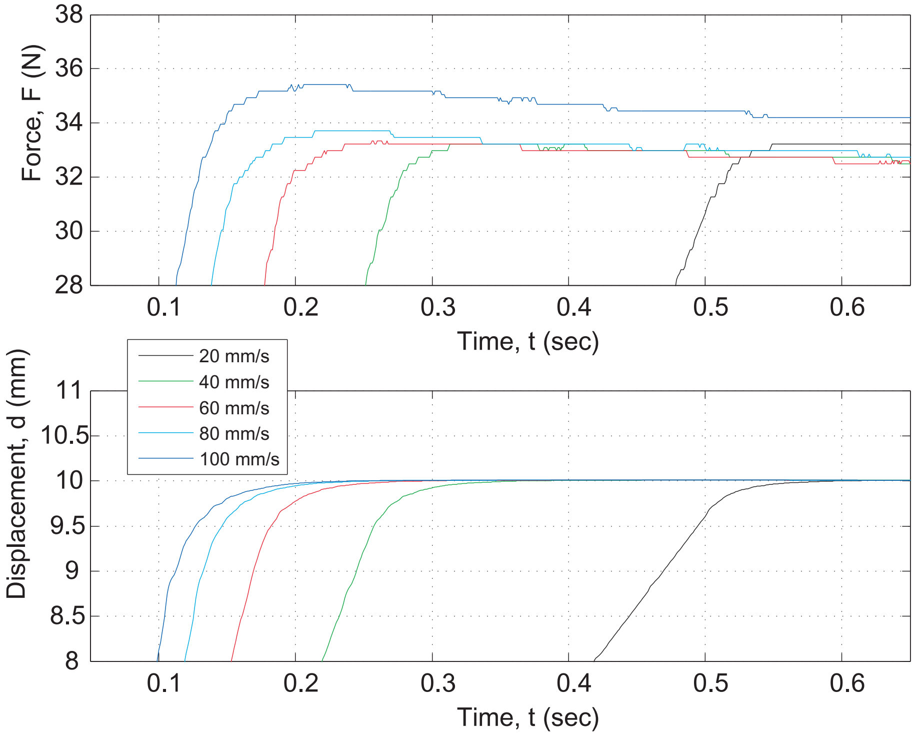

Figure 5.8: The zoom-in views of the force and displacement curves towards the end of the loading phase in Figure 5.6 for the soft silicone.

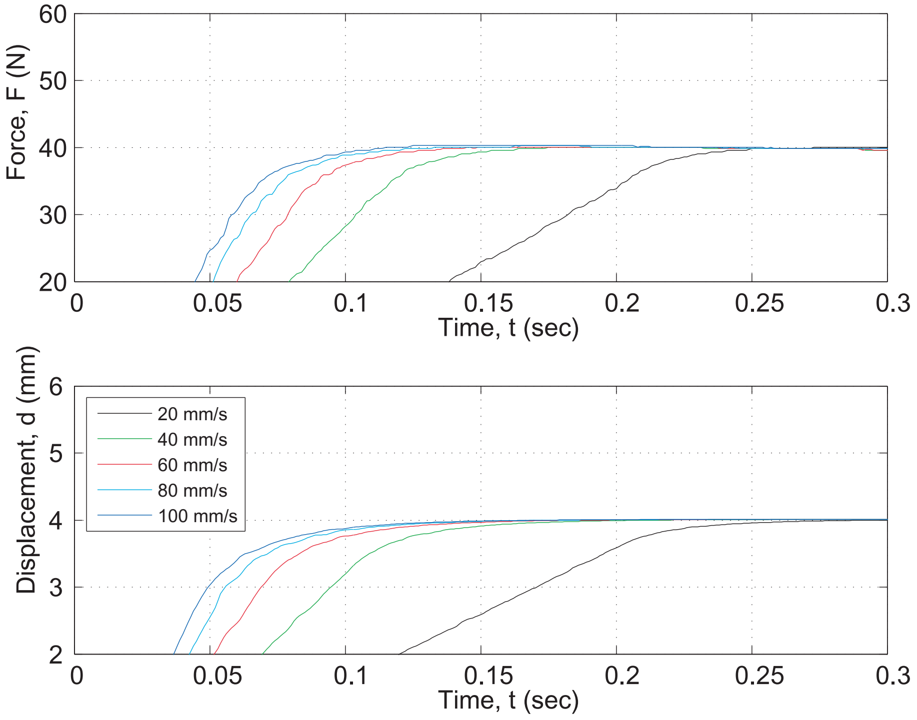

Figure 5.9: The zoom-in views of the force and displacement curves towards the end of the loading phase in Figure 5.7 for the hard silicone.

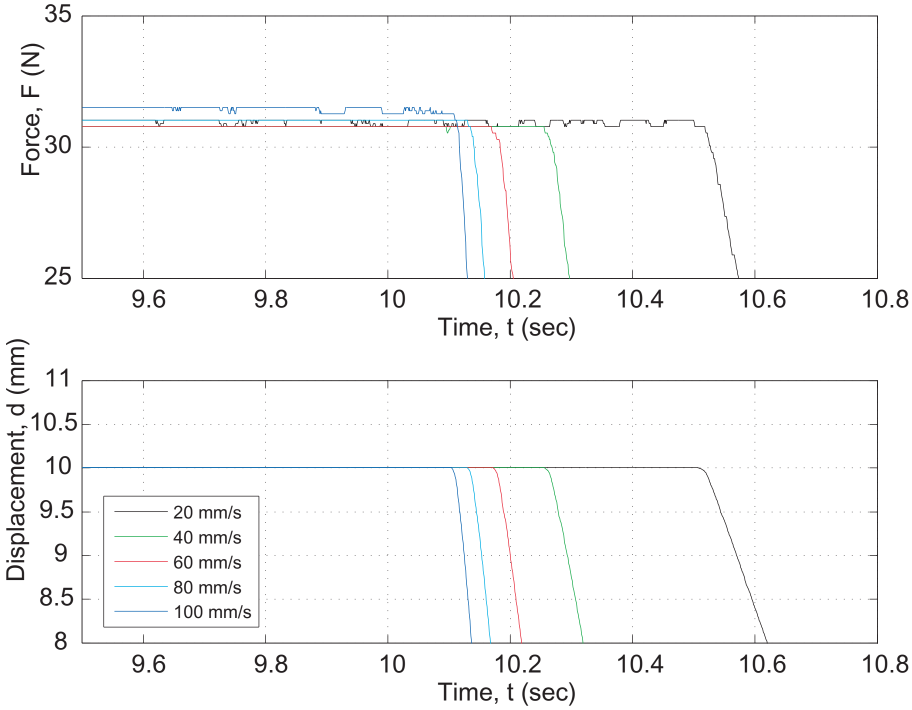

Figure 5.10: The zoom-in views of the force and displacement curves towards the end of the holding phase for the soft silicone in Figure 5.6.

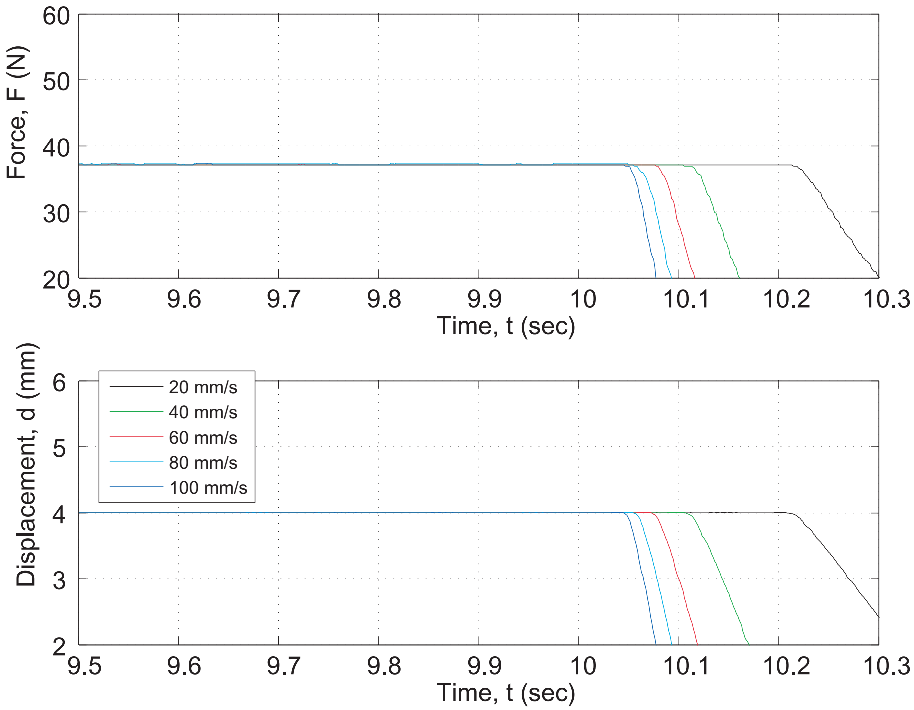

Figure 5.11: The zoom-in views of the force and displacement curves towards the end of the holding phase for the hard silicone in Figure 5.7.

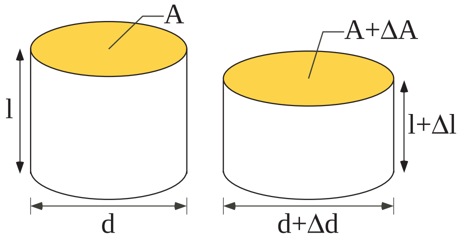

Figure 5.12: Change of nominal contact area due to the Poisson effect

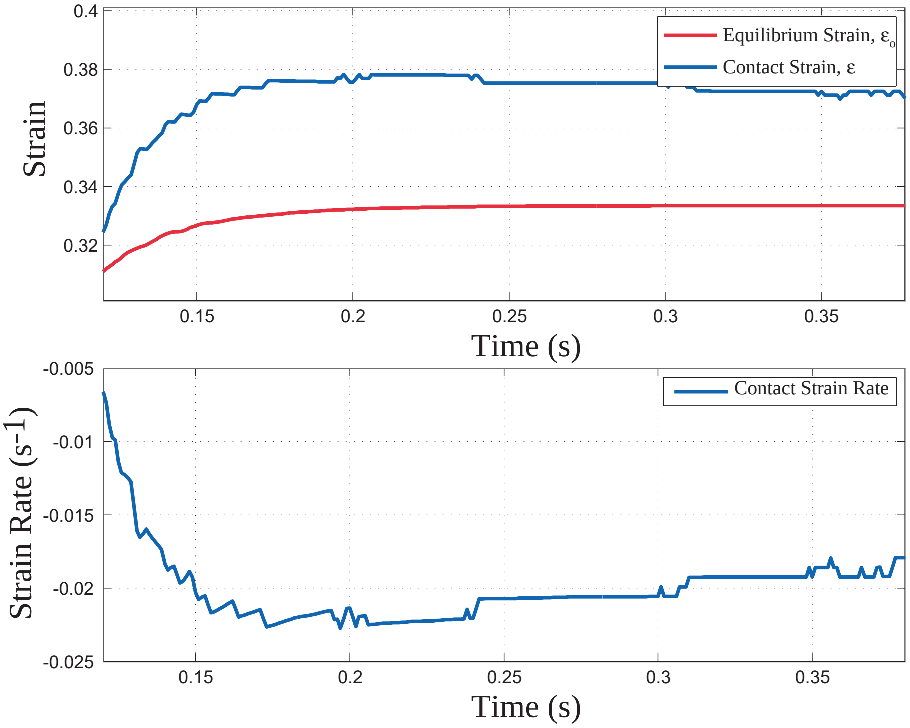

Figure 5.13: This figure shows an example of the strain on the contact surface of soft silicone at the end of *loading phase*. The loading rate is $100mm/s$.

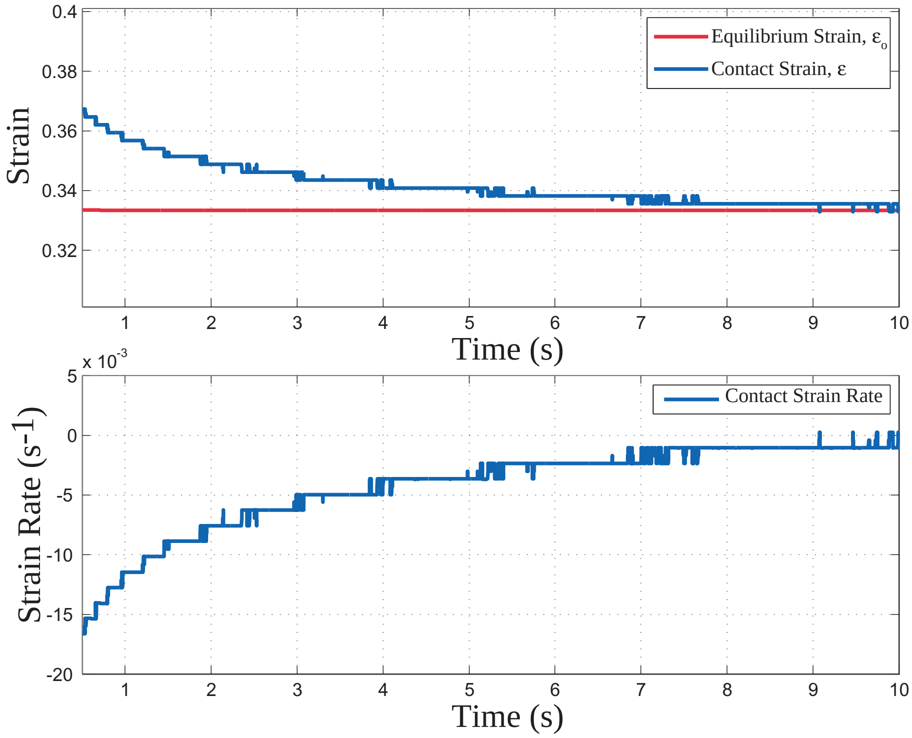

Figure 5.14: This figure shows an example of the strain on the contact surface of soft silicone during the *relaxation phase*. The loading rate is $100mm/s$.

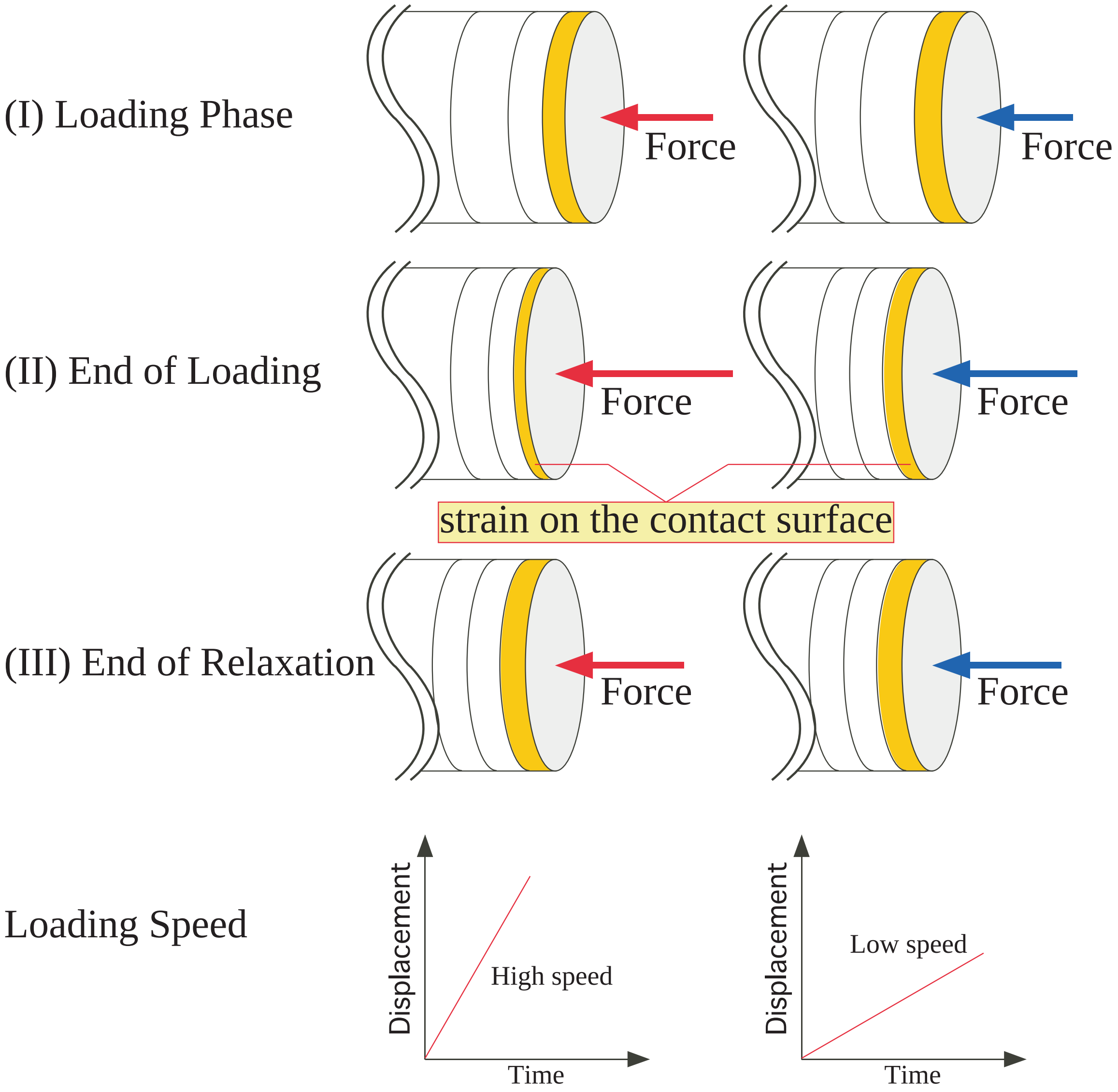

Figure 5.15: This figure illustrates the idea of the latency model with different loading rates. The left and the right columns show the change of the strain on the contact surface with high and low loading rates, respectively. We observe in (I) and (II) that the strain distribution is not even during loading and at the end of loading. With the same displacement being held, the material tends to rearrange the strains when enough time is allowed, as shown in (III), and the strain distribution becomes more uniform.

Chapter 6

EXPERIMENTAL STUDY OF CREEP RESPONSE OF VISCOELASTIC CONTACT INTERFACE UNDER FORCE CONTROL

Viscoelastic materials are known to exhibit both elastic response to external force or displacement, as well as temporal response that changes force or displacement at the contact interface under position or force control, respectively. Over the years, various dynamic models were proposed to describe the observation of both elastic and temporal responses of viscoelastic contact interface. In this chapter, we conduct experimental study using force control to explore and observe creep phenomenon in robotic grasping in order to better understand the nature of such contact interface, which has been widely used in soft robotic fingers, robotic feet, and contact surface of robotic arms. In addition to the force-controlled robotic gripper, we also employ high-speed vision sensor system to track four fiducial marks located throughout the grasped object to track the movements of elements between two contact surfaces. We found that the creep response under a constant external force exhibits the characteristics of exponentially increasing or decreasing temporal response. Such characteristics are similar in nature to those found in the *relaxation response* of viscoelastic materials when the grasping is under position control. Two different types of creep responses are found, depending on the state of grasping. When a constant force is held at the end of a loading phase, Type I creep is obtained with exponentially increasing displacement. On the other hand, when constant force is held at the end of a unloading phase, Type II creep is found with exponentially decreasing displacement. Both Types I and II in creep response mirror the Types I and II in relaxation response. We also found that different loading rates under force control result in different elastic response, in addition to the temporal response. This is an interesting finding because the Fung's model postulates for an elastic response that is independent of, and can be separated from, the temporal response. The experimental results do not show such independence. The creep phenomenon and grasp stability of viscoelasticity is studied in this chapter.

6.1 Introduction

Viscoelastic materials display the properties of both solid and fluid. Most biological materials are considered viscoelastic. Two important phenomena of viscoelastic materials in contact interface are *stress relaxation* and *strain creep* under constant displacement and force, respectively. In this chapter, we conduct experimental study on the creep response of viscoelastic contact interface by applying force control to deform viscoelastic material and hold the force constant in order to observe and measure the creep behavior of displacement under constant force. The experimental study reveals that the strain creep is a temporal response which can be modeled with combination of exponential functions, just as its counterpart in relaxation. High-speed camera vision sensor is employed to track the movement of fiducial fixated on the surface of the grasped viscoelastic material to capture the movement of fiducial marks between the two contact surfaces.

The study of the creep phenomenon of viscoelasticity is important because it is related to both stability and response of a contact interface. This is particularly useful when force control is employed in robotic grasping and manipulation. Furthermore, it can be used to optimize the energy consumption for robotic grasping. Understanding of the nature of viscoelastic contact interface can facilitate the modeling of robotic grasping which involves both elastic and temporal responses, such as those in soft fingers, biomedical contacts and tissues.

6.2 Theoretical Background

As we mentioned in the previous section, creep and relaxation are both time-delayed response of viscoelasticity. Fung's model [8] is used in [12] to study the temporal response of viscoelastic relaxation. A fundamental assumption of the Fung's model is that the elastic response and the temporal response are independent of each other and are separable. In this chapter, we applied similar assumption that the elastic response and the temporal response of the displacement under force control can be separated and expressed as

$$\delta(f,t) = \mathscr{D}^{(e)}(f) \cdot h(t) \tag{6.1}$$

where $\delta(f,t)$ is the displacement response, f is the external force, t is the time, $\mathscr{D}^{(e)}(f)$ is the elastic response which is a function of force, and $h(t)$ is the temporal response. Based on the experimental results, we assume that the temporal response is the combination of a series of exponential terms

$$h(t) = \sum_{i=0}^{n} c_i e^{-\nu_i t} \quad \text{with} \quad \nu_0 = 0 \quad \text{and} \quad c_0 = 1 \tag{6.2}$$

where c_i are constant coefficients, ν_i are the exponents of the exponential function, t is time, and n is the number of terms used in the equation.

It is noted that the constant $c_0 = 1$ is assumed in equation (6.2), instead of $\sum_{i=0}^{n} c_i = 1$ used in Fung's relaxation model. This is an expected outcome from the latency model [2], in which the initial elastic response is affected by the inhomogeneous movement of viscoelastic materials (*e.g.* hole displacement in polymeric materials) due to latent transmission of strain across the material when subject to external stimulus. As the time approaches infinity, the temporal effect will eventually decay, leaving an asymptotic elastic response that is the true value of homogeneous stress or strain. This phenomenon can also be observed from the experimental results of relaxation in which the value of force in relaxation will eventually become the same asymptotic value, in spite of different loading rates which result in different initial forces before relaxation takes place [2]. Such results clearly illustrate that the initial values of force or displacement in the relaxation or creep response do not represent the true elastic response. The homogeneous elastic response should be the steady-state (or asymptotic) value after the temporal effect dies out. Further discussions will be presented in Section 6.4.4.

The response of viscoelastic materials not only is time-dependent but also depends on the strain history. Thus, an additional assumption to this model is that the materials under force/displacement start from their equilibrium configuration.

6.3 Experimental Study

In order to conduct experiments to measure and observe the creep phenomenon of viscoelastic contact interface, force-controlled robotic gripper is employed. The experimental setup and procedures are explained in the following sections.

6.3.1 Experimental Setup

Fig. 6.1 illustrates the experimental setup using a robotic parallel-jaw gripper and a high-speed camera. A grasped object is shown between the two gripper surfaces in Fig. 6.2. The grasping force is measured by the load cell mounted on the gripper that has an accuracy of $0.25N$. The accuracy of displacement of the system is $1\mu m$. The resolution of the high-speed camera is 30 Mpixel with a spatial resolution of $50\mu m$ at a frame rate of 120 fps (frame per second). A ring of LEDs is used for illumination, as shown in Fig. 6.1.

A rectangular parallelepiped silicone is used in the experiment with a dimension of $50mm \times 40mm \times 25mm$. Four fiducial marks of different colors are positioned on the object for the vision sensor to track the continuous movement. The silicone is dyed in black using laser toner in order to eliminate the background noise when measured by the vision camera sensor. This is shown in Fig. 6.2.

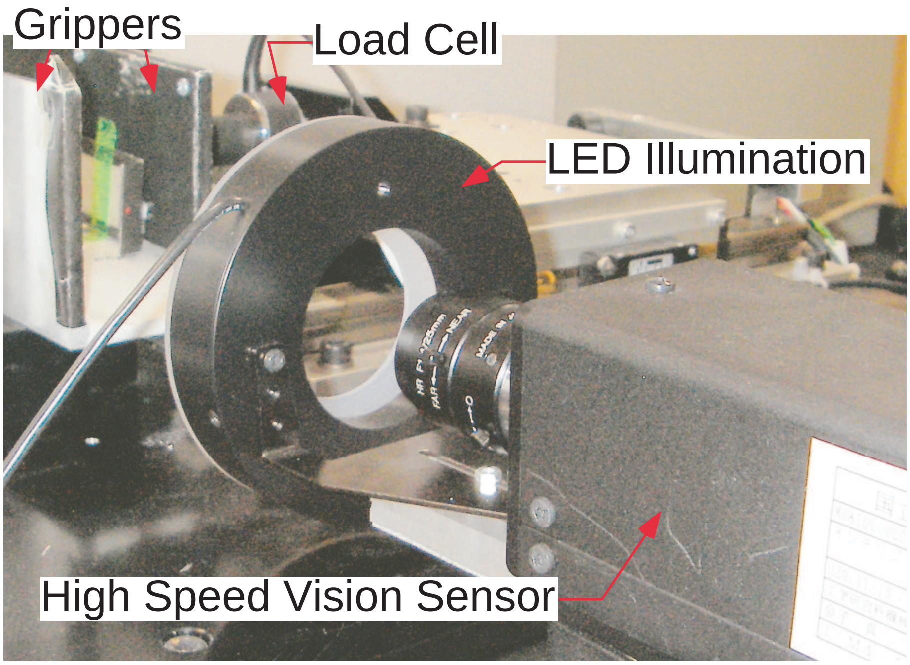

Figure 6.1: Experimental setup for the compressive loading and unloading tests, showing the parallel-jaw gripper, camera, and ancillary devices

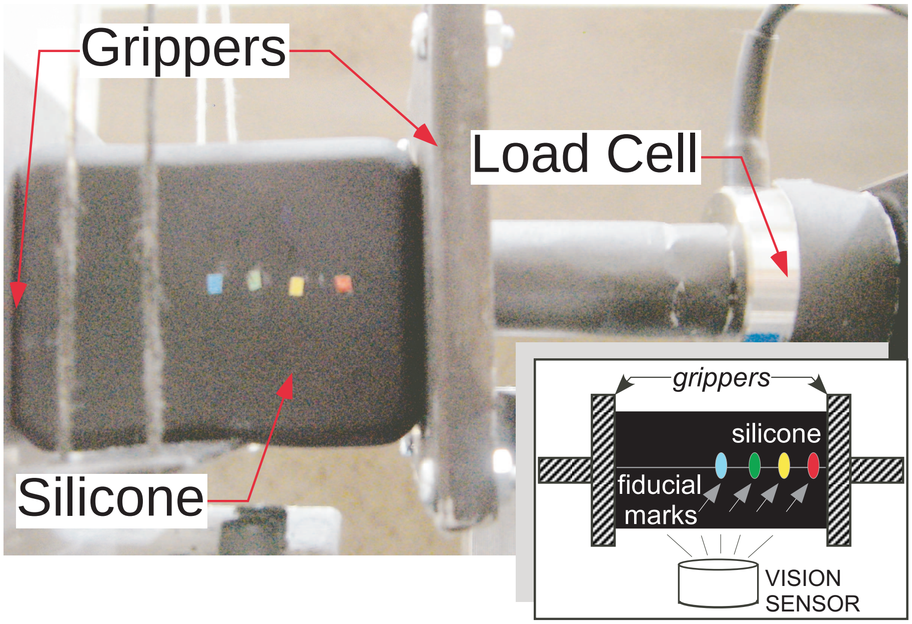

Figure 6.2: Four fiducial marks with different colors are placed on the silicone object, to be tracked by a high-speed camera (or vision sensor). The black silicone block is used to eliminate the background noise when using high-speed vision camera sensor.

The mass of the gripper mounted on the load cell is $14g$, which moves with an acceleration up to $100 mm/s^2$ in the experiments performed in this chapter. The grasped object has much smaller movement and thus its inertial effect can be neglected. With the operating parameters, we can estimate the maximum amount of inertial force to be about $0.0014N$ (during the ramp-up and ramp-down periods). This is much smaller than the accuracy level of the force sensor. As a result, we can neglect the inertial force of the gripper and the grasped object.

6.3.2 Procedures of Experiments

The procedures of various experiments conducted under different loading rates are enumerated in the following.

(1) The gripper is moved to barely touch the surface of the silicone solid. The silicone solid is supported freely by strings so that it will not fall due to gravity, but with least amount of interference to grasping in experiments. The high-speed vision sensor is calibrated with the colors of the fiducial marks on the silicone to track their positions.

(2) The loading process begins with a loading rate determined *a priori* by the amount of prescribed force and the duration of holding the force after loading (for creep). Several loading rates are employed in the experiments ranging from $0.1N/sec$ to $3N/sec$.

(3) When the contact force has reached the prescribed value, a PI (proportional-integral) controller is used to maintain a constant contact force for a duration of $9.5sec$. The displacement is recorded by the motion sensor mounted on the slider and the positions of the fiducial marks are tracked by the high speed vision sensor.

(4) After the loading-and-hold procedure, the gripper unloads to break contacts.

(5) The material rests for at least one minute before the next experiment is conducted. This one-minute rest allows for the material to restore to its original equilibrium state without affecting the subsequent experiments.

The measurements of force and displacement, as well as videos captured by high speed vision sensor are presented in the following section.

6.3.3 Experimental Results and Analysis

The results of experiments with force-controlled grasping of viscoelastic object are illustrated in Fig. 6.3 and Fig. 6.4. The figures plot experimental results based on different loading rates, and the resulting displacement of contact surface measured by the gripper (the black line in the position plot), as well as the displacements of the fiducial marks measured by the high-speed camera (the red, yellow, green, and blue colors, corresponding to the color of the fiducial marks). A low-pass Butterworth filter is utilized for conditioning the raw data obtained from load cell to filter out the high-frequency noise due to electromagnetic interference during experiments.

6.3.3.1 Different Loading Rates

Experiments with different loading rates are performed, with results plotted Figs. 6.3 and 6.4. The holding force of the experiments were maintained by a PI force feedback control algorithm at 2N. The charts on the right of Figs. 6.3 and 6.4 demonstrate the change of displacements and fitted curves based on (6.1) under a constant holding load. We can observe that, at begin of the holding, a lower loading rate causes a larger initial displacement, while a higher loading rate has a smaller initial rate. A further study of the effect of loading rate will be discussed in Section 6.4.3.

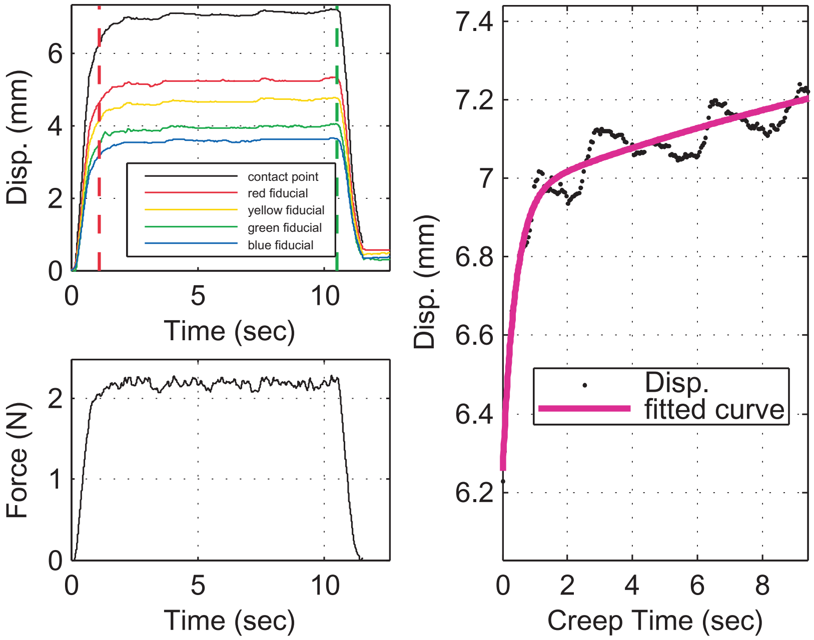

Figure 6.3: The results of loading-holding-unloading experiment under a lower loading rate with force control. The loading rate is $1.96N/s$. The four lower curves of displacement correspond to the four fiducial marks in Figure 6.2 of the same color.

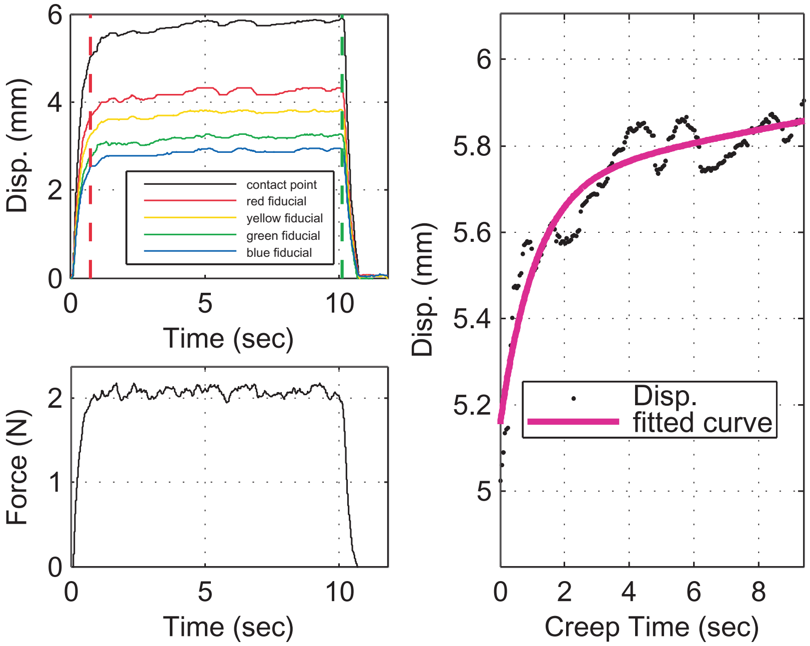

Figure 6.4: The results of loading-holding-unloading experiment under a higher loading rate with force control. The loading rate is $2.71N/s$.

6.3.3.2 Repeated Loading-Holding-Unloading

Experiments are also conducted with repeated loading-holding-unloading in order to examine the response of creep due to reversed direction of loading-holding and unloading-holding. Fig. 6.5 and Fig. 6.6 present the experimental results at a lower and a higher loading rate, respectively. The upper and lower values of holding forces were set at $4N$ and $2N$, as shown in the figures. The creep phenomenon in higher loading rate is more pronounced than that in lower loading rate. Furthermore, two different types of creep are observed. Further explanation and the definition of two types of creep responses will be presented in Section 6.4.2

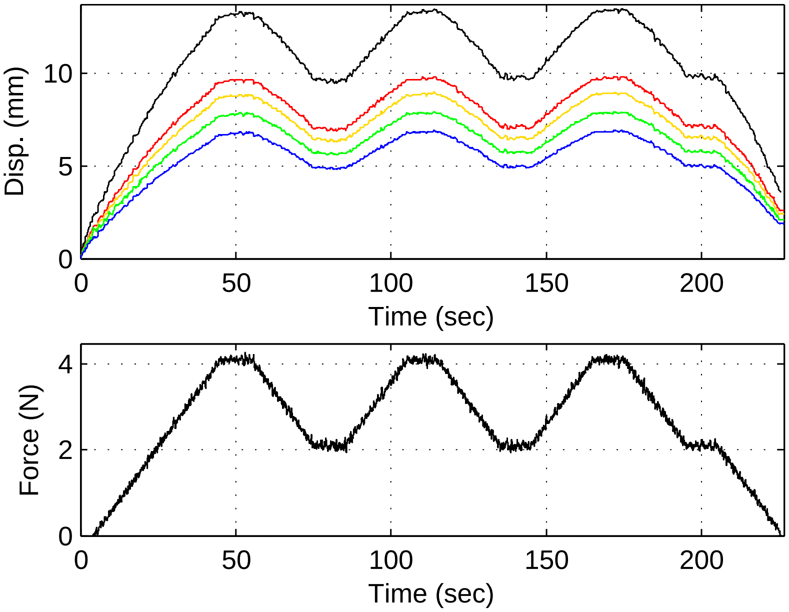

Figure 6.5: Repeated loading-holding and unloading-holding experiment with a lower loading rate of $0.092N/sec$

6.3.3.3 Creep response

As we discussed earlier, creep response is due to the temporal behavior of viscoelasticity, captured by equation (6.2). In this chapter, we choose two exponential terms for curve fitting with $n = 2$ in (6.2). The explanation of this choice is expounded in the Appendix. Note that in [12, 2, 43], two exponential terms were adopted also. It seems to

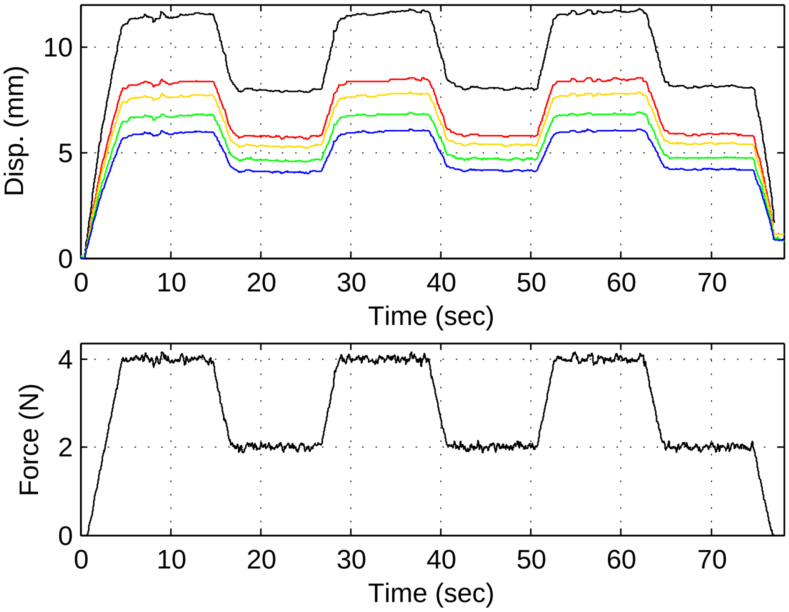

Figure 6.6: Repeated loading-holding and unloading-holding experiment with a higher loading rate of $0.85 N/sec$

suggest that such approximation and curve fitting with two exponential terms is valid for both relaxation and creep.

6.3.3.4 Displacement Sensor vs. Vision Sensor

The displacement of the contact surface is measured by the movement of the gripper. This is shown in black line in the plots. In addition to the displacement measurement afforded by the sensor on the gripper, the high-speed vision sensor is utilized in experiments to track the movements of the four fiducials. With the vision sensor, we can track the movement of materials away from the contact surface. The comparison shows the order of displacement in the plots. However, all four displacement curves show consistent trend of movement, including the exponential creep responses.

6.4 Discussions

Based on the preceding presentations of experimental results, some important results are discussed here.

6.4.1 Exponential creep response

As in the relaxation of viscoelastic contact interface [12, 2, 43], the temporal response of creep can be represented by curve fitting of experimental data using two exponential terms. This is due to the fact that relaxation and creep are two complementary effects, with the former being the temporal behavior under constant displacement and the latter under constant force. Since similar time-dependent force behaviors were observed in [12, 2, 43] with different materials, such as silicones of different compliance/composition and different soft rubbers, we believe that the creep response presented in this chapter is a general response of soft materials.

6.4.2 Type I and Type II Creep

Fig. 6.5 to Fig. 6.6 plot the results of experiments with repeated loading-holding and unloading-holding grasping tasks. In the figures, the displacement evolution (creep response) of the viscoelastic object depends on whether the object is under loading or unloading before holding at constant force. We defined them as Type I and Type II creep phenomena, respectively, as illustrated in Fig. 6.7(a).

(1) The Type I creep occurs under a constant external force of compression, at the end of a loading process in segment (1) in Fig. 6.7(a). The Type I creep is characterized by an exponential increases in the displacement, illustrated by segment (2) in the figure. This exponential increase is partly due to the latency of temporary response as that in the relaxation [12, 2, 43]. The nature of Type II creep response gives rise to the following constraint equation in (6.2)

$$c_i < 0 \quad \text{for} \quad i = 1, 2, \cdots, n \tag{6.3}$$

(2) In comparison, the Type II creep occurs under a constant external force in compression, at the end of a unloading process, represented by segment (3) in Fig. 6.7(a). The Type II creep is characterized by an exponential decrease in the displacement, illustrated by segment (4) in the figure. This exponential decrease is partly due to the latency of temporary response as that in the relaxation response [12, 2, 43]. The nature of Type II creep response gives rise to the following constraint equation in (6.2)

$$c_i > 0 \quad \text{for} \quad i = 1, 2, \cdots, n \tag{6.4}$$

It is noted that Type I and Type II creeps are with opposite trends of displacement evolution. This is akin to that in the Type I and Type II relaxation [12, 2, 43].

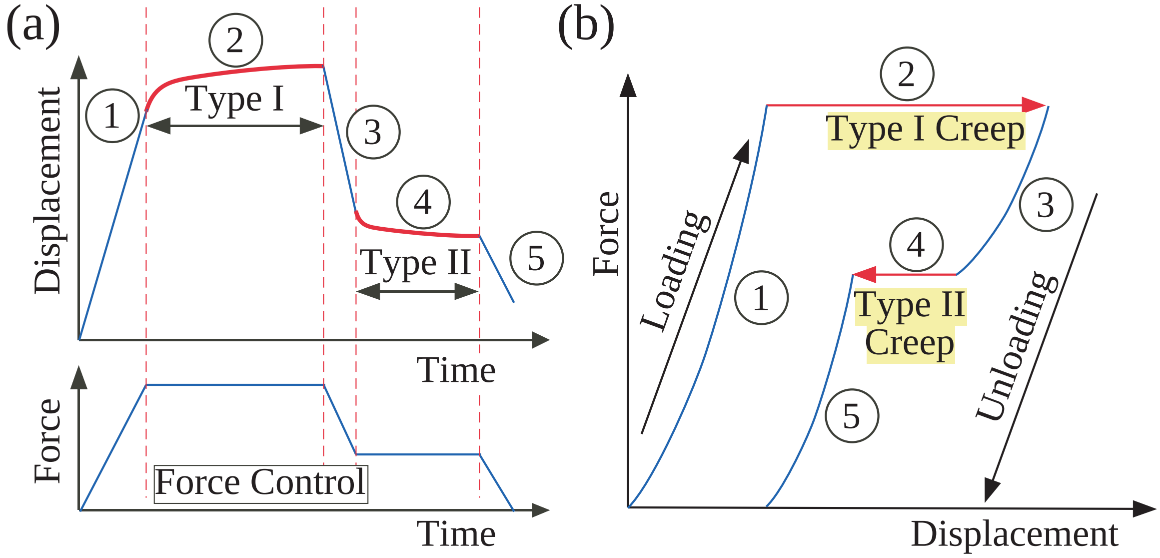

Figure 6.7: Two types of creep responses under force control. (a) Type I creep is the creep under constant force after loading; while Type II creep is under constant force after partial unloading. (b) The loading and unloading curves mainly depend on the elastic property of the material. The amount of creep (horizontal red lines) depends on the speed of sound in the material. The segment numbers, 1 through 5, correspond to each other.

Fig. 6.7(b) illustrates the two types of creep responses presented in Fig. 6.7(a) by plotting the history of loading-holding-unloading on the force-displacement plot. The segment numbers in Fig. 6.7(b) correspond to those in Fig. 6.7(a). As can be seen in Fig. 6.7(b), clockwise loop is traced starting from loading, followed by Type I creep when the force is held at constant. After that, segment 3 represents partial unloading followed by Type II creep when the force is held at constant. The issue of optimization of energy consumption when performing a stable grasping task, using a force-displacement plot such as Fig. 6.7(b), will be a topic of our follow-up research.

6.4.3 Effect of Different Loading Rates

Fig. 6.8 is an illustration of the response of viscoelastic contact interface under three different loading-unloading rates, as explained in the following. The origin of the plot in Fig. 6.8 indicates the initial state of the material.

(1) When a quasistatic loading-unloading is applied with very low loading rate, the loading and unloading curves nearly coincide with each other. The loading and unloading curves will cycle between the origin and the "point of pure elastic response" shown in Fig. 6.8. This is shown by the dashed blue lines.

(2) If the loading-unloading rate is increased, the loading curve will shift to the left as illustrated by the green arrows shown with the "increasing of loading rate." The unloading curve will shift to the right, causing the gap between the two curves to widen to form a clockwise loop. This is shown by the dashed green lines.

(3) When an even higher loading rate is applied to the material, the relationship between the grasping force and displacement will follow the blue solid curve. When the grasping force has reached the maxi-

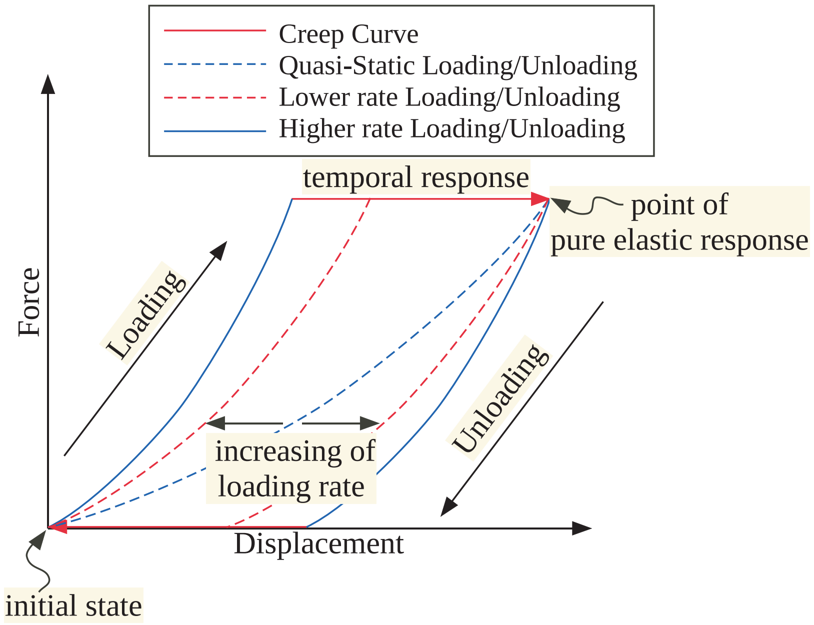

Figure 6.8: The ideal loop of a force-controlled loading-holding-unloading test. Different loading rates will result in different loops. Three loops: blue dash loop, red dash loop and blue solid loop, represent three loading rates: quasi-static, a low rate and a high rate, respectively. The loading and unloading curves depend on the elastic property of the material. Different loading rates will result in different loops. The blue dash line shows quasistatic loading/unloading curve with purely elastic response, without the temporal response of creep. With the increase of loading rate, the loading and unloading curve will shift as indicated by the green arrows to the dashed green lines. The loading-unloading rate corresponding to the solid line is the highest amongst the three rates.

mum, the force is held constant. At this point, the creep will start, as indicated by the red arrow at the top of the figure moving from left to right and reaching the point at top right, indicated by the "point of pure elastic response" in the figure. When the grasping force is released, the material will follow the unloading curve until the force returns to zero. Finally, the material will slowly go back to its initial state, following the red arrow at the bottom of the loop.

Two observations are in order from Fig. 6.8. First, the area of the loop increases with the increase of loading rate. In other words, the energy dissipated during the operation is higher with a high loading-unloading rate in grasping. Secondly, the higher loading rate will result in a "stiffer" loading-unloading curve. This phenomenon is known as the "strain stiffening" (*or strain hardening*) effect. The higher loading rate will be accompanied by a lower value of $\mathscr{D}^{(e)}$ for the same holding force in force control experiments. Here, $\mathscr{D}^{(e)}$ can be regarded as a compliance function of the material, with lower $\mathscr{D}^{(e)}$ representing a stiffer material. Therefore, if we let $t = 0$ in (6.1) and (6.2), we will have

$$\delta(f,0) = \mathscr{D}^{(e)}(f) \cdot h(0) = \mathscr{D}^{(e)}(f) \cdot \sum_{i=0}^{n} c_i \tag{6.5}$$

Different value of $\mathscr{D}^{(e)}$ shows different elastic property of the material, consistent with the results presented in [43]— the higher loading rate leads to a stiffer response, also known as the *strain stiffening effect*.

6.4.4 Asymptotic Value of Displacement in Creep

Based on equation (6.2), the temporal response of the displacement will converge exponentially to an asymptotic value during the creep period, represented by the horizontal arrows at top and bottom of the loop in Fig. 6.8. When the time approaches infinity, the transient temporal response will fade out and only the elastic response, $\mathscr{D}^{(e)}$, will remain. Consequently, the point at the top right of the loop in Fig. 6.8 represents the pure elastic response.

$$\delta(f,\infty) = \mathscr{D}^{(e)}(f) \cdot h(\infty) = \mathscr{D}^{(e)}(f)\, c_0 = \mathscr{D}^{(e)} \tag{6.6}$$

We also observed that the steady-state creep response always converges to an asymptotic value regardless of the loading rate. This shows that the static state of the same input is consistent. The difference only happens when the material is in a dynamic transient state.

6.4.5 Grasp Stability with Creep Response

The time-dependent displacement response of creep under force control can significantly affect the stability of a robotic grasp. In this section, we study how the creep phenomenon can affect the grasp stability by using the friction *limit surface* [44].

Limit surface is a surface defining the stable region of tangential force and normal moment in grasping with finite area of contact. As long as the actual tangential force and normal moment fall within the region of limit surface, it will not slide; in other word, the contact is stable. The tangential friction force and moment are defined and derived in the following equations

$$\mathbf{f}_t = -\int\int \mu\, \hat{\mathbf{v}}\, p(x,y)\, dxdy \tag{6.7}$$

$$\mathbf{m}_n = -\int\int \mu [\mathbf{r} \times \hat{\mathbf{v}}] p(x,y)\, dxdy \tag{6.8}$$

where $\mathbf{f}_t$ is tangential force, μ is the coefficient of friction, $\hat{\mathbf{v}}$ is the unit vector of velocity, $p(x,y)$ is the pressure distribution, $\mathbf{m}_n$ is normal moment, and $\mathbf{r}$ is the position vector.

Fig. 6.9 illustrates the contact between a flat, rigid surface and a soft silicone material with center of rotation (COR) along x-axis. We define the unit vector along the direction of the velocity $\hat{\mathbf{v}}$ as

$$\hat{\mathbf{v}} = \frac{1}{\sqrt{(d_{cr}+x)^2+y^2}} \begin{bmatrix} -y \\ (d_{cr}+x) \end{bmatrix}, \quad \mathbf{r} = \begin{bmatrix} x \\ y \end{bmatrix} \tag{6.9}$$

We apply the general pressure distribution [10] in (6.10) by assuming that it is only a function of x with $k = 4$.[1]

$$p(x) = C_k \frac{N}{L \times W} \left[1 - \left(\frac{x}{L} \right)^k \right]^{\frac{1}{k}} \tag{6.10}$$

where N is the normal force, L and W are the length and width of the contact area, C_k is a coefficient, a function of k, that adjusts the profile of pressure distribution to satisfy the equilibrium condition at the contact interface.

The limit surface can be obtained by scanning the COR along the X-axis, corresponding to the experiment. This friction limit surface with creep response is shown in Fig. 6.10. Since the normal force is held constant, the tangential force will not be affected by the creep phenomenon. However, due to the expansion of contact area, the margin of limit surface also expands with time, making the contact more stable. This proves that the creep phenomenon can enhance the stability of a soft contact.

6.5 Summary

In this chapter, we present an experimental study to examine the creep phenomenon of viscoelastic materials using a parallel-jaw gripper under force control, equipped with a high-speed vision sensor system to track the fiducial marks located on the surface of the grasped object. We found that the creep response under constant external force features the characteristics of exponentially increasing or decreasing temporal response. Such characteristics are similar in nature to those found in relaxation of viscoelastic materials when the grasping is under position control. Two types of creep are observed, and both Types I and II in creep response mirror the Types I and II in relaxation response. In addition, it appears that different loading rates under force control result in different elastic response, $\mathscr{D}^{(e)}$. It is found that force control with creep response can enhance the stability of soft contacts. This is a subject of future investigation because the Fung's model postulates an elastic response that is separable from and independent of the temporal response.

---

[1] Hertzian pressure distribution is a special case when $k = 2$. Softer materials usually have higher values of k. As a result, we chose $k = 4$.

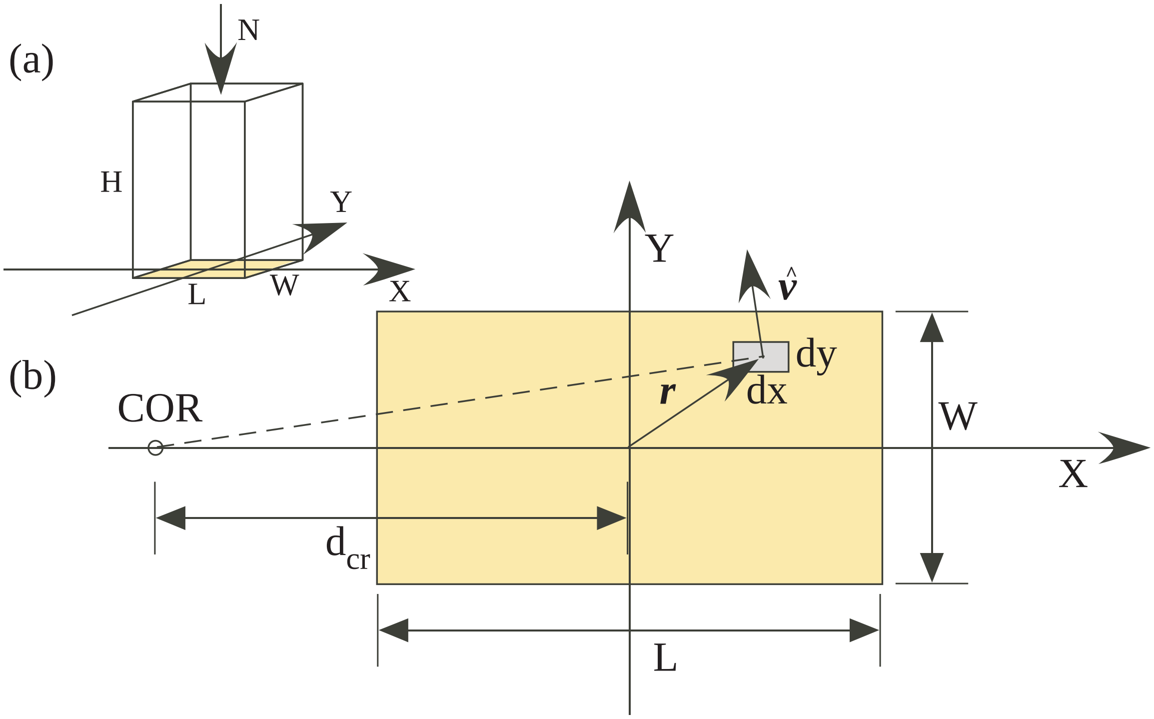

Figure 6.9: (a) Rectangular parallelepiped viscoelastic silicone, with a dimensions of $L \times W \times H$. (b) The dimensions of the rectangle contact area is $L \times W$. The coordinate is centered at the center of the contact area. COR indicates the center of rotation, and d_{cr} is the distance from COR to the center of the contact area. The vector $\mathbf{r}$ is the position vector, and $\hat{\mathbf{v}}$ is the unit vector along the direction of the velocity.

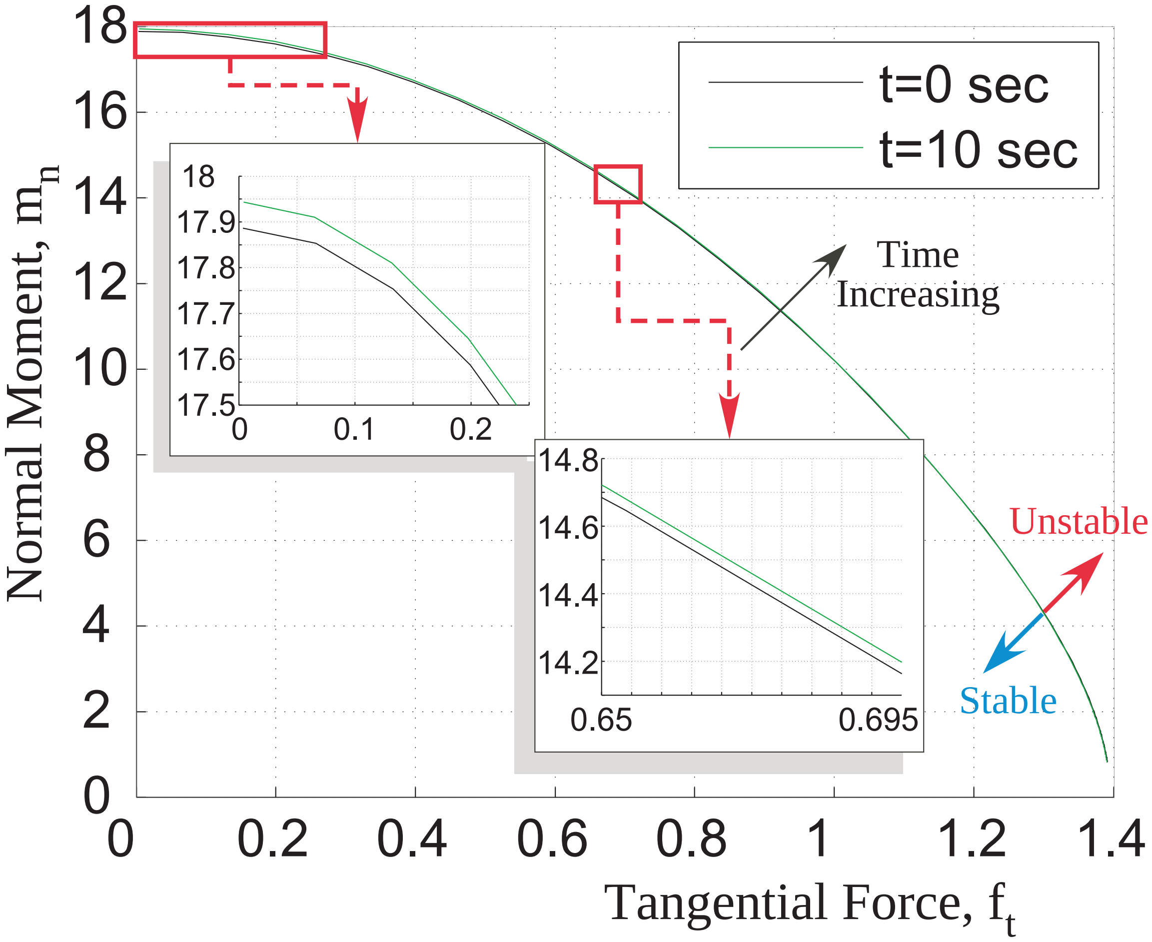

Figure 6.10: Evolution of the limit surface as a function of time in the case of a constant normal force. In this analysis, we let coefficient of friction, μ, equal to 0.7, and the constant normal force, N, equal to 2N. The contact area changes based on (6.1) and Poisson ratio. The length of the contact area evolves from 42.22 to 42.39, and the width of the contact area evolutes from 26.38 to 26.50

Chapter 7

STUDY OF THE RELATIONSHIP BETWEEN THE STRAIN AND STRAIN RATE FOR VISCOELASTIC CONTACT INTERFACE IN ROBOTIC GRASPING

In this chapter, a nonlinear latency model is presented to describe the relationship between the strain and strain rate of the temporal responses in robotic grasping that involves viscoelastic contact interface. The results from experiments and simulation are presented, and are found to match well with each other. The nonlinear latency model was able to adequately represent both Type I and Type II relaxation responses. For the successive loading and holding with a soft contact, the model describes the behavior of step-wise increase of equilibrium strain and a polynomial relationship between the strain rate and the strain. The nonlinear latency model can successfully predict and model the behavior of anthropomorphic soft contact interface in grasping and manipulation when the grasped object is held in certain posture of prehension with repeated loading and/or unloading.

7.1 Introduction

Viscoelastic materials display the properties of both elastic solids and viscous fluids. As a result, viscoelastic materials exhibit both elastic (linear or nonlinear) response and temporal response when subject to external stimuli, such as force or displacement. Most biological materials are considered viscoelastic. Viscoelastic materials exhibit two impor-

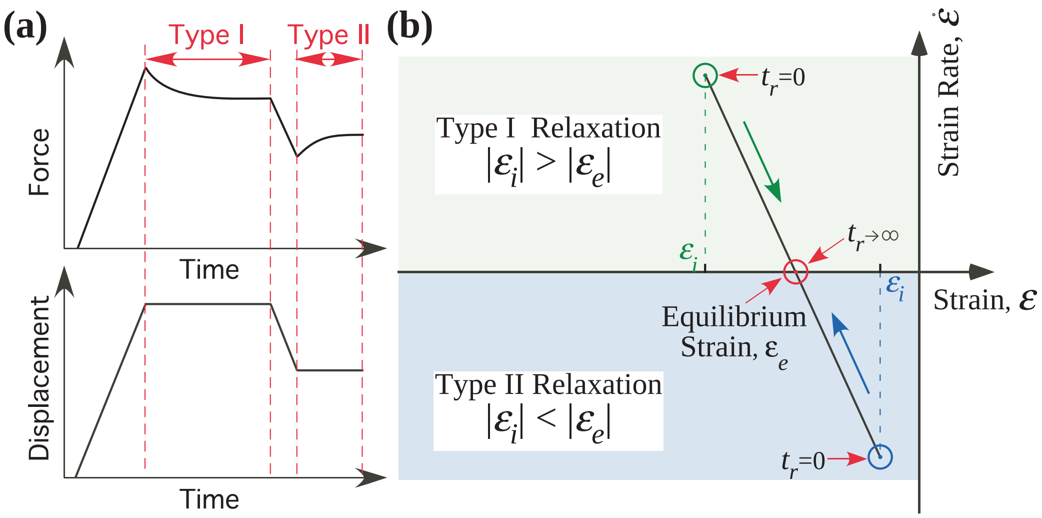

Figure 7.1: (a) Type I and Type II relaxation as observed experimentally in association with the latency model. (b) The latency model with linear relationship between strain and strain rate [2].

tant temporal responses when subject to displacement and force in contact interface. They are *stress relaxation* and *strain creep*, respectively. In this chapter, the nonlinear relationships between the strain and strain rate of viscoelastic materials are studied and derived based on the linear latency model presented in [2]. Furthermore, simulation studies using the latency model also produce results of stress relaxation and strain creep responses that correlate well with the experimental data.

Stress relaxation and strain creep are two well-known properties of viscoelastic materials. Stress relaxation, normally called *relaxation*, depicts the varying contact force/stress with time when a constant displacement is applied to the material [8]. Two types of relaxations are defined in [2] and shown in Figure 7.1. Type I relaxation exhibits decreasing stress under a constant displacement, typically at the end of loading. Type II relaxation exhibits increasing stress under a constant displacement, typically at the end of unloading. (See Fig. 7.1.) Creep response, the other important property, is the displacement/strain change when a constant force is applied to viscoelastic materials. Creep and relaxation illustrate the delayed temporal responses with the application of displacement or force.

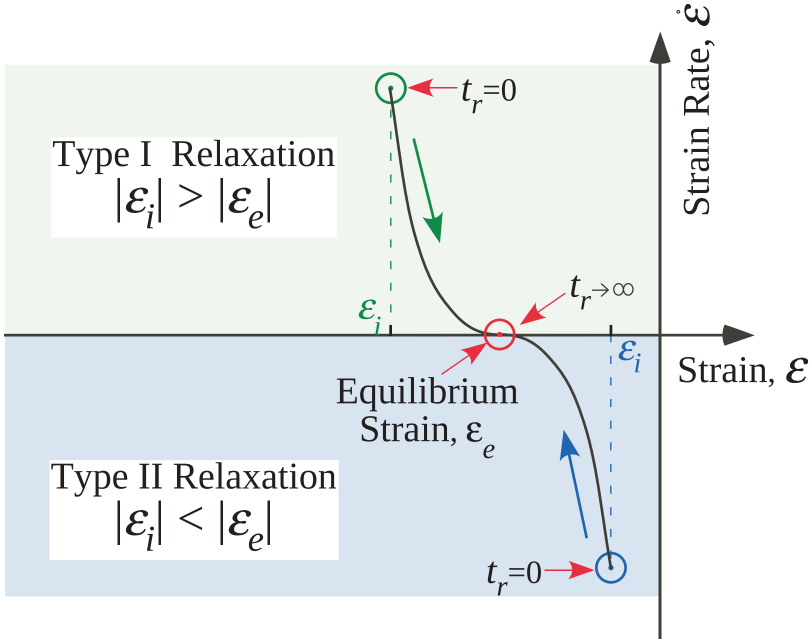

Figure 7.2: The nonlinear latency model

7.2 Theoretical Background

Based on the experimental observation and the fundamental concept in physics, we postulate the following two aspects of viscoelastic contact behaviors.

(1) The two viscoelastic phenomena, stress relaxation and strain creep, are caused by unbalanced stress states within the material subject to transition of external stimuli. Such response in some literature was referred to as hole displacement, especially in polymeric materials [20]. The velocity of stress propagation inside the material determines the time constants of exponential decay or growth for stress relaxation or strain creep.

(2) The material, given enough time, will always approach the equilibrium state at which internal stress is balanced and stress propagation ceases. This state is called the equilibrium state.

The latency model [2] proposed by Tsai and Kao is described by the following equations

$$\dot{\varepsilon}_c = -\nu_1(\varepsilon_c - \varepsilon_e) \quad \& \quad \varepsilon_e = -\frac{N_0 c_0}{\alpha_c} \tag{7.1}$$

where ε_c is the compressive strain measured externally at the contact interface, $\dot{\varepsilon}_c$ is the strain rate, and ε_e is the strain when equilibrium state is reached. The parameters ν_1, N_0, c_0 and α_c are constants pertaining to material properties [2].

The latency model elucidates a process for viscoelastic materials to reach equilibrium after being subjected to external stimuli. When a new equilibrium state is reached, the strain becomes the equilibrium strain, $\varepsilon = \varepsilon_e$, with the strain rate becoming zero, $\dot{\varepsilon} = 0$. In [2], stress relaxation was discussed and modeled by assuming one exponential term in the exponentially decaying temporary response. Based on the latency model with this assumption, an intuitive and straightforward linear relationship (with a closed-form solution) between the strain and strain rate can be obtained, as shown in Fig. 7.1. The temporal response in Fig. 7.1 is a function of the time t, with $0 \leq t \leq \infty$.

The experimental results suggest that the relationship is nonlinear, as shown in the nonlinear latency model in Fig. 7.2. As a result, we propose the following empirical model to represent the nonlinear polynomial relationship between the strain and strain rate in the following equations with respect to odd or even exponent

$$\dot{\varepsilon} = \begin{cases} -\nu(\varepsilon - \varepsilon_e)^n & \text{if } n \text{ is odd} \\ -[\operatorname{sgn}(\varepsilon - \varepsilon_e)]\,\nu(\varepsilon - \varepsilon_e)^n & \text{if } n \text{ is even} \end{cases} \tag{7.2}$$

where ε_e is the equilibrium strain, ν and n are constants of the empirical polynomial function, and ε is the instantaneous strain at any point within the material. Eq. (7.2) shows that the magnitude of strain rate can be determined from the current strain, ε, and the equilibrium strain, ε_e. In other words, if the current strain is further away from the equilibrium strain, a larger magnitude of strain rate will be expected.

In this chapter, we adopt odd exponents in equation (7.2) for the convenience in analysis. With n being odd, we can re-write (7.2) as follows

$$\dot{\varepsilon} = -\nu(\varepsilon - \varepsilon_e)^n \tag{7.3}$$

Eqs. (7.2) and (7.3) extends the linear model in Fig. 7.1 to include the nonlinearity observed in experiments. The experimental study will be presented in Section 7.3. This model has two assumptions. First, the material is assumed to be homogeneous. Second, every infinitesimal element within the material is assumed to have similar property, such that we can apply the empirical model from the exterior contact surface to the core of the material.

The solution of the differential equation in (7.3), before reaching the equilibrium state ε_e, can be obtained as follows.

(I) When $\varepsilon_e > \varepsilon_0$:

$$\varepsilon = \varepsilon_e - [(n-1)(\nu t + c)]^{\frac{1}{1-n}} \quad \text{with} \quad c = \frac{(\varepsilon_e - \varepsilon_0)^{1-n}}{(n-1)} \tag{7.4}$$

(II) When $\varepsilon_e < \varepsilon_0$:

$$\varepsilon = \varepsilon_e + [(n-1)(\nu t + c)]^{\frac{1}{1-n}} \quad \text{with} \quad c = \frac{(\varepsilon_0 - \varepsilon_e)^{1-n}}{(n-1)} \tag{7.5}$$

where $\varepsilon_0 = \varepsilon(0)$ is the boundary condition, which represent the initial strain when $t = 0$.

Eqs. (7.4) and (7.5) are the solutions of the differential equation of the nonlinear latency model. The solutions of the strain ε is a function of time, the exponent n, and the coefficient ν. When $t \to \infty$, the second term on the right-hand side of the equal sign will vanish, resulting in $\varepsilon = \varepsilon_e$. Physically, this means that the strain will converge asymptotically to an equilibrium strain when time approaches infinity. This is consistent with the latency model and observation based on the experimental data.

7.3 Experimental Study

A tensile test machine is employed to conduct experiments for measuring and observing the temporal responses of viscoelastic contact interface. The experimental setup and procedures are explained in the following sections.

7.3.1 Experimental Setup

Experiments were conducted using a tensile testing machine with a pair of parallel flat fixtures pressing upon the object, as shown in Fig. 7.3. The system is identical to a parallel-jaw gripper, and will be so referred to in this chapter. The load cell has a range of $2\,kN$ force with an accuracy of $0.2\,N$ and high repeatability. The displacement measurements have an accuracy of $10^{-3}\,mm$. Multiple experiments with varying loading rates, stationary and relaxation phase, and unloading phase were conducted. The parameters of the experiments are tabulated in Fig. 7.3.

The inertia of the fixture is compensated by the design of the equipment in order to minimize the effect of force measurement due to acceleration or deceleration. Calibration experiments were conducted to measure the inertia force without contact to identify the amount of inertia force due to the fixture alone. The results indicate a maximum of $0.35\,N$ of inertia force (within the range of acceleration and deceleration used in the experiments) measured by the load cell, which is only slightly larger than the accuracy of the load cell. Based on the parameters used in the experiments, we conclude that the inertia effect is less than 1% of the typical range of forces; therefore, it is negligible.

The material of the grasped object is a viscoelastic soft rubber ball with a radius of $35\,mm$.

7.3.2 Procedures of Experiments

The procedures of various experiments conducted with different loading rates are enumerated in the following.

(1) The gripper is moved to barely touch the surface of the viscoelastic object.

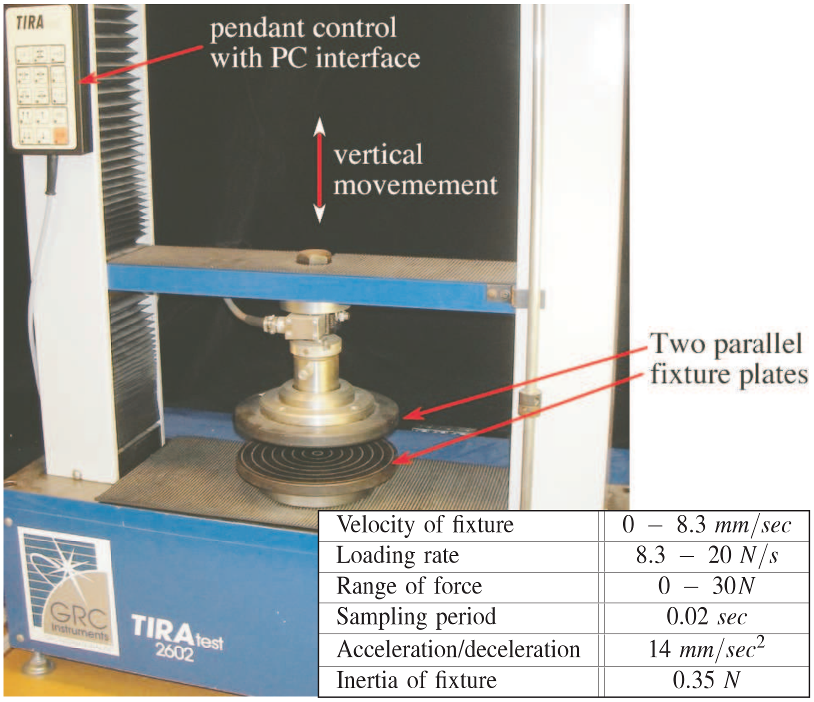

Velocity of fixture	$0 - 8.3\ mm/sec$
Loading rate	$8.3 - 20\ N/s$
Range of force	$0 - 30N$
Sampling period	$0.02\ sec$
Acceleration/deceleration	$14\ mm/sec^2$
Inertia of fixture	$0.35\ N$

Figure 7.3: The experimental setup of a tensile testing machine with a pair of flat parallel fixture plates.

(2) The upper fixture moves in vertical direction for loading, unloading, and holding by following a prescribed control sequence of displacements.

(3) The gripper unloads and breaks contact.

Two different tests were conducted. In the first test, as shown in Fig. 7.4(a), the fixture moves to compress the viscoelastic object in an increment of $5\,mm$ with the displacements of 5, 10, 15, 20, and $25\,mm$. At the end of each loading sequence and increment, the fixture was held at that displacement for 10 seconds. This is shown in the bottom plot of Fig. 7.4(a). In the other test, the fixture first compressed the object to a displacement of $25\,mm$. After that, the displacements were reversed to go through the descending order of 25, 20, 15, 10, and $5\,mm$. The fixture was also held at each displacement for 10 seconds at every step and with the same loading/unloading rate, $500 mm/min$. This is shown in the bottom plot of Fig. 7.4(b).

7.3.3 Experimental Results and Analysis

The experimental results of the two tests are presented in Figs. 7.4(a) and 7.4(b). The normal forces at the contact surface are measured and plotted in the top plots in Figs. 7.4(a) and 7.4(b).

To obtain strains and strain rates from the experimental results, we assume a linear relationship between the strain, ε, and stress, σ, for the sake of convenience in analysis; that is,

$$\varepsilon = \frac{\sigma}{E} = \frac{f/A}{E} \tag{7.6}$$

where A is the area of contact at the exterior surface, f is the measured force, and E is the Young's modulus of the material which has an average value of $2.8 \times 10^4\,Pa$. The area of contact grows with the amount of depression, d, of the fixture onto the surface of the

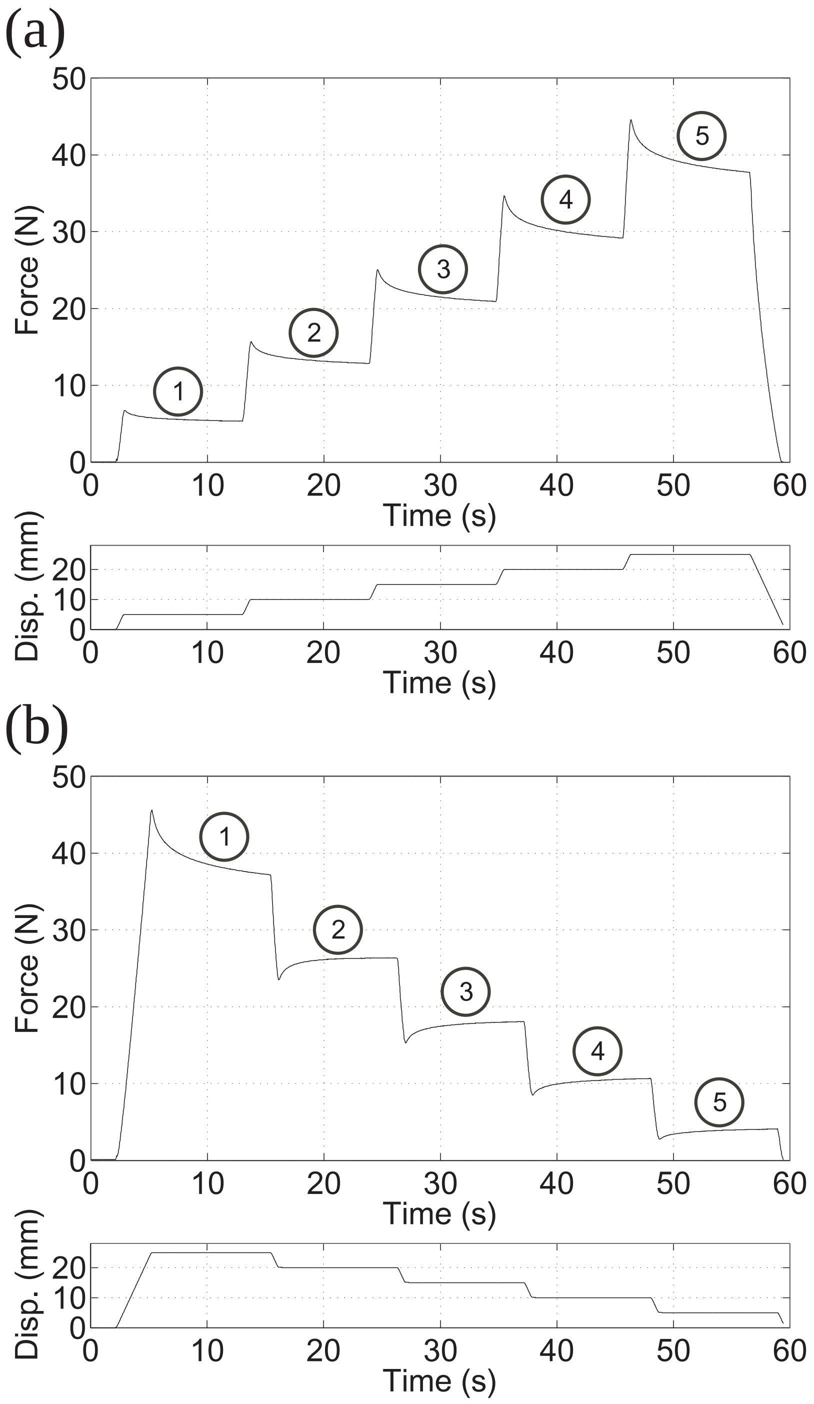

Figure 7.4: Experimental results from a tensile test with a pair of flat parallel fixture plates. (a) loading and relaxation; (b) loading followed by successive unloading and hold. Bother Types I and II relaxation are present.

object, and can be written as follows

$$A = \pi a^2 = \pi\,[(r)^2 - (r-d)^2] \tag{7.7}$$

where r is the radius of the ball, a is the radius of the contact area, and d is the displacement (or depression) in the vertical direction, as shown in Fig. 7.5

Finally, we can calculate the strains and strain rates as functions of time

$$\begin{aligned} \varepsilon(t) &= \frac{f(t)}{E\pi[r^2 - (r-d(t))^2]} && (7.8) \\ \dot{\varepsilon}(t) &= \frac{d\varepsilon(t)}{dt} && (7.9) \end{aligned}$$

The strains and strain rates can be calculated based on the measured force and displacement, and are plotted as blue curves in Fig. 7.6(a) and Fig. 7.6(b).

Next, we chose $n = 5$ in (7.2) because it is the lowest order of polynomial which fits the experimental results the best. The nonlinear latency model becomes

$$\dot{\varepsilon} = -\nu(\varepsilon - \varepsilon_e)^5 \tag{7.10}$$

The least-square (LS) curve fitting technique is applied using Eq. (7.10) with the results plotted as red curves in Fig. 7.6(a) and Fig. 7.6(b). The parameters are listed in Table 7.1 for loading and Table 7.2 for unloading.

The fitting results indicate that the equilibrium strains, ε_e, are consistent for the same displacement in both continuous loading and continuous unloading experimental results. In addition, we found that the parameter, ν, in the continuing loading experiment in Table 7.1 shows consistent decrease with the increase in corresponding equilibrium strain, ε_e. This trend, however, is not repeatable in unloading (Table 7.2). It may be due to the different mechanisms of loading and unloading. For loading, the test machine gave a direct displacement for compression. But for unloading, the gripper moved backward and let material expand freely. We believe this may be a reason for the inconsistent phenomenon of ν between the two sets of parameters in Tables 7.1 and 7.2.

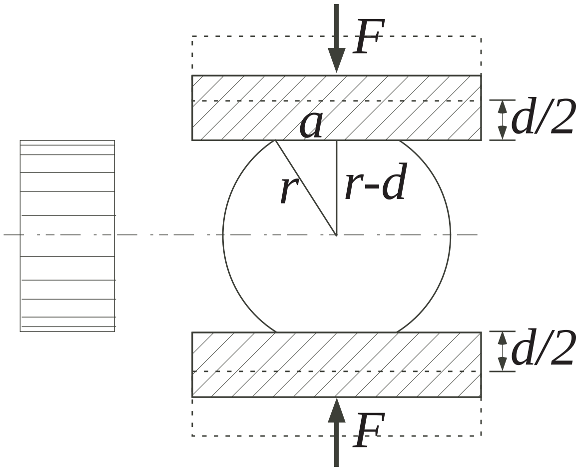

Figure 7.5: A model of a nonlinear viscoelastic ball making contact with a parallel-jaw gripper. The contact area is assumed to be circular. The plot to the left of the grasped object is the plot of equivalent latency model.

Table 7.1: fitting results of Fig. 7.6(a) (loading) $\dot{\varepsilon} = -\nu(\varepsilon - \varepsilon_e)^5$

curve #	1	2	3	4	5
ε_e	-0.1661	-0.2193	-0.2623	-0.3031	-0.3144
ν	4.1×10^4	2.6×10^4	2.0×10^4	1.4×10^4	1.2×10^3

Table 7.2: fitting results of Fig. 7.6(b) (unloading) $\dot{\varepsilon} = -\nu(\varepsilon - \varepsilon_e)^5$

curve #	1	2	3	4	5
ε_e	-0.3144	-0.3031	-0.2623	-0.2193	-0.1661
ν	1.4×10^3	1.4×10^6	1.4×10^5	7.0×10^4	2.8×10^4

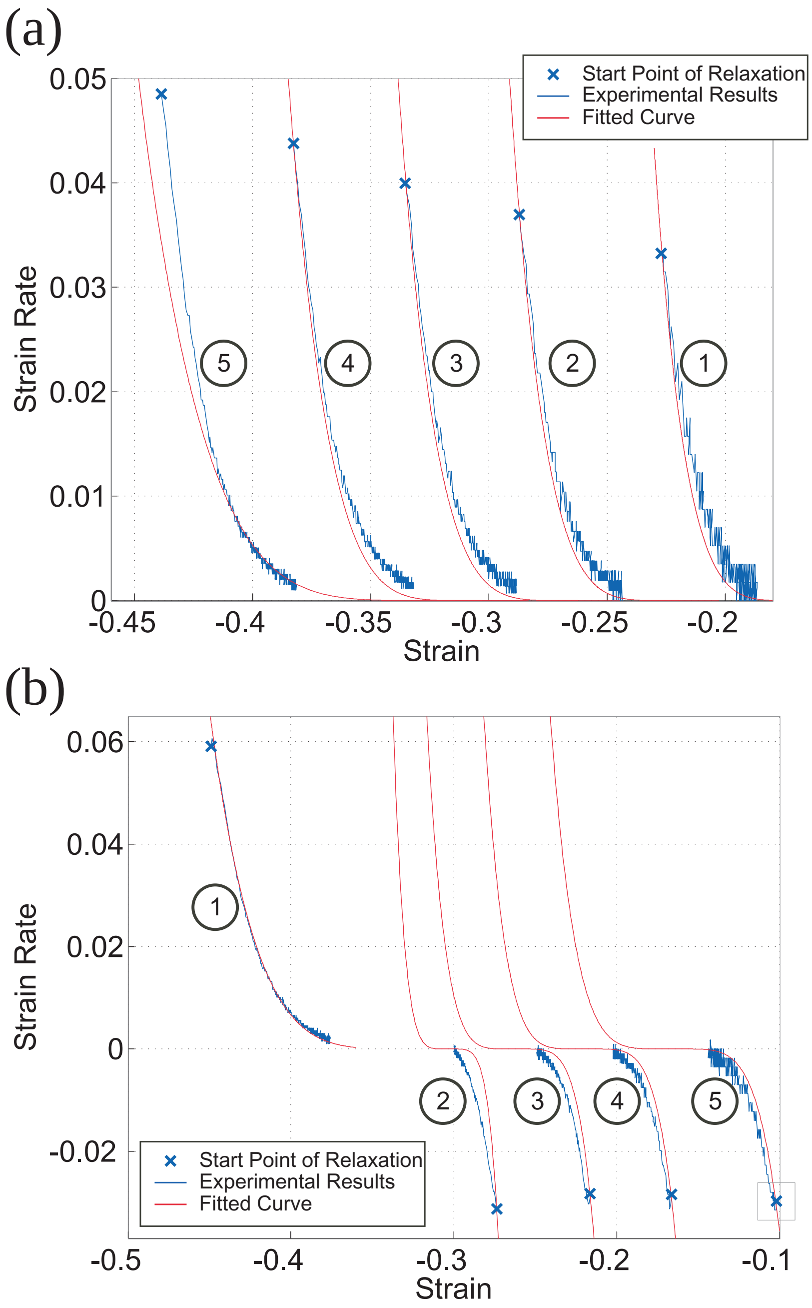

Figure 7.6: Plots (a) and (b) are the analysis of strain rate versus strain of the experimental results (a) and (b) in Fig. 7.4, respectively. The blue points are the values calculated from the experimental results, using (7.6) and (7.7). The red curves are the best fit using (7.10).

7.4 Simulation

Based on the model presented in (7.2), we use MATLAB to simulate the force response with the same displacement profile as that in the experiments, shown in Figs. 7.4(a) and 7.4(b). As the fixture of the tensile machine moves the distance of d, the movement is kinematically identical to each contact surface moving with a distance of $d/2$, with respect to the plane of symmetry in the middle of the ball, as illustrated in Fig. 7.5. The procedures of simulation are presented in the next section.

7.4.1 Simulation Procedures

(1) First, we divide the material into m segments axially, as illustrated in Fig. 7.7.

(2) The displacement of contact surface is updated with the progress of compression. We assume the displacement will eventually be evenly distributed when time approaches infinity. As a result, the equilibrium strain, ε_e at the i-th element equals the displacement of i-th node divided by the original length from i-th node to the symmetric center.

(3) The model in (7.10) is applied to each of the segments from the contact element from the exterior surface to the plane of symmetry. The strain of each element changes according to the corresponding strain rate calculated by (7.10).

(4) The force at the contact interface will simply be equal to the product of the stress at the contact interface, σ_1 (the first element), and the contact area, A. That is,

$$F = \sigma_1 \times A = (E\varepsilon_1) \times \left\{\pi[r^2 - (r - d_1)^2]\right\} \tag{7.11}$$

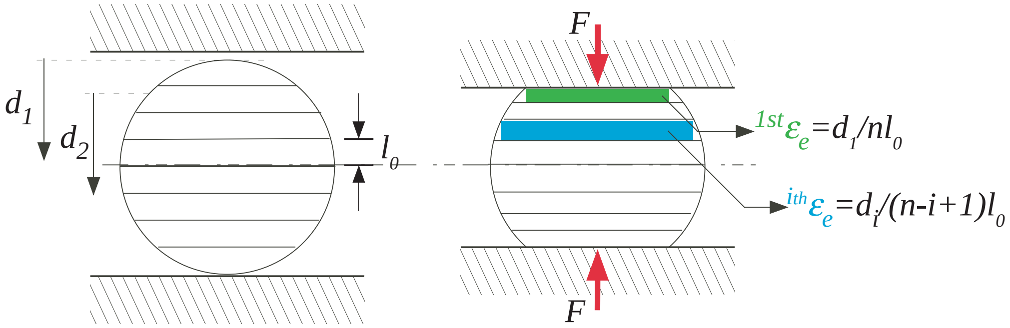

Figure 7.7: This diagram shows the discrete model used in the simulation. The object is divided into m segments ($m = 8$ in this figure). When an external force, F, is applied, the stress/strain wave will propagate toward the plane of symmetry of the grasped object, consistent with the latency model illustrated in Figure 7.5. In order to apply the model in (7.10) to the simulation, we estimate the equilibrium strain, $^{ith}\varepsilon_e$, of the i-th element by assuming the strain between the i-th element and plane of symmetry is uniformly distributed.

7.4.2 Simulation Results

Fig. 7.8 shows the results of simulation based on the model presented in (7.10), corresponding to the experimental results in Fig. 7.4(a). The procedures of simulation are described in the previous section. It can be seen from the results that the trend of Type I relaxation in simulation is similar to that of the experimental results. In addition, the amount of relaxation in each step also matches quite well with the experimental data in Fig. 7.4(a). This suggests that the proposed model can capture the relaxation responses of such grasping task adequately. We note that the unloading curve at the end of Fig. 7.8 (at $t \cong 53\,sec$) drops faster than the experimental results, which is probably due to the different mechanisms in loading and unloading as discussed in the end of the previous section. Overall, the simulation employed here can capture the relaxation responses of successive loading, and can model the nonlinear latency response well. This simulation tool will be useful in studying the robotic grasping or prehension that involves soft viscoelastic contacts.

7.5 Discussions

Based on the preceding presentation of the results of experimental study and simulation using the nonlinear latency model, observation and results are presented in the following.

7.5.1 Amount of relaxation versus displacement

As experimental results in Fig. 7.4(a) and Fig. 7.4(b) show, a larger amount of relaxation is always resulted when the displacement of loading is larger. This is due to the higher equilibrium strain, ε_e.

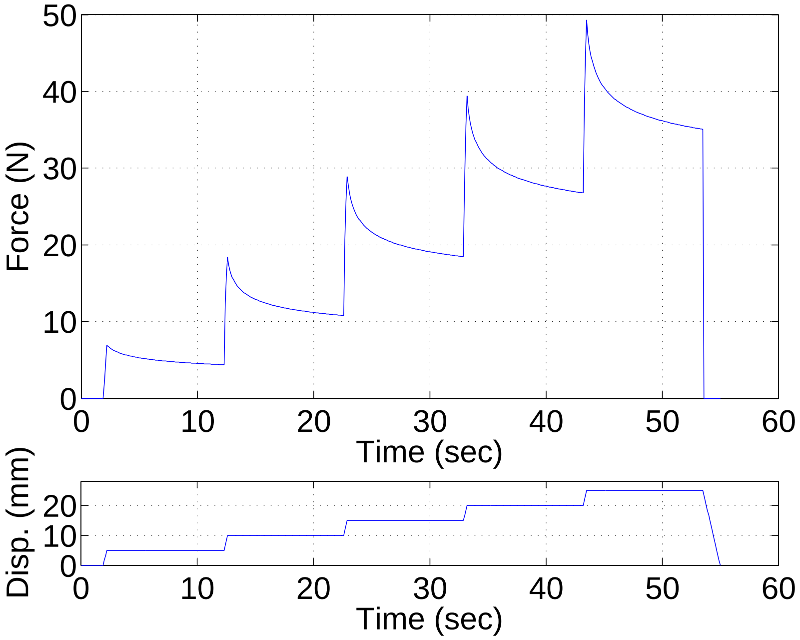

Figure 7.8: The results of simulation corresponding to Fig. 7.4(a).

7.5.2 Results in Tables 7.1 and 7.2

In Table 7.1, it is observed that the magnitudes of the equilibrium strain, $|\varepsilon_e|$, increase as the loading-holding procedure repeats itself from steps 1 to 5. This causes a larger amount of relaxation, as alluded to in Section 7.5.1. In addition, the values of the coefficient, ν, decrease as the loading-holding process progresses from steps 1 to 5. It is also noted that with the increase of the magnitude of the equilibrium strain, $|\varepsilon_e|$, the coefficient, ν, decreases.

In Table 7.2, it is observed that the magnitudes of the equilibrium strain, $|\varepsilon_e|$, decrease as the unloading-holding procedure repeats itself from steps 2 to 5, after the initial loading to the maximum displacement of $25\,mm$. The values of the coefficient, ν, decrease when the unloading-holding cycles start after step "2". (Step 1 is the loading process.) The values of the equilibrium strains at the various displacement steps are the same as the corresponding ones in Tables 7.1.

7.6 Summary

In this chapter, a contact model for nonlinear viscoelastic materials is presented with both simulation and experiments. The model describes the relationship between the strains and the strain rates of infinitesimal element within the material. The proposed model postulates that the values of strain will asymptotically reach an equilibrium strain. The nonlinear latency model attempts to characterize the path by which the strain varies from the initial value to the equilibrium strain, with successive loading, unloading, and holding—a situation which occurs often in robotic grasping and manipulation involving soft contacts. The simulation tool developed based on the latency model appears to match well with the experimental results.

Future study will be focused on the physical meaning of the exponent, n, of the nonlinear latency model and its correlation to the material structure or property of soft contacts.

Chapter 8

CONCLUSIONS AND FUTURE WORK

8.1 Conclusions

Various topics of viscoelastic contact have been investigated and presented both theoretically and experimentally. The conclusions are summarized as follows:

(1) **Stress relaxation and strain creep** are two sides of the same coin in viscoelastic contact interface. They both represent the same latent behavior of viscoelasticity. Stress relaxation happens when a constant displacement is applied to a viscoelastic material. On the other hand, strain creep occurs when a constant force is applied to the material. The temporal responses of both stress relaxation and strain creep can be obtained analytically with curve fitting by the Fung's model with two exponential terms in the temporal function. This demonstrates that the material consistently exhibits temporal responses which can be captured by this model, as reflected in the experiments of stress relaxation and strain creep.

(2) **Strain stiffening** refers to the phenomenon for viscoelastic materials to have different instantaneous elastic modulus when subject to different loading rates of external stimuli. The *instantaneous elastic modulus* of the materials usually increases when the loading rate is high. Based on both theoretical modeling and experimental studies, it is believed that the stiffening phenomenon results from the latent behavior of

viscoelastic materials. In other word, the strain stiffening is due to the strain on the contact surface which has not been propagated throughout the viscoelastic material yet. The actual strain on the contact surface is larger than the strain is supposed to be in an equilibrium state. Macroscopically, the material shows the phenomenon of becoming stiffened.

(3) A novel viscoelastic model, the **latency model**, is proposed. The latency model was inspired by experimental observation of latent behavior of viscoelastic response, and derived by applying the Fung's model. The analytical equation that describes the consistent relation between strain and strain rate was derived. Subsequently, the latency model was extended to model the strain and strain rate in a nonlinear relation. The experimental results and simulation show the consistency of the parameters of the latency model.

(4) The study of **grasp stability** of soft contact shows that, theoretically and experimentally, the grasp stability is improved by using soft contact instead of rigid contact with a force control manipulation. The analysis of grasp stability is based on the limit surface and pressure distribution of a soft contact.

The topics with theoretical modeling and experimental studies were conducted in the context of the research project between Stony Brook and Osaka Universities under NSF-JST international research collaboration between Professors Imin Kao and Makoto Kaneko. Some experiments have been conducted at Dr. Kaneko's laboratory in Osaka University and at Dr. Korach's laboratory in State University of New York at Stony Brook.

8.2 Future Work

Based on the preceding research studies and results, future research topics for viscoelastic applications are proposed: (1) bio-inspired tactile sensor, and (2) modeling of viscoelastic contact for calibrating cochlear models.

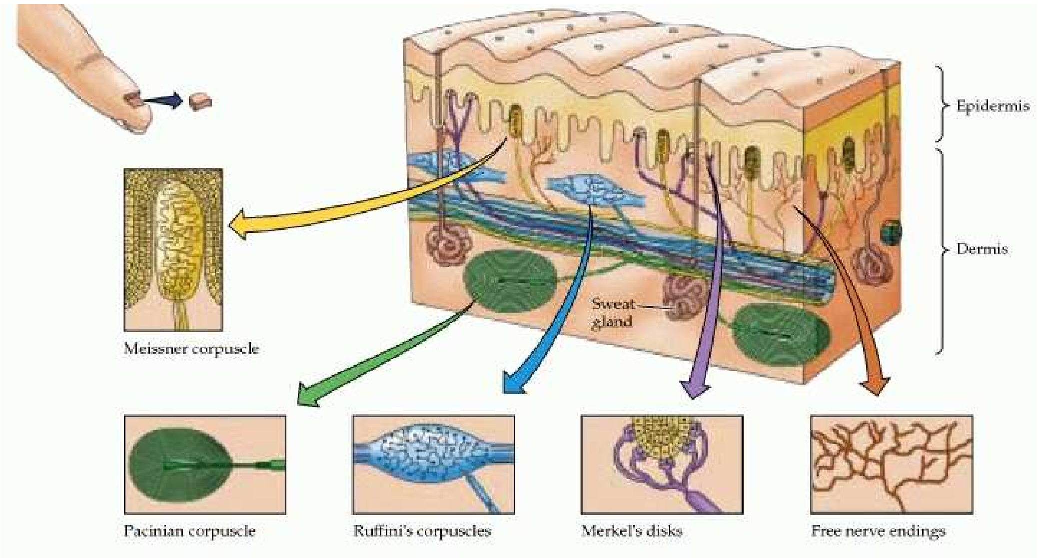

Figure 8.1: Schematic drawing of skin. [3]

8.2.1 Bio-Inspired Tactile Sensor with Viscoelastic Properties

Human's tactile senses has two different kinds of receptors: fast adapting receptors (FA) and slow adapting receptors (SA), which are similar to the two different time constants of the relaxation/creep characteristics of viscoelastic material from the experimental results presented in previous chapters.

To build a human-like tactile sensor, a specimen made of silicone polymer with strain gauges embedded is shown in Fig. 8.2. Four specimen were made for the experiments, and their composition and dimensions are listed in Table 8.2

Preliminary experiments of pressing the specimen with different shapes of indenters have been conducted, with the results shown in Fig. 8.4. The results show that, due to stress concentration, the strain gauge signals quickly reach the saturation limit while indenting with a sharp tip. With a blunt tip, the signals are within measurable range. But interestingly, both types of stimuli caused the temporal response, that is, the strain creep, when the indenter is removed.

Future investigation includes:

(1) Experiments with different frequencies of stimuli: The expected results should have

Table 8.1: The Major Classes of Somatic Sensory Receptors [3]

Receptor Type	Location	Function	Rate of Adaption
Meissner’s Corpuscles	Epidermis	Touch, Pressure (Dynamic)	Rapid
Pacinian Corpuscles	Dermis	Deep Pressure, Vibration (Dynamic)	Rapid
Merkel’s Disks	Epidermis	Touch, Pressure (Static)	Slow
Ruffini’s Corpuscles	Dermis	Stretching of Skin	Slow

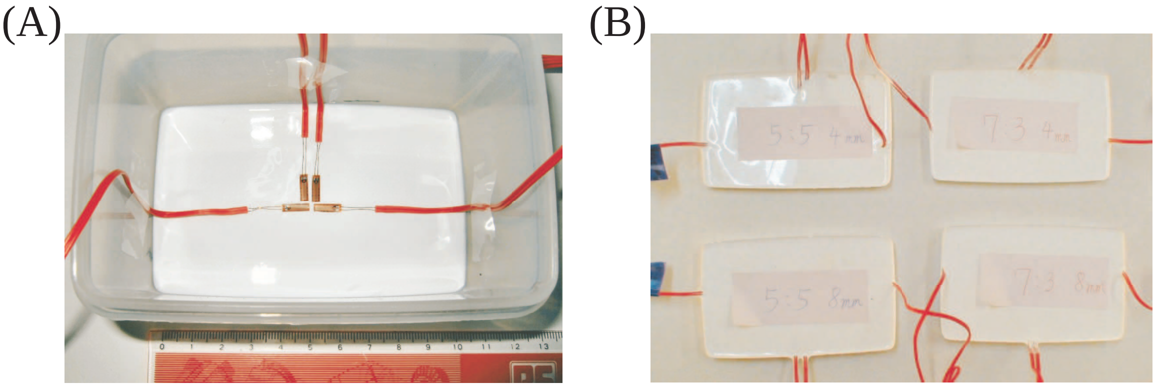

Figure 8.2: Manufacturing of human-like tactile sensor. (A) Pour silicone polymer into the mold as the bottom layer and place four strain gauges as shown. After the bottom layer is cured, pour a top layer of silicone polymer on it to complete a human-like tactile sensor; (B) Different compositions of silicone polymers are used in making the tactile sensors with different dimensions.

Table 8.2: The Composition and Thickness of the Specimens

Specimen#	Silicone:Thinner	Thickness
1	5 : 5	4mm
2	7 : 3	4mm
3	5 : 5	8mm
4	7 : 3	8mm

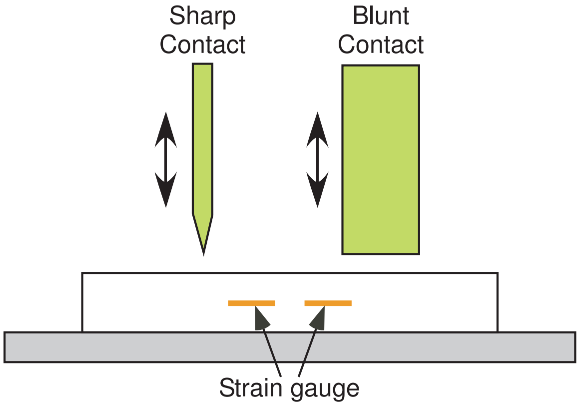

Figure 8.3: Illustration showing two different types of indentors.

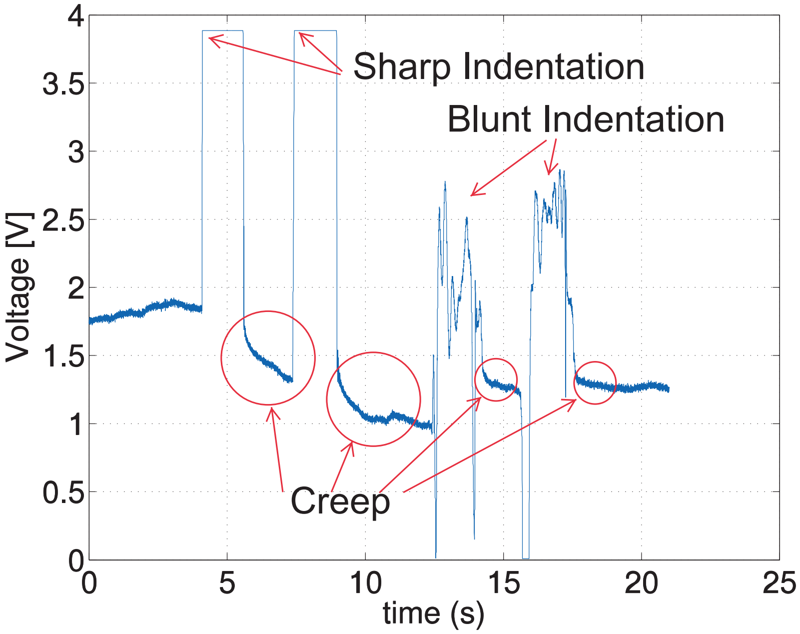

Figure 8.4: The signals captured by a strain gauge subject to different indentation. The sharp contact and blunt contact are illustrated in Fig. 8.3

different responses under different stimuli with different frequencies. It should be feasible to identify the characteristics of the material by examining the dynamic damping effect.

(2) Research results from literature suggest that fingerprint helps human tactile sensation. In the future work, contact surface similar to human fingerprint can be added on the surface to quantitatively examine the relation between such fingerprint and signals.

8.2.2 Modeling of Contact Mechanics for Calibrating Cochlear Models

Mammal hearing systems can sense and discriminate the sound of different frequencies and intensities quite well. The sense of hearing is initiated when oscillations in air pressure are converted into fluid pressure and travel down the inner ear. In the inner ear, cochlea is the organ where mechanical energy from vibrations of membranes and hair bundles, in the form of sound waves, transforms into neural signals. As a result, understanding intrinsic properties, such as the mechanical properties and contact interface, of cochlear membranes is essential for understanding cochlea. This future work will focus on developing a novel methodology, which takes the special properties of viscoelasticity into consideration, to determine the mechanical properties of cochlear membranes, such as hardness and elastic modulus. Furthermore, the proposed research also seeks to apply the techniques for calibrating cochlear models of human inner ear.

Cochlea is snail-shaped organ in the inner ear as shown in Fig. 8.5. [4]. As shown by the illustration, the tectorial membrane (TM), hair cell bundles, and Basilar membrane (BM) are connected together; therefore, the dynamic responses are coupled and challenging to model. Cai *et al.* [45] used Navier-Stokes fluid and Voigt solids to construct a cochlear model. Shoelson *et al.* [46] mapped the shear modulus of the TM using atomic force microscopy (AFM), and presented the evidence of inhomogeneity in TM elasticity. Nanoindentation is a popular methodology to measure the mechanical properties of materials, and there are numerous advantages of nanoindentation, such as the capability of measuring the

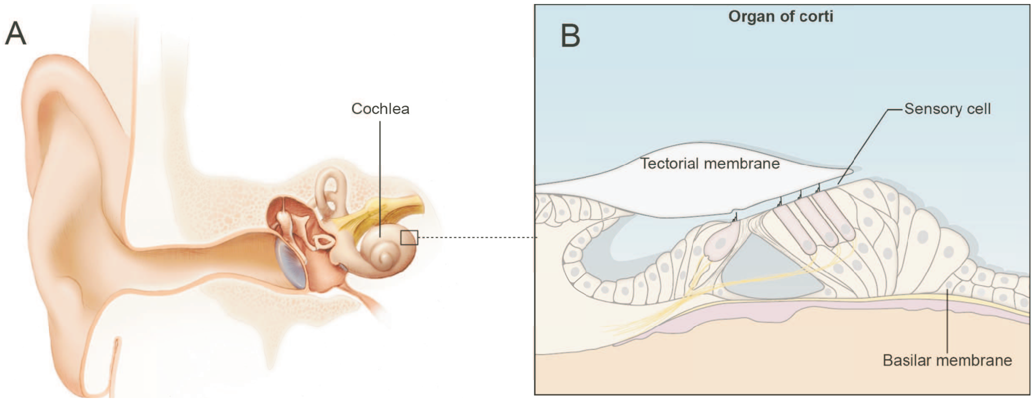

Figure 8.5: (A) The cochlea is located in the inner ear. (B) The organ of Corti. [4]

mechanical properties of a localized area and substrate effect. Oliver and Pharr proposed an empirical model by using a power law function to describe the relation between strain and stress in a nanoindentation test [47]. The model is based on an elastic solution and works well for hard ceramic materials. AFM and the modified AFM, atomic force acoustic microscopy (AFAM), are broadly used as an important tool for measuring mechanical properties [5, 48]. Taber and Steele modeled the cochlea with a straight rigid-walled tube and modeled membranes with viscoelastic, orthotropic, tapered plate with hinged edges [49].

Fig. 8.6 illustrates experiments of nano indentation with an AFM. The Hertzian contact model is usually applied for the contact mechanics. In reality, pressure distribution of a contact interface differs with different properties of materials. Although the Hertzian contact model has been widely used and accepted, a more general model is necessary in the study of bio-tissues. In [34], Xydas and Kao observed a more general formulation of pressure distribution with viscoelastic contact, and proposed the contact model, which subsumes the Hertzian contact model, as follows:

$$p(r) = C_k \frac{N}{\pi a^2} \left[1 - \left(\frac{r}{a} \right)^k \right]^{\frac{1}{k}} \tag{8.1}$$

where $p(r)$ is the pressure as a function of radius in a polar coordinate, N is the normal force, a is the radius of contact area. C_k is a coefficient, a function of k, that adjusts the profile of pressure distribution to satisfy the equilibrium condition at the contact interface,

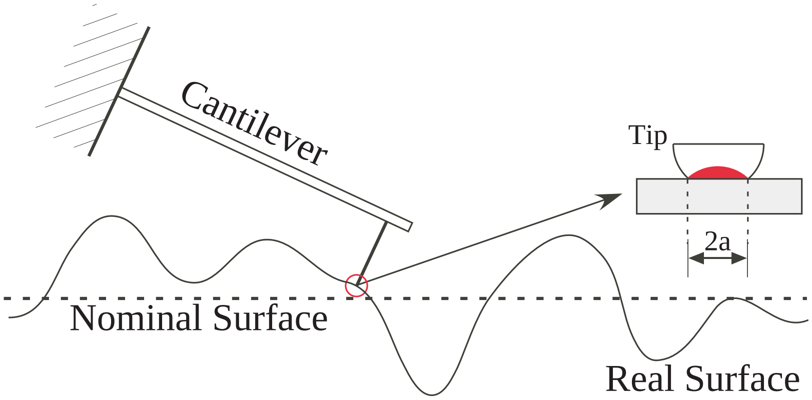

Figure 8.6: The diagram illustrates how an atomic force microscopy (AFM) measures the surface roughness or mechanical properties of materials.

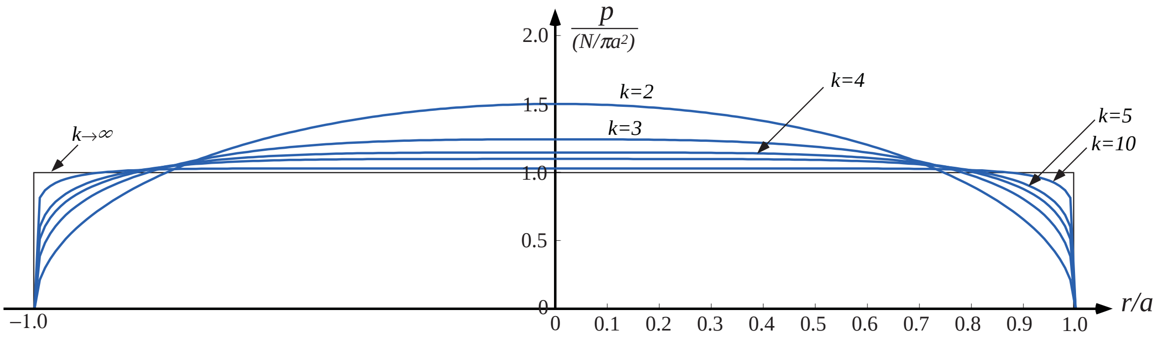

Figure 8.7: The pressure distribution of viscoelastic contact based on equation (8.1) for different values of k. As $k \longrightarrow \infty$, the distribution becomes uniform with normalized maximum pressure of 1.0. Selected values of C_k is tabulated in Table 8.3.

and is:

$$C_k = \frac{3}{2}\frac{k\Gamma\left(\frac{3}{k}\right)}{\Gamma\left(\frac{1}{k}\right)\Gamma\left(\frac{2}{k}\right)} \tag{8.2}$$

where Γ is the Gamma function, and k is a positive real number, although integer values are often used. It is apparent from equation (8.2) that C_k is only a function of k.[1] The pressure profile varies with different k, and can be plotted in a normalized coordinate as shown in Fig. 8.7. In this model, Hertzian model is a special case when $k = 2$. In general, softer materials usually tend to have higher values of k.

Future investigation includes:

(1) The contact of bio-tissue always involves not only elastic response but also temporal responses. A relevant viscoelastic model is essential for the study. An application of the latency model for the investigation of contact mechanics using probe tip and bio-tissue is shown in Fig. 8.8

(2) As opposed to the deterministic modeling, stochastic modeling is usually more accurate, especially for biological contact interface; however, it requires large computing power and time. A standard AFM process is shown in Fig. 8.6. One end of the cantilever is mounted on the AFM, while the other end has a nano-scale probe attached.

---

[1] Equation (8.2) can also be expressed in an alternative form with $C_k = \frac{3\Gamma\left(\frac{3}{k}\right)}{\Gamma\left(\frac{1}{k}\right)\Gamma\left(1+\frac{2}{k}\right)}$ because $\Gamma(z+1) = z\Gamma(z)$.

Table 8.3: Table of values of C_k for selected values of k. The values of k can be integer or real numbers, depending on the characteristics of the materials and geometry of contact.

k	C_k
1.8	1.6080
2	1.5000
3	1.2405
4	1.1441
10	1.0274
100	1.00032

The real surface is not truly smooth on an atomic scale. Cochlear membranes also have asperities as illustrated in Fig. 8.6. The roughness can affect the measurement of force and displacement of the probe tip. As a result, a stochastic model is necessary for the measured data corresponding to the surface roughness. An optimized stochastic model with adjustment of parameters can be obtained based on experimental results.

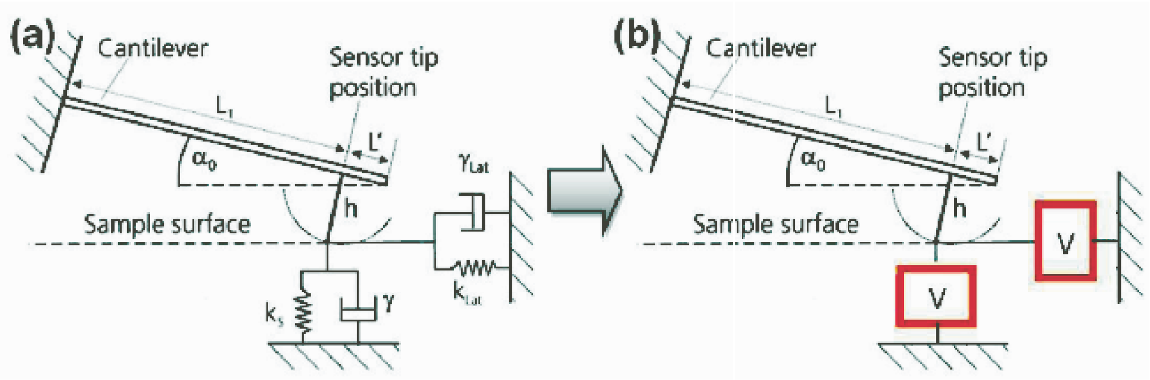

Figure 8.8: Replace the Kelvin Voigt contact model in [5] by the latency model.

Bibliography

[1] N. Sakamoto, M. Higashimori, T. Tsuji, and M. Kaneko. An optimum design of robotic hand for handling a visco-elastic object based on maxwell model. In *Proc. IEEE Int. Conf. on Robotics and Automation, ICRA 2007*, pages 1219–1225, Roma, Italy, April 10-14 2007.

[2] C. D. Tsai and I. Kao. The latency model for viscoelastic contact interface in robotics: Theory and experiments. In *Proc. 2009 IEEE Int. Conf. on Robotics and Automation (ICRA 2009)*, pages 1291–1296, Kobe, Japan, May 2009.

[3] D. Purves, G. Augustine, D. Fitzpatrick, L. Katz, A. LaMantia, J. McNamara, and S. Williams, editors. *Neuroscience*. 2nd edition.

[4] M. Schwander, B. Kachar, and U. Muller. The cell biology of hearing. *Journal of Cell Biology*, 190(1):9 – 20, 2010.

[5] E. Kester, U. Rabe, L. Preqsmanes, Ph. Tailhades, and W. Arnold. Measurement of young's modulus of nanocrystalline ferrites with spinel structures by atomic force acoustic microscopy. *J. Phys. Chem. Solids*, 61:1275–1284, 2000.

[6] M. A. Meyers and K. K. Chawla. *Mechanical Behavior of Materials*. Prentice-Hall, Inc, 1999.

[7] Y. Li and I. Kao. A review of modeling of soft-contact fingers and stiffness control for dextrous manipulation in robotics. In *Proc. IEEE Int. Conf. on Robotics and Automation, ICRA*, pages 3055–3060, Seoul, Korea, 2001.

[8] Y. C. Fung. *Biomechanics: Mechanical Properties of Living Tissues*. Springer-Verlag, 1993.

[9] P. Tiezzi and I. Kao. Characteristics of contact and limit surface for viscoelastic fingers. In *IEEE Int. Conf. on Robotics and Automation, ICRA 2006*, pages 1365–1370, Orlando, Florida, May 15-19 2006.

[10] P. Tiezzi and I. Kao. Modeling of viscoelastic contacts and evolution of limit surface for robotic contact interface. *IEEE Transaction on Robotics*, 23(2):206–217, April 2007.

[11] P. Tiezzi, I. Kao, and G. Vassura. Effect of layer compliance on frictional behavior of soft robotic fingers. *Advanced Robotics*, 21(14):1653–1670, 2007.

[12] C. D. Tsai, I. Kao, N. Sakamoto, M. Higashimori, and M. Kaneko. Applying viscoelastic contact modeling to grasping task: an experimental case study. In *International Conference on Intelligent Robots and Systems, IROS*, pages 3737–3743, 2008.

[13] W. Yang. The contact problem for viscoelastic bodies. *Journal of Applied Mechanics*, 33:395–401, June 1966.

[14] W. Flugge. *Viscoelasticity*. Blaisdell Publishing Company, 1967.

[15] J. C. Maxwell. *Philosophical Transactions of the Royal Society London*, 157:49–88, 1867.

[16] D. P. Noonan, H. Liu, Y. H. Zweiri, K. A. Althoefer, and L. D. Seneviratne. A dual-function wheeled probe for tissue viscoelastic property indentification during minimally invasive surgery. In *Proc. IEEE Int. Conf. on Robotics and Automation, ICRA 2007*, pages 2629–2634, Roma, Italy, April 10-14 2007.

[17] M. Kimura, Y. Sugiyama, S. Tomokuni, and S. Hirai. Constructing rheologically deformable virtual objects. In *Proc. IEEE Int. Conf. on Robotics and Automation, ICRA*, pages 3737–3743, 2003.

[18] W. N. Findley and J. S. Y. Lay. A modified superposition principle applied to creep of non-linear viscoelastic material under abrupt changes in state of combined stress. *Trans. of the Society of Rheology*, vol. 11(3):361–380, 1967.

[19] D. B. Adolf, R. S. Chambers, and J. Flemming. Potential energy clock model: Justification and challenging predictions. *Journal of Rheology*, 51(3):517–540, 2007.

[20] A. Z. Golik and Y. F. Zabashta. a molecular model of creep and stress relaxation in crystalline polymers. *Mekhanika Polimerov*, pages 969–975, 1971.

[21] B H. Zimm. Dynamics of polymer molecules in dilute solution: Viscoelasticity, flow birefringence and dielectric loss. *The Journal of Chemical Physics*, 24(2):269–278, 1956.

[22] T. Alfrey. A molecular theory of the viscoelastic behavior of an amorphous linear polymer. *The Journal of Chemical Physics*, 12(9):374–379, 1944.

[23] JR. P. E. Rouse. A theory of the linear viscoelastic properties of dilute solutions of coiling polymers. *The Journal of Chemical Physics*, 21(7):1272–1280, 1953.

[24] F. Bueche. The viscoelastic properties of plastics. *The Journal of Chemical Physics*, 22(4):603–609, 1954.

[25] L. R. G. Treloar. *The Physics of Rubber Elasticity*. Clarendon Press, Oxford, 1975.

[26] T. G. Goktekin, A. W. Bargteil, and J. F. O'Brien. A method for animating viscoelastic fluid. In *Special Interest Group on Graphics and Interactive Techniques, SIGGRAPH*, 2004.

[27] P.S. Theocaris and N. Papadopoulou. Propagation of stress waves in viscoelastic media. *Polymer*, 19(2):215 – 219, 1978.

[28] D. Turhan and Y. Mengi. Propagation of initially plane waves in nonhomogeneous viscoelastic media. *International Journal of Solids and Structures*, 13(2):79 – 92, 1977. NONHOMOGENEOUS VISCOELASTIC MEDIA;WAVE PROPAGATION;.

[29] Paul Stucky and William Lord. Finite element modeling of transient ultrasonic waves in linear viscoelastic media. *IEEE Transactions on Ultrasonics, Ferroelectrics, and Frequency Control*, 48(1):6 – 16, 2001. Linear viscoelastic media;.

[30] J.M. Pereira, J.J. Mansour, and B.R. Davis. Dynamic measurement of the viscoelastic properties of skin. *Journal of Biomechanics*, 24(2):157 – 162, 1991. Collagen Network;Dynamic Wave Propagation Method;Proteoglycan Gel;Skin Strain Properties;Skin Viscoelastic Properties;.

[31] R. Fowles and R. F. Williams. Plane stress wave propagation in solids. *Journal of Applied Physics*, 41(1):360 – 363, 1970.

[32] D. T. V. Pawluk and R. D. Howe. Dynamic contact of the human fingerpad against a flat surface. *ASME Jour. of Biomechanical Engineering*, vol. 121(6):605–611, 1999.

[33] R. D. Howe, N. Popp, I. Kao, P. Akella, and M. R. Cutkosky. Grasping, manipulation, and control with tactile sensing. In *Proc. IEEE Int. Conf. on Robotics and Automation, ICRA*, Cincinnati, OH, 1990.

[34] N. Xydas and I. Kao. Modeling of contact mechanics and friction limit surface for soft fingers in robotics, with experimental results. *Int. J. of Robotic Research*, 18(8):941–950, 1999.

[35] N. Xydas and I. Kao. Modeling of contacts and force/moment for anthropomorphic soft fingers. In *Proc. of Int. Conf. on Intelligent Robots and Systems, IROS*, pages 488–493, Victoria, Canada, 1998.

[36] T. Inoue and S. Hirai. Elastic model of deformable fingertip for soft-fingered manipulation. *IEEE Trans. in Robotics*, 22:1273–1279, 2006.

[37] K. B. Shimoga and A. A. Goldenberg. Soft robotic fingertips - part I and II: A comparison of construction materials. *Int. Jour. of Robotic Research*, 15(4), 1996.

[38] F. Barbagli, A. Frisoli, K. Salisbury, and M. Bergamasco. Simulating human fingers: a soft finger proxy model and algorithm. In *Proc. IEEE Int. Symp. on Haptic Interface, HAPTICS'04*, 2004.

[39] I. Kao and F. Yang. Stiffness and contact mechanics for soft fingers in grasping and manipulation. *the IEEE Trans. of Robotics and Automation*, 20(1):132–135, February 2004.

[40] D. T. V. Pawluk and R. D. Howe. Dynamic lumped element response of the human fingerpad. *ASME Jour. of Biomechanical Engineering*, vol. 121(2):178–183, 1999.

[41] Y. C. Fung. *Biomechanics: Mechanical Properties of Living Tissues*. Springer-Verlag, 1993.

[42] M. L. Gardel, J. H. Shin, F. C. MacKintosh, L. Mahadevan, P. Matsudaira, and D. A. Weitz. Elastic behavior of cross-linked and bundeled actin networks. *Science*, 304:1301–1305, May 2004.

[43] C. D. Tsai, I. Kao, K. Yoshimoto, M. Higashimori, and M. Kaneko. An experimental study and modeling of loading and unloading of nonlinear viscoelastic contacts. In *International Conference on Intelligent Robots and Systems, IROS*, pages 3737–3743, October 2009.

[44] J. W. Jameson. *Analytic Techniques for Automated Grasp*. PhD thesis, Department of Mechanical Engineering, Stanford University, June 1985.

[45] H. Cai, B. Shoelson, and RS. Chadwick. Evidence of tectorial membrane radial motion in a propagating mode of a complex cochlear model. *Proc Natl Acad Sci*, 101:6243 – 6248, 2004.

[46] B. Shoelson, EK. Dimitriadis, H. Cai, and B. Kachar. Evidence and implications of inhomogeneity in tectorial membrane elasticity. *Biophys J*, 87:2768 – 2777, 2004.

[47] W. Oliver and G. Pharr. An improved technique for determining hardness and elastic-modulus using load and displacement sensing indentation experiments. *Journal Mater Res*, 7:1564 – 1583, 1992.

[48] U. Rabe, S. Amelio, M. Kopycinska, S. Hirsekorn, M. Kempf, M. Goken, and W. Arnold. Imaging and measurement of local mechanical material properties by atomic force acoustic microscopy. *Surface and Interface Analysis*, 33:65 – 70, 2002.

[49] L.Taber and C. Steele. Cochlear model including three-dimensional fluid and four modes of partition flexibility. *J. Acoust. Soc. Am.*, 70(2):426–436, 1981.

Appendix A

JUSTIFICATION OF CHOOSING TWO EXPONENTIAL TERMS IN RELAXATION

The question we are trying to answer is: “What is the reasonable number of exponential terms required in equation (3.3) to render a good curve fitting?” We justify the choice of two exponential terms by comparing the results and adequacy of fitting of equation (3.4) with one to four exponential terms. The results of a typical set of data are listed in the following:

$$\begin{aligned}
f(t) &= 1.0870 + 0.7820\,e^{-1.208t} && \text{(A.1)}\\
f(t) &= 0.9987 + 0.4780\,e^{-3.672t} + 0.5144\,e^{-0.5145t} && \text{(A.2)}\\
f(t) &= 0.8852 + 0.4264\,e^{-4.009t} + 0.3421\,e^{-0.8896t} \\
&\quad + 0.3399\,e^{-0.1758t} && \text{(A.3)}\\
f(t) &= 0.8597 + 0.3866\,e^{-4.206t} + 0.2227\,e^{-1.4000t} \\
&\quad + 0.4255\,e^{-0.3545t} + 0.09962\,e^{-8.5\times10^{-5}t} && \text{(A.4)}
\end{aligned}$$

The graphical results of curve fitting is shown in Figure A.1. It is obvious from visual inspection that all equations in (A.2) to (A.4) render very good fit, except equation (A.1) which has only one exponential term. In addition, the correlation factor (R^2) of the curve fitting with two or more exponential terms are $R^2 \geq 0.9988$, confirming the good curve fitting as seeing visually in Figure A.1. If we define the time constant of each of the exponential term as $\tau_i = 1/\nu_i$, we can obtain the shortest time constants for each of the

Table A.1: Time constants of each exponential term in equations (A.1–A.4)

Eq	*exp*. terms	τ_1 (sec)	τ_2 (sec)	τ_3 (sec)	τ_4 (sec)
(A.1)	1	0.8278	N/A	N/A	N/A
(A.2)	2	0.2723	1.9436	N/A	N/A
(A.3)	3	0.2494	1.1241	5.6883	N/A
(A.4)	4	0.2378	0.7143	2.8209	11628.0

curve fitting in equations (A.1) to (A.4) in Table A.1.

Since τ_1 is the shortest time constant, it affects the exponential decaying response of relaxation most dominantly. It can be seen from Table A.1 that as long as two or more exponential terms are adopted, the results of τ_1 do not vary too much. As a result, two exponential terms are used in modeling.

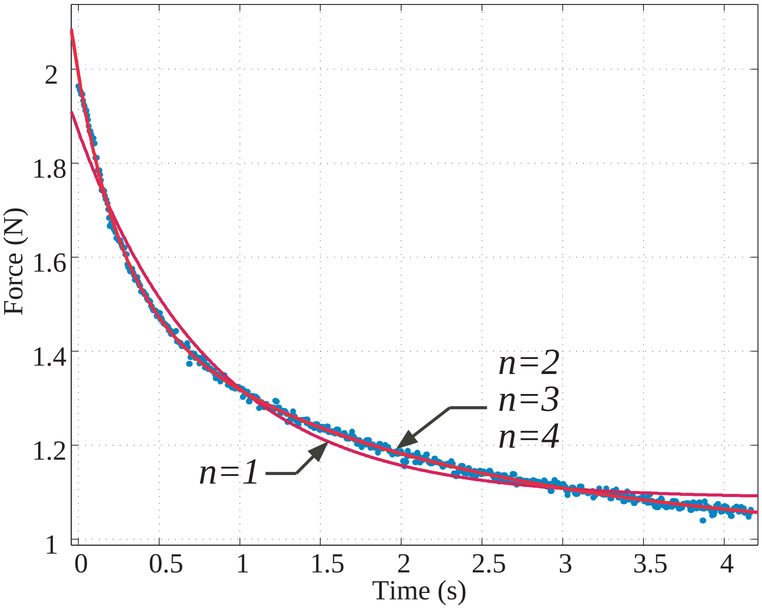

Figure A.1: Overlaid plot of curve fitting using different number of exponential terms in equation (3.3), where *n* is the number of exponential terms. It is evident that when $n \geq 2$, the curve fittings are practically the same over the span of the time interval.

Appendix B

JUSTIFICATION OF CHOOSING TWO EXPONENTIAL TERMS IN CREEP

As an illustration for the choice of the parameter n in equation (6.2), we apply curve fitting to the experimental results in Fig. 6.4 by using equation (6.2). The creep response, based on different choice of $n = 1, 2, 3$, are listed in the following for comparison.

$$d(t) = 6.480 - 0.6787\,e^{-0.5907t} \tag{B.1}$$

$$d(t) = 8.100 - 0.5977\,e^{-0.8229t} - 1.733\,e^{-0.007805t} \tag{B.2}$$

$$\begin{aligned} d(t) &= 7.622 - 0.5973\,e^{-0.8235t} - 0.7719\,e^{-0.01161t} \\ &\quad -0.4833\,e^{-0.009946t} \end{aligned} \tag{B.3}$$

The graphical results of curve fitting are plotted in Figure B.1. The normalized coefficients of curve fitting and R^2 are summarized in Table B.1. It is obvious from visual inspection that the good curve fitting results can be obtained with two or more exponential terms ($n \geq 2$).

Therefore, we choose to use $n = 2$ in equation (6.2) for the analysis of the creep response.

Table B.1: The normalized results of curve fitting using (6.2)

	$n = 1$	$n = 2$	$n = 3$
$D^{(e)}$	6.48	8.10	7.62
c_0	1.00	1.00	1.00
c_1	-1.05×10^{-1}	-7.38×10^{-2}	-7.84×10^{-2}
c_2	N/A	-2.14×10^{-1}	-1.01×10^{-1}
c_3	N/A	N/A	-6.34×10^{-2}
v_1	5.91×10^{-1}	8.23×10^{-1}	8.24×10^{-1}
v_2	N/A	7.81×10^{-3}	1.16×10^{-2}
v_3	N/A	N/A	9.95×10^{-3}
R^2	0.9162	0.9411	0.9411

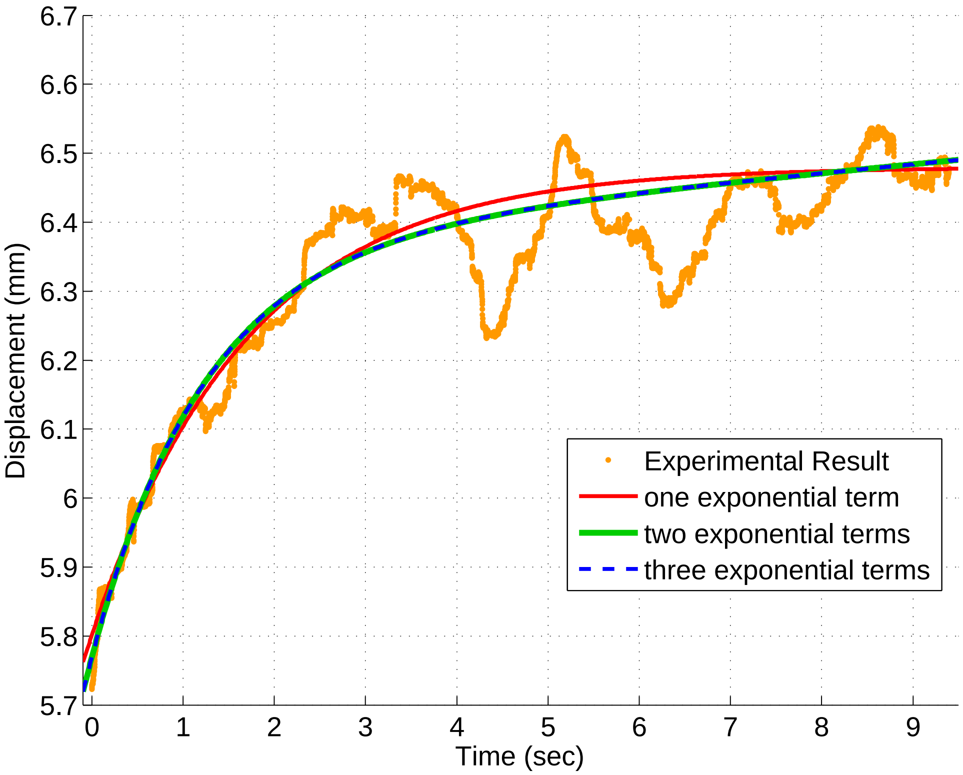

Figure B.1: The plots of curve fitting using different number of exponential terms in equation (6.2)